Fundamental Experiments on the Response of Solutions, Polymers, and Modified Polymeric Materials to Electromagnetic Radiation

by

George Dallas

Dissertation submitted to the Faculty of the
Virginia Polytechnic Institute and State University
in partial fulfillment of the requirements for the Degree of

DOCTOR OF PHILOSOPHY

in

Materials Engineering Science

APPROVED

Thomas C. Ward, Chairman

James E. McGrath

Garth L. Wilkes

Thomas J. Fabish

Robert W. Hendricks

November, 1991

Blacksburg, VA

Fundamental Experiments on the Response of Solutions, Polymers, and Modified Polymeric Materials to Electromagnetic Radiation

by

George Dallas

Committee Chairman: Dr. Thomas C. Ward
Materials Engineering Science

(ABSTRACT)

This dissertation is divided into two sections. In the first section dielectric and magnetic properties were analyzed for a series of materials: bisphenol A solutions, a poly(amide-imide), and polymers filled with either carbon black, iron particles, or aluminum flake. The second section deals with the influence of volatiles and low temperature aging on the dynamic mechanical and dielectric properties of a poly(amide-imide).

In the first investigation, solutions of bisphenol A in tetrahydrofuran (THF) or diglycidylether of bisphenol A (DGEBA) in either toluene or tetrahydrofuran were used to identify the influence of chemistry, solvent, and concentration (0 - 2.6M) on dielectric loss (ε'') and storage (ε') at (2.45 GHz). A number of solutions were examined as a function of frequency and temperature to obtain a mechanistic explanation for the single frequency data. The results showed the relaxation time shifting to higher frequencies with increased temperature and shifting to lower frequencies after a critical concentration. A polymer derived from bisphenol A and the diglycidylether of bisphenol A was sandwiched between two microwave inactive quartz plates to show selective

heating of a 0.002" film. The poly(amide-imide's) dielectric storage and loss values (ε', ε'') were examined as a function of temperature. The metal filled systems showed nonlinear behavior for dielectric loss (ε''), magnetic loss (μ''), and normalized magnetization (Gauss), which were explained by a percolation model. A critical volume fraction (Φ_c) was identified in the 0.15 - 0.25 volume fraction range. Scaling of dielectric and magnetic properties above Φ_c was 1.2 for aluminum flake, 1.5 for iron, and 5 for carbon black. The development of structure that occurred with increased filler content was monitored by scanning electron microscopy (SEM) and showed qualitative agreement with percolation behavior. At low volume fractions, there were individual particles, then clusters, then veins of material that extended many particle lengths.

The second part of this dissertation dealt with the influence of volatiles on the dynamic mechanical and dielectric values of a poly(amide-imide). Experiments were conducted in both the temperature and time domains. These data were complemented by thermogravimetry (TG), thermogravimetry-mass spectrometry (TG-MS), and thermomechanical analysis (TMA). The isothermal desorption of volatiles (150 - 165°C) could be monitored by either mechanical, dielectric, or gravimetric techniques. The mechanical experiments revealed two peaks for water: one a low temperature peak (-90 - -50°C) and the other at (100 - 190°C). The dielectric analysis revealed two peaks for <u>as received</u> poly(amide-imide). The first was between -50 to 0°C, the other was between 0 to 50°C. The low power dielectric analysis and volatile desorbtion behavior were combined to explain the structure that developed after poly(amide-imide) spheres were subjected to similar thermal or microwave processing conditions. Thermal processing produced a closed cell structure and a rough surface, while microwave processing produced an open cell structure at a smooth air-surface interface.

Acknowledgements

I would like to acknowledge VPI&SU professors Thomas C. Ward, James E. McGrath, G. L. Wilkes, Robert W. Hendricks, who presented me with quality lectures on synthesis and characterization of polymers and other aspects of material science. I appreciate Dr. Ward for financial assistance and maintaining a group of intelligent graduate students with whom I could discuss polymer characterization. The presence of Saikat Joardar made Room 1016 an entertaining lab. A special thanks goes to Dr. Tom Fabish for helping me while I visited American Cyanamid and for extending my understanding of materials response to electromagnetic radiation by giving me one of the most thorough prelim questions and an internship at Alcoa. Also, I appreciate Dr. Richard Zallen for helping clarify my understanding of percolation.

The many dielectric measurements were performed on a variety of instruments not in our labs. The data could not have been collected without the help of Jim Rancourt, Ken Baker, and Ron Perry (Alcoa), who maintained their instruments and made them available. The films could not have been made without the help of Leon Bretzski and Mark Wyzack, both of whom work at Mobay in Pittsburgh. Lastly, I would like to acknowledge the secretarial staff, librarians, and Physics machine shop for their timely and consistent support.

Dedication

This dissertation is dedicated to my parents, who did not receive their degrees but had the foresight and offered the support so I could pursue mine.

Table of Contents

List of Tables

List of Figures

Chapter 1

1.1 Introduction

This project was initiated by a DARPA grant to study microwave processing of materials. The work was divided into fundamental and applied research. The applied research included the microwave processing of epoxy [1] and polyimide [2] systems. They showed accelerated curing in a microwave field compared to the thermally processed system and the ability to control morphology in a rubber toughned epoxy [3]. The fundamental research focused on structure-property relationships for microwave heating [4]. This research is an extension of the fundamental work and includes solutions, polymers, and polymers filled with conductive and magnetic particles.

The objective of this research was to characterize materials response to electromagnetic radiation. A second goal was to investigate the influence of volatiles and low temperature aging on the dynamic mechanical or dielectric properties of a poly(amide-imide). To process materials by microwave energy it is helpful to view the task from a materials standpoint by considering all the constituents in the material, including volatiles. Fundamental insights of materials response to electromagnetic radiation can be gained by focusing on low power dielectric experiments. A range of materials with varying degrees of electrical complexity is shown in Figure 1.1, the electrically simple being the dilute solutions, and continuing in electrical complexity with polymers, a layered structure, and polymers filled with carbon black, aluminum flake, and iron particles. The materials excluded from this series are on the electrically simple end, gasses and on the electrically complex region, ceramics. The idea of presenting experimental data in order of electrical complexity was not mine. It comes from work by Arthur von Hippel

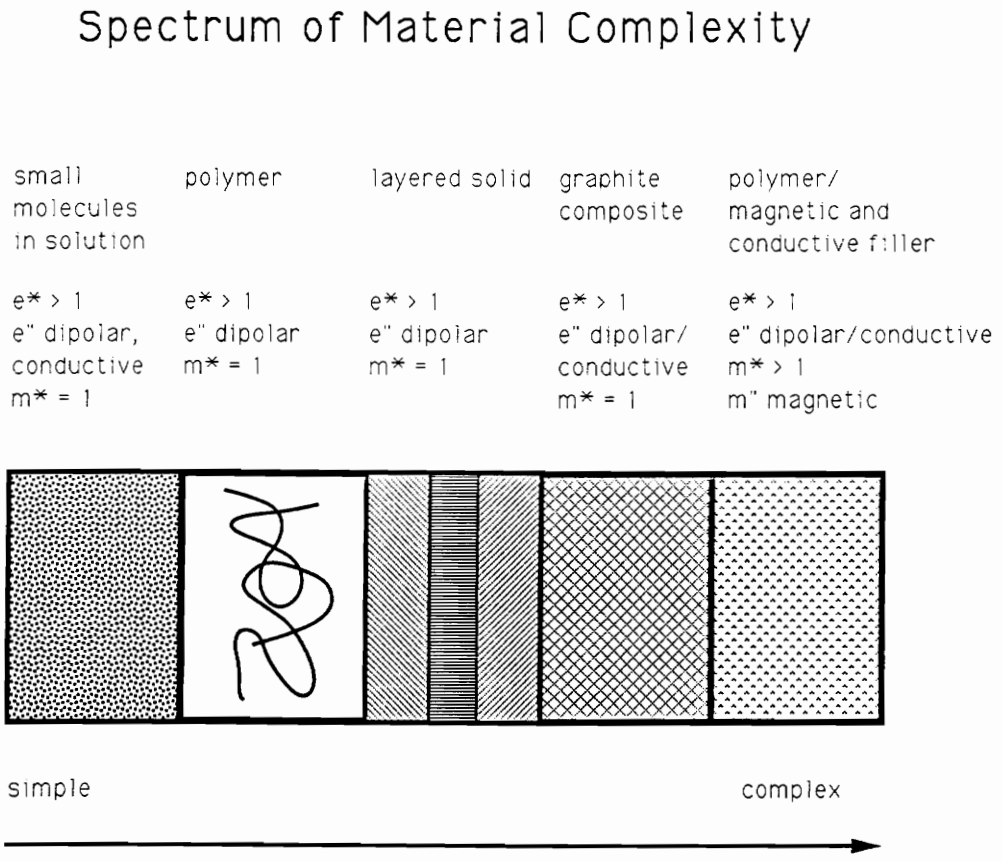

Figure 1.1

Schematic of materials investigated for dielectric analysis, presented in terms of dielectric complexity.

[5], though his work was more extensive and included gasses and ceramics. The volatiles, while not covalently bonded to the polymer structure, increased the dynamic mechanical and dielectric loss values of a poly(amide-imide) within specific temperature regions. Low temperature aging below the β transition, though reported not to have an influence on mechanical properties [6], had transient mechanical effects on the polymer.

The dissertation is divided into two parts. In Chapter 2, low power dielectric and magnetic analysis of the materials was accomplished on a state-of-the-art network analyzer as a function of temperature, time, and frequency.

In Chapter 3, the results of the influence of volatiles and low temperature aging on mechanical and dielectric properties and dimensional stability of a poly(amide-imide) were obtained. Occasionally, in both chapters high-powered microwave experiments were done to complement the low-power findings.

It is hoped that this work will make a meaningful contribution to the area of materials processing by electromagnetic radiation (2.45 GHz) by providing a broad range of experimental results on a wide range of materials, and to the field of low temperature aging of polymers.

The reader should be alert to a thought that is reapplied throughout this dissertation and its application to material science, "Think of everything as transient." Its application to material science generates the question, "What molecular motions occur on the temperature and time scale of the experiment?"

References

1. Lewis, D.A., *et al.*, *The Accelerated Curing of Epoxy Resins Using Microwave Radiation.* Polymer Preprints, 1987. **28**(2): p. 330 - 331.

2. Lewis, D.A., *et al.*, *Cure Kinetics and Mechanical Behavior of Electromagnetically Processed Polyimides.* Polymer Preprints, 1988. **29**(1): p. 174 - 175.

3. Hedrick, J.C., *et al.*, *Morphology and Fracture Toughness of Thermoplastic Modified Epoxy Resin Networks Prepared Via Electromagnetic Processing.* Polymer Preprints, 1988. **29**(1): p. 363 - 365.

4. Chen, M., *Electromagnetic Radiation Calorimetry of Thermoplastics, Elastomer, and Composites Systems.* 1989, Virginia Polytechnic Institute and State University:

5. von Hippel, A.R., *Dielectrics and Waves.* 1954, New York: John Wiley and Sons.

6. Struik, L.C.E., *Physical Aging in Amorphous Polymers and Other Materials.* 1978, Amsterdam: Elsivier.

Chapter 2

Dielectric Properties of Solutions, Polymers, and Filled Polymers

2.1 Introduction

Initial applications of electromagnetic shielding commenced during World War II [1]. The purpose was to shield aircraft from radar. The fundamentals of reflection and absorption extend to materials for electronics applications and recently to microwave processing of foods and polymers. A review of materials interaction with electromagnetic waves has been presented by Smyth [2] and von Hippel [3]. In these studies materials response to electromagnetic radiation at 2.45 GHz was conducted as a function of concentration or volume fraction filler, with complementary experiments performed as a function of temperature, time, or frequency. A series of materials shown in Figure 1.1 had their dielectric storage (ε') and loss (ε'') properties, with units of s^2 $C^2/kg\ m^3$, and magnetic storage (μ') and loss (μ'') properties, with units of $kg\ m/C^2$, examined. The materials included solutions of bisphenol A compounds; the polymer was a poly(amide-imide); the layered system was a quartz-polyhydroxyether-quartz sandwich. The polymers filled with conductive particles were polypropylene filled with carbon black and polyurea filled with aluminum flake. The last system was polyurea filled with both aluminum flake and iron particles.

The purpose of examining the concentration behavior of the solutions was to identify an absorptivity or slope of the dielectric property vs. concentration plot. The intention was to compare the "microwave absorptivity" of individual functional groups and determine those that coupled more with the applied field. The layered structure was chosen to demonstrate the concept of selective heating of dielectric layers in a controlled electric

field. The filled systems were selected to examine percolation and scaling behavior as a function of volume fraction and shape of filler. The iron particles were spherical, with ferromagnetic and dielectric properties, while the aluminum flake was flat and had electrical properties. The carbon black also had only electrical properties. While these were specific goals for each material, the general behavior that unites them is that reflection and absorption properties are governed by a material's dielectric and magnetic values.

To calculate the reflection and absorption properties of materials it is necessary to know their dielectric storage (ε') and loss (ε'') and magnetic storage (μ') and loss (μ'') properties at the frequency of interest (2.45 GHz)[4, 5]. The power of the electromagnetic wave dissipated within a material can be calculated from experimentally derived dielectric and magnetic properties, but these properties cannot be calculated from known chemistries and compositions. To provide insights into how these properties scale with composition, a fundamental analysis was made into how the materials properties (ε', ε'', μ', μ'') change as a function of composition. Knowing the low power dielectric values can assist with high power microwave processing.

Microwave processing of reactive and nonreactive material systems at 2.45 GHz is accomplished by coupling electromagnetic energy through loss mechanisms within the molecular structure. The magnetic and electric dipoles or electrons are forced to oscillate and dissipate their energy with their local environment, generating thermal energy. The heating rate and dielectric loss for nonreactive systems are a function of temperature, frequency, number of dipoles, and their mobility. The heating rate for the reactive systems is more difficult to predict since the number of dipoles and their

chemistry change with time.

Microwave processed liquids are typically in a highly concentrated melt or resin form with many chemistries being used. Thus, a fundamental understanding of how the liquids dielectric properties varied with **concentration, local environment**, and **molecular structure** were determined. The influence of concentration was explored by covering concentrations from 0.0 to 2.6 M using toluene or tetrahydrofuran as solvents. The effect of local environment was examined by using the same small molecules and changing the solvent. Investigation into the influence of chemical structure was made by using the same solvent while changing the small molecules used. To reduce the influence of a spectrum of relaxations, which are encountered in polymers, small molecules are used. Two typical small molecules used for composite and adhesive applications are diglycidyl ether of bisphenol A (DGEBA) and bisphenol A. The frequencies examined were from the kHz to GHz range. The purpose was to examine the ionic and dipolar loss mechanisms. A product of the bisphenol A compounds was a polyhydroxyether that was sandwiched as a 0.002" film between two low loss quartz plates. The purpose was to examine selective heating of thin polymeric films.

The dielectric properties of the poly(amide-imide) were examined vs. temperature, frequency, and time. The dielectric changes vs. temperatures between 20 - 285°C were exaimed to identify the effects of water and the glass transition temperature at the frequencies used. The frequencies used were from the kHz to GHz range. The change in ε'' vs. time was compared to the weight loss of water vs. time as determined by thermogravimetry.

The dielectric and magnetic properties of filled polyurea films (< 0.020") were manipulated by adding aluminum flake and iron particles. The aluminum flake had dielectric properties and the iron had both ferromagnetic and dielectric properties. The volume fraction of these fillers ranged from 0.0 to 0.5 for iron particles, and from 0.0 to 0.3 for aluminum flake. A percolation model was used to explain property vs. volume fraction trends. The theoretical development of connectivity of filler particles vs. volume fraction filler was compared to scanning electron micrographs of the films. The effect of the filler on the initial GHz wave was calculated from measured optical properties to identify one wavelength film thicknesses.

The literature review will provide an explanation and illustration of concepts useful to understanding the following experimental data.

2.2 Literature Review

The determination of the dielectric and magnetic properties is essential for calculating the reflection and absorption properties of a material [4] and for anticipating its microwave processability. It is therefore understandable why much experimentation has been carried out to determine dielectric and magnetic properties of materials [3]. Many methods are used to determine these properties in the GHz frequency region. Waveguide techniques were used for determination of dielectric and magnetic properties at a single frequency, while two coaxial techniques were used to sweep frequency for the solutions and filled systems in this study. Thus, the influence of the above variables as applied to the selected materials will be given below.

2.2.1 Dielectric Loss

Dielectric loss is the ability of an absorbing species to dissipate electromagnetic energy into its local environment. Understanding the fundamentals of how small molecules generate loss in the GHz frequency range can be visualized by focusing on the dipoles. Dipolar loss for dilute solutions of non-associated polar liquids was first correctly modeled by Onsager [6]. An illustration of an Onsager sphere is shown in Figure 2.1a. In the dilute concentration region, the total dielectric loss scales with the concentration of dipoles. Onsager assumed a model of a dipole that occupied a sphere of radius (r), that its polarizability is isotropic, and that its interaction with the surroundings can be described by the polarizing action of its dipole field. The important concept is that the *dipole interacts with its local environment.* This local field was neglected by Debye in his calculations. He explains the assumptions of his derivation on page 10 of his book: Polar Molecules [7]. This local electric field, E_c, exerts a torque on the dipole as described by Equation 2.1:

$$T = |\mu||E_c|\sin\Theta \qquad \text{Eq. 2.1}$$

where: T = torque
μ = dipole moment
E_c = local electric field
Θ = angle between applied field and the dipole.

A magnetic analogy can be constructed for Equation 2.1, where magnetic induction, B, is substituted for, E_c, and a magnetic dipole, m, is substituted for, μ,. The Onsager model is described more completely by von Hippel. The sphere is thought to be filled by a medium of the optical dielectric constant (ε'_a) and surrounded by a continuum of the static dielectric constant (ε'_b). A homogeneous field, E_o, is applied and acts as such at large

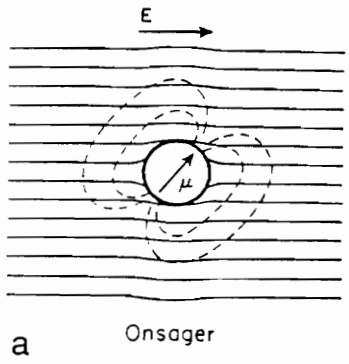

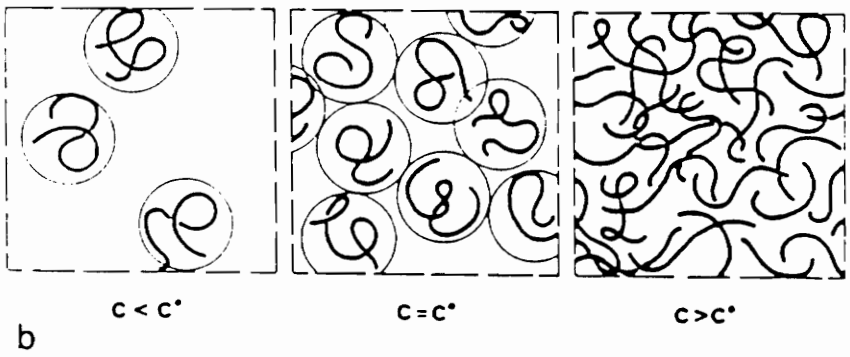

Figure 2.1

a. A schematic of the Onsager cavity [3]; b. A schematic of the influence of concentration on average distance between polymer coils [8].

distance from the sphere. Near the sphere it is distorted by the existence of the cavity; therefore, instead of, E_o, the cavity field, E_c, exercises its torque on the dipole. The dipole in the sphere also polarizes the continuum. This polarization of the surroundings in turn creates, by its free charges, a reaction field, E_{re}, parallel to the dipole itself and the medium in its cavity, but the reaction field turns with the dipole and cannot contribute to the torque. Thus, the Onsager theory introduces two fields: the cavity field, E_c, as the directing field, and the vector sum of the cavity field, E_c, and the reaction field, E_{re}, designated as the internal field, E_i, as the field that induces polarization.

Therefore, solvent, chemistry, and concentration can influence the local electric field. Chemical structure changes the dipole moment of the functionalities present. Solvent influences the local electric field by increasing or decreasing the total electronic interactions with the dipoles. Concentration affects the local electric field, in two ways: first, by changing the static dielectric constant ε_b, and, second, when the dipoles reach a concentration where they become associated.

2.2.2 Concentration

An illustration of how the average distance between polymer coils decreases with increasing concentration is shown in Figure 2.1b. In the dilute region the concentration is low and the molecules are completely surrounded by solvent and do not frequently collide with other polymer molecules. In the transition region the concentration is high enough so that the polymer coils are in contact with another coil. In the concentrated region of Figure 2.1b, the concentration is high enough to prohibit unhindered motion of

the polymer coil. Analogously, an explanation can be made for small molecules in solution. At low concentration the dielectric properties will scale with the number of dipoles per unit volume. After a critical concentration (c*) the dipoles will collide frequently enough to hinder their motion. This slows their characteristic relaxation time, shifting the relaxation to lower frequencies or longer times.

Determining dielectric structure-property relationships can be accomplished with small molecules in solution. The loss due to a specific functionality vs. concentration can be obtained. The response of many small molecules has been tabulated in the book Dielectric Properties of Binary Solutions by Akhadov [9]. The influence of temperature, frequency, and solvent is also shown. The advantage of small molecules compared to polymers is the lack of multiple relaxations that occur with covalently bonded nearest neighbors. Theoretical calculations of nearest neighbor or stereoregularity on dipole moments of polymer coils have been proposed by Marc Mansfield [10].

A review of molecular dielectric analysis of polar liquids has been performed by von Hippel [11]. The influence of intra- and inter-molecular relaxations has been identified for propylene glycol and glycerol. The change in relaxation time as a function of concentration and temperature was investigated for water/ethanol mixtures. The nonlinear relationship between $\Delta\varepsilon$ (Δk) is shown in Figure 2.2. Arthur von Hippel describes the data as follows. They showed that: (a) the relaxation spectrum of the water molecules moves systematically toward lower frequencies(larger relaxation times) with increasing alcohol content of the solutions; the alcohol spectrum at 50°C with increasing water dilution moves toward higher frequencies and then reverses itself; and (b) at low

temperatures these opposing trends lead to a partial overlapping of the two spectral regions; at higher temperatures they remain separate. Complemented by activation energy calculations, the conclusion was that the water structure that formed made dipolar reorientation easier to proceed for water than for ethanol.

The complex relationship between relaxation time, concentration, and temperature for interacting systems is illustrated in Figure 2.2. The response could not have been predicted in advance. Therefore, it is always preferable to obtain the data at the concentration of interest and substantiate it with complementary experiments.

Fundamental dielectric investigations by Kauzman [12] have been done on a wide variety of small molecules and polymers in solution to obtain their activation enthalpy and entropy for motion. Dielectric measurements from the semi-dilute to concentrated regions have been obtained for cis-poly(isoprene) [13]. The variation of the dielectric constant near the liquid-liquid critical point for polystyrene also has been investigated [14]. In addition, poly(phenylacetylenes), polyacrylate, and poly(vinyl carbazole) solutions have been investigated by North, Phillips, and Singh [15-18]. Finally, a study on poly(isoprene) comparing dielectric properties and mean end-to-end polymer distance as a function concentration revealed the different concentration regions and that concentration normalized dielectric data decreased with end-to-end distance [19]. From this research it can be concluded that concentration affects the amount of contact solute molecules have, which changes their mobility or relaxation time.

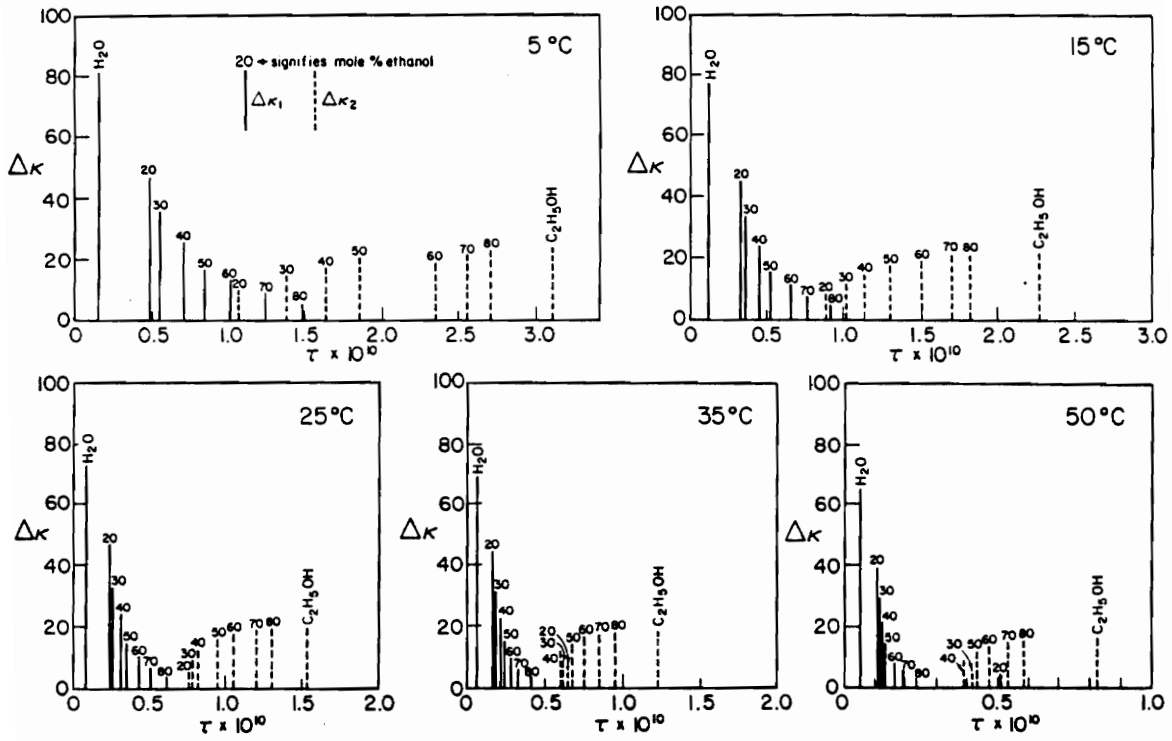

Figure 2.2

Water and ethanol relaxation times as a functon of concentration. $\Delta\varepsilon$ is represented by $\Delta\kappa$[3].

Though not directly related to this work the interested reader may find the following references useful for understanding concentration effects on polymers in solution and melt. The overlap concentration has been investigated dielectrically by Ying and Chu [20]. The theory of entangled solutions has been proposed by De Gennes [21, 22] and Doi and Edwards [23]. De Gennes also has studied polymer-polymer interdiffusion [24]. The influence of molecular weight and molecular weight distribution on polymer-polymer interdiffusion and the viscoelastic properties of polymers have been investigated [25-29]. Also, tracer interdiffusion coefficients of polystyrene in the melt form havw been examined [30].

2.2.3 *Interactions*

The types of interactions that occur between molecules are random dipole-induced dipole, dipole-induced dipole, dipole-dipole, ion-dipole, and hydrogen bonding. The spacially averaged energies of random dipole-induced dipole, dipole-induced dipole, and dipole-dipole energies decrease inversely as distance^6. The average ion-dipole and ion-induced dipole interactions decrease inversely as distance^2 and distance^6, respectively. Ionic interaction energies scale inversely with distance. Hydrogen bonding involves electron sharing between a hydrogen covalently bonded to an electron withdrawing atom and a structure with available donatable electrons. The energies that respond with 1/distance^6 have energies in fraction of a kJ/M range, while hydrogen bonds have energies 10 - 30 kJ/(M of hydrogen bonds). A typical ionic bond like NaCl is 40 kJ/M.

These small scale interactions can be measured by macroscopic measurements and by certain spectroscopies. The enthalpic interactions between small molecules in solution

have been characterized by Fowkes by surface tension measurements [31], NMR [32], and infrared and calorimetric methods [33], along with work by van Oss using surface tension and contact angle measurements [34]. The interested adhesive scientist should be alert to the condition that interactions in solution are only indications of how well a polymer may bond to a surface. According to Fowkes, "The accuracy of predictions of values verifiable by experiment lead one to expect that predictions of unverifiable quantities, such as magnitude of attractive forces at solid-solid interfaces, are to be trusted" [31]. A theory of molecular attractive forces between solids has been proposed by Lifshitz to determine the van der Waals forces between solids [35].

2.2.4 *Frequency and Temperature*

Dielectric structure-property relationships can be identified when a material's dielectric properties are evaluated for a wide frequency region. Figure 2.3 is a schematic of dielectric storage and loss as a function of frequency. Loss occurs when the applied frequency couples with a molecular motion and that energy is dissipated into the surroundings. Dielectric storage occurs when a molecular motion is elastically distorted by an applied electric field.

Starting at low frequencies and proceeding to higher frequencies, the first relaxation is due to interfacial polarization. This occurs at interfaces between conductive and dielectric materials. A relaxation time is an exponential decay of the polarization with time when an externally applied field is removed.

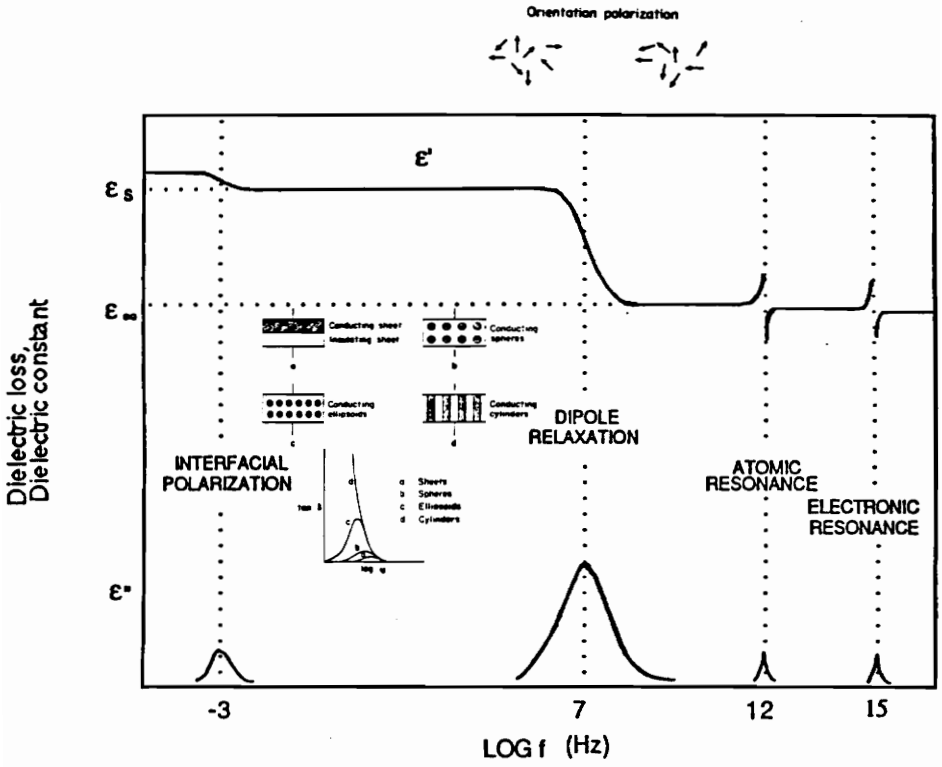

Figure 2.3

Schematic diagram of the dielectric spectra vs. frequency.

The shape of the curve resembles a relaxation as long as the geometry of the conductive material is not continuous, from one plate to the other. Geometries that will produce this dispersion are sheets, spheres, and elipsoids [3]. Conductivity from one capacitor plate to another will produce a ε'' response that varies inversely with frequency, see Equation 2.2. This behavior is illustrated in the insert of Figure 2.3.

$$\varepsilon'' = \sigma/f \qquad \text{Eq. 2.2}$$

Where: σ = conductivity
f = frequency

An explanation of conductive losses in solutions is given by Barrow [36].

Dipolar orientation occurs when applied frequency couples with a permanent dipole within the material. The dipole is forced to oscillate and has friction with its local environment. The dipole relaxation ranges in time from 10^{-12} s for gasses to 10^{-6} s for viscous liquids. In the kHz to MHz frequency region where conductive and dipolar losses can occur simultaneously, the total dielectric loss (ε''_t) is given by Equation 2.3 .

$$\varepsilon''_t = \varepsilon''_{conductive} + \varepsilon''_{dipole} \qquad \text{Eq. 2.3}$$

Substituting for $\varepsilon''_{conductive}$, Equation 2.2, into Equation 2.3 and multiplying by frequency gives Equation 2.4

$$f\varepsilon''_t = f\varepsilon''_{dipole} + \sigma \qquad \text{Eq. 2.4}$$

A plot of $f\varepsilon''_t$ vs. frequency will be linear with the slope proportional to the dipolar losses ε''_{dipole} and the intercept related to conductivity. Much research has been conducted in this frequency region.

Initial work on thermosetting alkyd resins in the 1930's indicated that vitrification was a dielectric event and gelation was not [37]. Also, the influence of conductive ionic impurities was identified [38]. Taylor and Rancourt have investigated the surface and bulk resistivities of polyimides doped with metal ions [39]. Further work has been done by Senturia et al. on epoxy systems [40-47], where they investigated both the conductive and dipolar contributions. A review article summarizes most of their work in this field [48]. Atomic and electronic relaxations occur due to atomic or electronic polarization. The applied electric field will either displace two atoms or an electron cloud from its equilibrium position. These relaxations occur in the infrared and ultra-violet frequency regions.

The relationship between relaxation time and temperature is exponential and given by Equation 2.5:

$$\ln \tau = \Delta H/RT \qquad \text{Eq. 2.5}$$

where: τ = relaxation time
ΔH= activation enthalpy
R = gas constant
T = temperature in degrees K

Thus, an increase in temperature will result in a lowering of the relaxation time, or complementarily, increased thermal agitation increases the frequency of the peak of the dielectric loss curve. For polymer systems relaxations occur for the β transition, glass

transition temperature (T_g), and melting. The amount that relaxations shift with temperature is dependent upon the activation enthalpy for motion. Typically, at the microwave frequencies, these motions have merged to one continuous dispersion. A review of polymeric materials responses to electromagnetic radiation has been written by Pochan and Pai [49]. They consider block copolymers, polymer blends, and identify the influence of absorbed gasses, water, plasticizers, process control, and chemical aging.

2.2.5 *Percolation*

The behavior of the dielectric and magnetic properties to concentration of iron, carbon black, and aluminum flake will be described by percolation theory. This theory deals with effects of varying the number of short-range interconnections within a system. The interconnections are generated in a random manner. The increase in concentration, volume fraction, or density of interconnections eventually leads to long-range connectivity which extends indefinitely far. This transition is called the percolation point. Essentially, percolation is the development of connectivity as a function of volume fraction filler. This is illustrated in Figure 2.4, where S_{av} is the weight average size of a cluster, l_{av} is its average length, p_c is the critical bond fraction necessary to form an infinite cluster, P(p) is the probability of the particle or bond being connected to the infinite cluster, and ($\sigma/\sigma o$) is the normalized conductivity. These are all plotted as a function of the filled bonds (p) for bond percolation on a two dimensional square lattice. The development of S_{av} and P(p) will be described as the number of bonds increases. S_{av} is described by Equation 2.6.

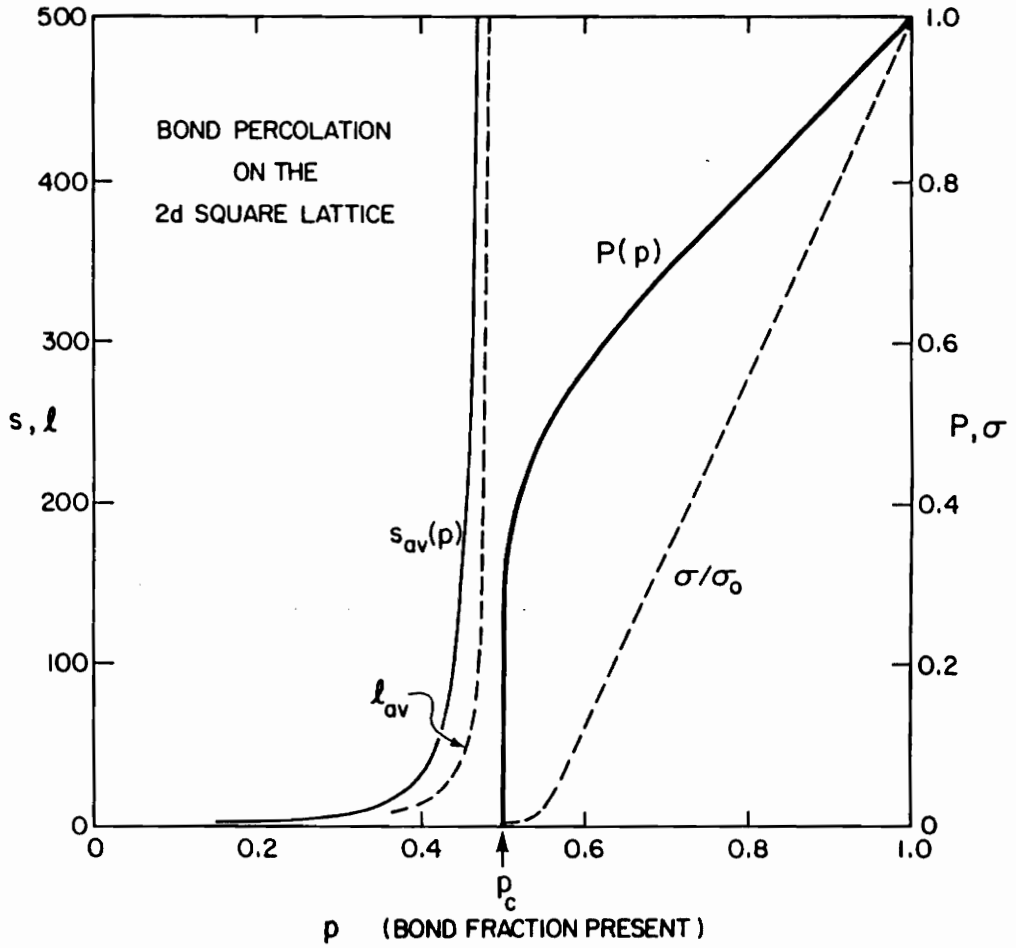

Figure 2.4

The behavior, as a function of the fraction (p) of filled bonds, of key properties that characterize bond percolation on the square lattice in two dimensions [50].

$$S_{av} = \frac{\sum_{s=1}^{s=\infty} n_s s^2}{\sum_{s=1}^{s=\infty} n_s s} \qquad \text{Eq. 2.6}$$

where n_s is the number of clusters of size s. The direct analogy between S_{av} and M_w or weight-average molecular weight of a polymer coil should be recognized. At low bond fractions, S_{av} is dominated by isolated bonds. As the number of bonds is randomly increased, clusters are formed. These clusters grow in size until there is a cluster that extends, without limit in the bulk: i.e., $S_{av} = \infty$. In a two dimensional square lattice with bond percolation, this occurs at 0.5 bond fraction. Thus, 0.5 is p_c, or the critical bond fraction for percolation. The critical bond fraction p_c is a function of dimensionality and lattice type. The formation of an infinite cluster does not mean that all clusters are connected. At p_c the infinite cluster exists alongside clusters of finite size. Above the critical bond fraction for percolation, focus on P(p), the probability of a particle being connected to the infinite cluster. It increases dramatically above p_c and moves steadily toward unity as the bond fraction increases. The response is different for the normalized conductivity σ/σ_o. Conductivity reflects the number of parallel connected pathways present. As clusters become bonded to the infinite cluster, it does not necessarily mean that additional parallel pathways of connectivity from one end to the other have been formed.

The response of conductivity above p_c is shown to have a power law dependence upon fraction of filled bonds or sites $\sigma(p) \sim (p - p_c)^t$. The number t is called a scaling exponent. *The scaling exponent does not depend on the lattice type in a given dimensionality.* For two and three dimensions it has been experimentally determined to

be 1.1 and 1.65, respectively [50]. These values were determined in computer experiments by a site percolation model assuming non-overlapping circles for two dimensions or spheres for three dimensions. The values for the scaling exponent determined by Kirkpatrick are 1 - 1.3 for two dimensions and 1.5 - 1.6 for three dimensions [51, 52].

Their exists a measure of the percolation threshold that is appropriate to filler/binder systems that is insensitive to the details of local geometry. It is called the critical volume fraction (ϕ_c) and was introduced by Scher and Zallen in the context of site percolation processes. With each site we associate a circle of radius equal too half the nearest-neighbor separation, shaded circles for filled sites and open circles for empty sites. Now p is the fraction of shaded circles, the volume fraction is defined as the fraction of space that is taken up by the shaded circles. The relationship between ϕ and p is dictated by geometry: $\phi = vp_c(site)$, where v is the filling factor for the lattice, the fraction of space occupied by all the circles. The critical volume fraction ϕ_c is the value of ϕ that applies at the site percolation threshold: $\phi_c = vp_c(site)$ [50, 53]. The critical volume fraction for percolation is shown to be *insensitive to dimensionality*, and is 0.15 for three dimensions and 0.45 for two dimensions [50, 53]. The critical volume fractions were determined to be 0.25 for two dimensions and 0.5 for three dimensions, assuming critical bond fraction is directly related to volume fraction [14, 51, 52]. The critical volume fraction calculated by modeling will be compared to the critical volume fraction derived graphically from plots of ε'', μ'', and normalized magnetization vs. volume fraction carbon black, iron, and aluminum within a polymer. This comparison is shown in Chapter 2 in Table 2.2 on page 81.

As a function of volume fraction filler, percolation shows the random development of structure from independent particles to clusters, to an infinite cluster and finally to a completely filled system. The identifying traits of a properties vs. volume fraction plot are: one, the critical volume fraction for percolation and two, the scaling above percolation. Some properties like conductivity of a 2 dimensional lattice are 0, while $S_{av} < \infty$ and only develop after p_c. Above p_c there is electrical connectivity within the lattice. The conductivity, above p_c, increases with a power law dependence on volume fraction filler. The scaling exponent and critical volume fraction for conductivity, μ", and magnetic susceptibility will be shown to be modeled by percolation behavior.

The volume fraction instead of mole fraction is the appropriate variable in the percolation equation, because volume fraction is related to interparticle distance. Interparticle distance relative to the communication distance is a physically significant length [54]. Information about average interparticle separation is contained in volume fraction (Φ). The distance, r, between spherical particles of diameter, d, arranged in a cubic array is given in Equation 2.7:

$$r = (\pi/6)^{1/3}\ d\ (\Phi)^{-1/3} \qquad \text{Eq. 2.7}$$

Using for iron particles, d = 6 μm and Φ = 0.2, an average of Zallen's and Kirkpatrick's critical volume fraction points results in an interparticle distance of 8 μm. Though the idealized array does not represent random packing of filler in the films used, the dependence of interparticle distance on volume fraction will be a useful marker when analyzing scanning electron micrographs of these films.

2.2.6 Reflection and Absorption

Figure 2.5 is a schematic of a transverse electromagnetic wave at an air-material boundary. The wave's power is divided into four components: input, reflected, transmitted, and absorbed. Equation 2.8 shows the expanded form of the reflection coefficient which governs the amount of the power reflected. The expanded form of impedence (Z) has been substituted for where $Z = (\mu^*/\varepsilon^*)^{1/2}$. The point of the equation is to illustrate the relationship between material properties and the reflection coefficient. The reflection coefficient can be manipulated by selectively adding conductive, dipolar, or magnetic fillers. The absolute values of the reflection can range from 0 to 1. A reflection coefficient of zero means that impedences are matched and the wave will propagate through the boundary. This implies that the complex permittivity and permeability of materials 1 and 2 are equivalent, which means that their loss and storage values are also equal. A reflection coefficient of 1 means that the impedences are completely mismatched. This can occur with either a short or an open circuit. The high conductivity of a metal can produce an short circuit. This is seen by substituting a large value for ε''. A polymeric substrate would have a $\mu' = 1$ and a $\mu'' = 0$; its dielectric properties are some complex value. Thus, some the energy is transmitted, while the rest is reflected. The transmitted wave propagating through dielectric 2 is attenuated by the loss component. The amount of attenuation will be calculated for a 12.2 cm wave propagating through 0.6 m of dielectric material with $\varepsilon' = 4$ and tan delta 0.02. These calculations are found in Rizzi section 2.6 [55]. The wavelength in the material $\lambda = \lambda o/(\varepsilon')^{1/2}$, where λo is the initial wavelength in meters. Thus, $\lambda = 0.122/4^{1/2} = 6.1 \times 10^{-2}$ m. The attenuation constant $\alpha = (\pi/\lambda)$ tan delta = 1.03 Napier/m. The ratio of amplitudes is given by Equation 2.9 .

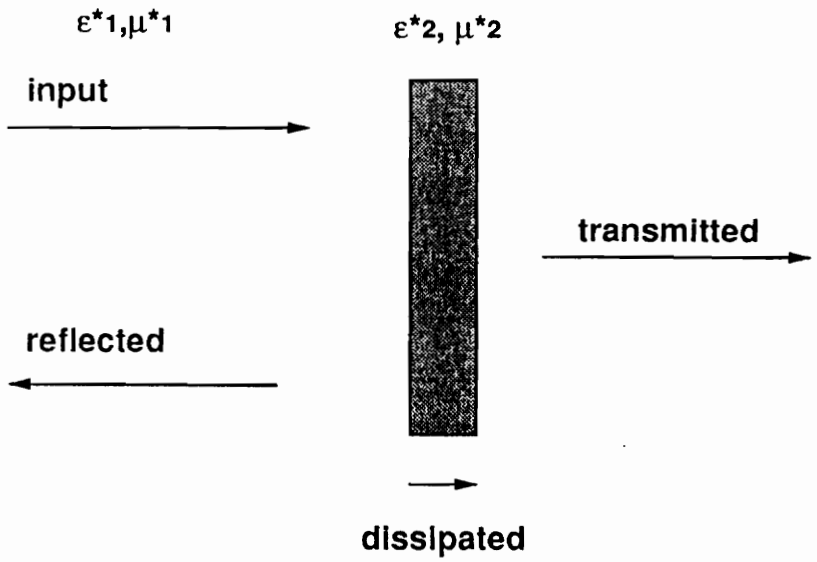

$$\text{Reflection Coefficient} \quad \Gamma = \frac{\left(\frac{\mu'_2 + \mu''_2}{\varepsilon'_2 + \varepsilon''_2}\right) - 1}{\left(\frac{\mu'_2 + \mu''_2}{\varepsilon'_2 + \varepsilon''_2}\right) + 1} \qquad \text{Eq. 2.8}$$

Figure 2.5

Schematic of a transverse electromagnetic wave at an air-material boundary.

$$\frac{Ez = 0.6}{Ez = 0} = e^{-\alpha(0.6)} = 0.539 \qquad \text{Eq. 2.9}$$

The ratio of amplitudes squared is the power ratio. It is 0.29. This means over a distance of 0.6 m the electric field wave has been attenuated 70%. Equation 2.10 is an equivalent attenuation equation for calculating skin depth of the electric field in a good conductor. Typical skin depths are in the micron range:

$$\text{depth} = 1/(\pi\mu\sigma f)^{1/2} \qquad \text{Eq. 2.10}$$

where: f = frequency
μ = permeability
σ = conductivity

The above calculations are helpful in that the processing engineer can visualize the part sizes that can be processed. Microwave processed polymer parts can be approximately 10 - 20 cm thick. The use of a 7" cylindrical cavity, described in Chapter 3, can reduce the amount of reflection by tuning the cavity to match impedences of the cavity and sample, though a filled sample with highly dielectric or magnetic property particles can attenuate the incoming wave within a centimeter as shown in Figure 2.28.

A review of the theory of how materials interact with electromagnetic waves has been compiled by Rizzi [55], Lekner [4], Lederer [56], and Knott [5, 55, 57]. Lekner and Knott also review the structural dependence of the reflection properties of a material. A recent experimental review also has been conducted by researchers at Georgia Tech [58] on a wide range of materials in the GHz frequency region.

For radar absorbent applications, a film coated on a conductive substrate, called a Dallenbach layer (D-layer) is of interest. The theoretical behavior of a D-layer has been reviewed [5, 56]. It is not the same as a typical material-air interface. With the limit of film thickness (d) going to zero it can be shown that the reflection coefficient (R) is only a function of one material property, the magnetic loss (μ''), see Equation 2.11 [54]; where c is the speed of light and w is the angular frequency.

$$\frac{\partial |R|}{\partial d} = -2\frac{w}{c}\mu'' \qquad \text{Eq. 2.11}$$

This is obtained from the derivative of the impedence ratio and reflection coefficient with respect to film thickness, see Appendix 1. Power absorbed is proportional to one minus the reflection coefficient squared. Thus, the amount of electromagnetic energy dissipated for thin D-layer films is related to the magnetic loss. Therefore, reflection and absorption characteristics of dielectric layers less than one wavelength are not only dependent upon (ε', ε'', μ', μ''), but on the overall structure of the material.

2.3 Experimental

2.3.1 Samples and Sample Preparation

The experimental section focuses on sample preparation and instrumentation used to evaluate the samples. The diglycidylether of bisphenol A was recrystallized from the Epon 828 resin and the bisphenol A was used as received; both were dried before use. The structure of diglycidylether of bisphenol A is shown in Figure 2.7 as Epon 828 with n = 0. The diglycidylether of bisphenol A was dried under vacuum at room temperature and the bisphenol A at 70 - 80 °C overnight. Both bisphenol A and diglycidylether of

bisphenol A are shown in Figure 2.7, diglycidylether of bisphenol A is Epon 828 with n equal to 0. Diglycidylehter of bisphenol A was recrystallized by the following procedure. 1100 g of Epon 828 or Dow Der 332 was poured into a 2 l beaker. This was mixed with 450 ml of 2-ethoxyethyl ether and 350 ml of methylisobutyl ketone. The mixture was stirred over low heat for 15 to 20 minutes, until dissolved. It was covered with aluminum foil and placed in a refrigerator for five days. The solution was seeded with purified diclycidylether of bisphenol A. The precipitated crystals were suction filtered and air dried for three to four hours. The crystals were washed with 1 l of cold methanol and air dried. Then they were washed in 2 l of hexanes and air dried. The crystals were put in a 4 l beaker and covered with 3.5 l of hexanes and soaked for five days, with regular stirring. The crystals were suction filtered and vacuum dried. The HPLC grade solvents toluene and tetrahydrofuran were used as received from Fisher Scientific.

2.3.1.1 Poly(amide-imide)

The poly(amide-imide) was solution polymerized in N-methylpyrolidone by a supplier of polymers. The exact synthetic route for the poly(amide-imide) is not known, but typical steps are as follows. A review of poly(amide-imide) synthesis is written in the Encyclopedia of Polymer Science [59]. The starting materials were trimellitic anhydride and 4-4' oxydianiline, possibly in 1 - 5% excess as shown in Figure 2.6. Due to the lower reactivity of aromatic amines compared to aliphatic amines [60] the carboxylic acid group on the trimellitic anhydride was converted to the acid chloride, possibly by PCl_5 or $SOCl_2$. The acid chloride was reacted with the amine at -20 - 0°C to form the amide. Base, possibly triethylamine, was present to scavenge the HCl. The complex, triethylamine hydrogen chloride precipitates from solution. The temperature was raised to room temperature and the amine reacts with the anhydride to form the

amic acid. At the higher temperatures between 150 to 220°C ring closure results in evolution of water. Usually, an azeotroping agent such as toluene or chlorobenzene was used to remove the water. Though the commercial product may not use an azerotroping agent, a chemical one [61] such as, acetic anhydride may be added to react with the water. The reaction was stopped at 95% conversion and the product was collected. The powder was formed and taken through a final cure to temperatures of 260°C resulting in a final Tg of 285°C. The poly(amide-imide) samples were molded into ~0.65 mm sheet, 1.5 mm rod, and 10 mm (0.4") or 13 mm (0.5") balls. Drying was performed under vacuum in a National Appliance Company model 5831 vacuum oven at temperatures from 155 to 165°C from 3 to 24 hours. The curing of the poly(amide-imide) balls was done in a Hewlett Packard model 5890A Gas Chromatography oven preheated to 288°C or a Fisher programmable oven. To monitor the temperature of the balls during isothermal curing, one ball was drilled and a temperature probe placed inside it, as shown in Figure 3.3. The balls were held so their interior temperature was ~280°C for 900 seconds. The full cured sheet or rod was either used as received from the manufacturer or cured in a nine day cure cycle in house. The diameter of the rod used for dielectric measurement was determined by averaging at least 10 measurements, five on each axis. The samples for thermogravimetry were small pieces cut from the poly(amide-imide) sheet weighing between 10 to 15 mg.

2.3.1.2 Polyhydroxyether

The polyhydroxyether was synthesized in a microwave cavity from bisphenol A and the diglycidylether of bisphenol A as shown in Figure 2.7. They were mixed in a 1:1 molar ratio. They were put in a teflon container 3 cm off the cavity bottom. The temperature was monitored by a Luxtron Fluoroptic probe. The input power ranged from 20 -14 W.

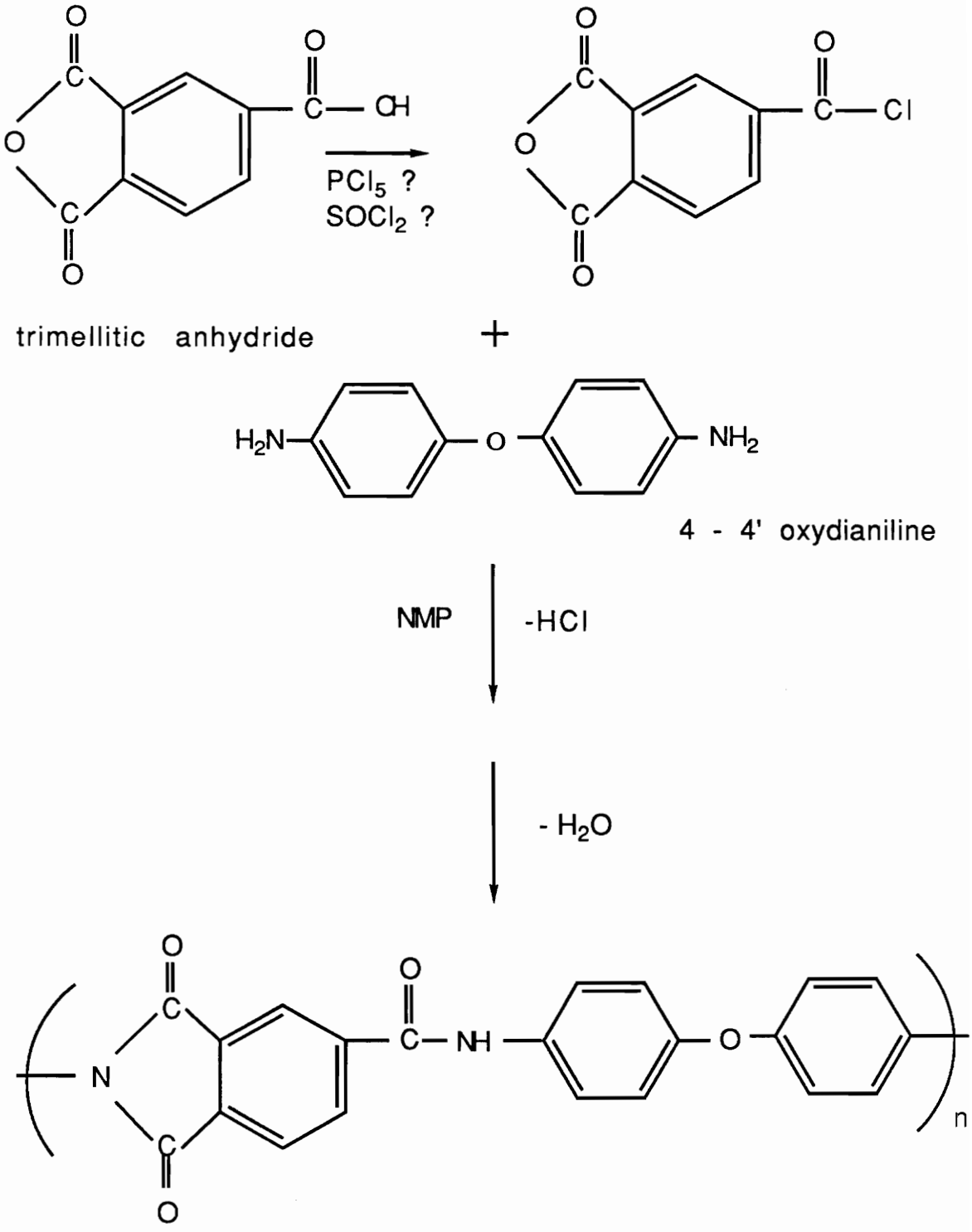

Figure 2.6

Schematic for the synthesis of a poly(amide-imide).

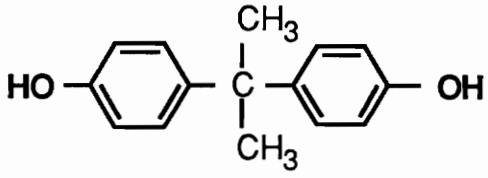

Bisphenol A

+

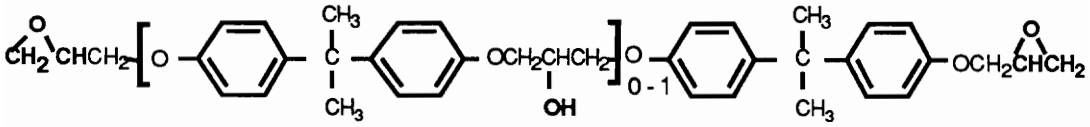

Epon 828

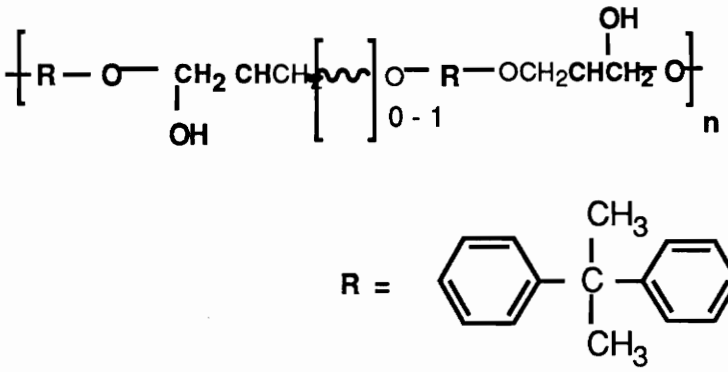

R =

Figure 2.7

Scheme for synthesizing polyhydroxyether from Bisphenol A and Epon 828.

The temperature time profile was 170°C/ 15 min, 200°C/ 5 min, 250°C/ 5 min. The material was cooled and dried in a vacuum oven at ~100°C for several hours until volatiles stopped evolving. The temperatures the monomers were subjected to would not only produce the polyhydroxyether, but also epoxy-epoxy reaction and dehydration of aliphatic hydroxyls ~200°C. The final product was probably a cross linked system. The material formed gell balls in tetrahydrofuran. Its use was for the thin films heated in the microwave cavity. The Tg of the material was determined from the second heat in a DSC as 125°C.

2.3.1.3 Polypropylene Filled with Carbon Black

The polypropylene filled systems were made by weighing different amounts of Kodak (Tenite) polypropylene and AKZO 600JD carbon black. The weights of the carbon black ranged from 0.5 to 3 grams per 50 grams of polypropylene. The samples were blended in a Haake Master Motor 100 melt blender at 204°C and 40 rpm for 10 minutes. The mixed material was then extruded through a 0.07" capillary die at a temperature of 204°C at a plunger rate of 6 cm per minute. The purpose was to make ~0.05" rods for dielectric analysis in the 430 waveguide to be described in section 2.3.2.4. For the volume fraction calculations the density of the carbon black was 0.115 g/cm^3, and the polypropylene was assumed to be 0.9 g/cm^3.

2.3.1.4 Polyurea Films

In this research polyurea films were synthesized by a room temperature polymerization from materials commercially available from Mobay. The polyurea was synthesized from Desmodur E-41, Desmodur Z-4370, and DT. Desmodur E-41 is a cycloaliphatic polyisocyanate based on isophorone diisocyanate. It is a linear prepolymer with 100%

solids. Desmodur Z-4370 is a isocyanurate trimer based on isophorone diisocyanate, which was dissolved in propylene glycolmonomethyl ether acetate and xylene (1:1). It is 70% solids. DT is an alkylated aromatic diamine in a 67% solution of propylene carbonate. DT was reacted with the isocyanate system to form the polyurea. The starting materials were mixed in weight ratios as follows: 170 g E-41, 14.4 g Z-4370, 20.2 g DT. The prepolymer system was weighed so a predetermined amount of solids was available in 200, 175, or 150 grams and mixed with the appropriate amount of aluminum or iron. An illustration of the starting materials used in the reaction are shown in Figure 2.8. The aluminum flake paste was a Reynolds product 6-334 with 79 - 85% solids. These were flakes ~10 microns in diameter and less than 1 micron thick. The iron particles were GAF CIP type E. They were spherical particles ~5 microns in diameter.

Polyurea films were prepared by spraying a mixture of unreacted starting materials, aluminum flake, and iron with methylethylketone as a solvent. The mixture was sprayed on 0.016" aluminum foil. The aluminum was sprayed with Teflon® so it could be peeled off and analyzed for (ε', ε'', μ', μ''). The films were allowed to air dry for 24 hours.

The volume fractions (Φ) for the polyurea filled systems were determined by using the general volume fraction equation, Equation 2.12

$$\Phi_a = \frac{V_a}{V_a + V_b + V_c} \qquad \text{Eq. 2.12}$$

where: V_a, V_b, or V_c equal either the volume of the polymer, aluminum flake, or the iron. The volumes were determined from density and mass values, volume =

Isophorone Diisocyanate

Desmodur E-41

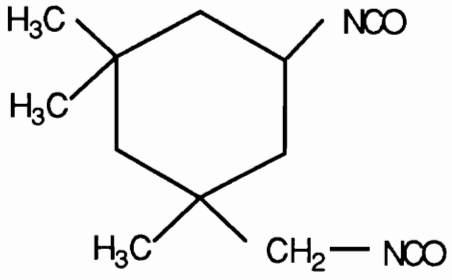

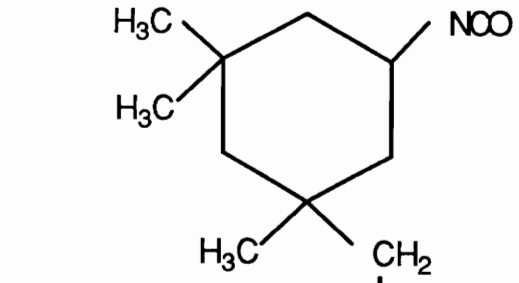

+

Isocyanurate Trimer of
Isophorone Diisocyanate

Desmodur Z-4370

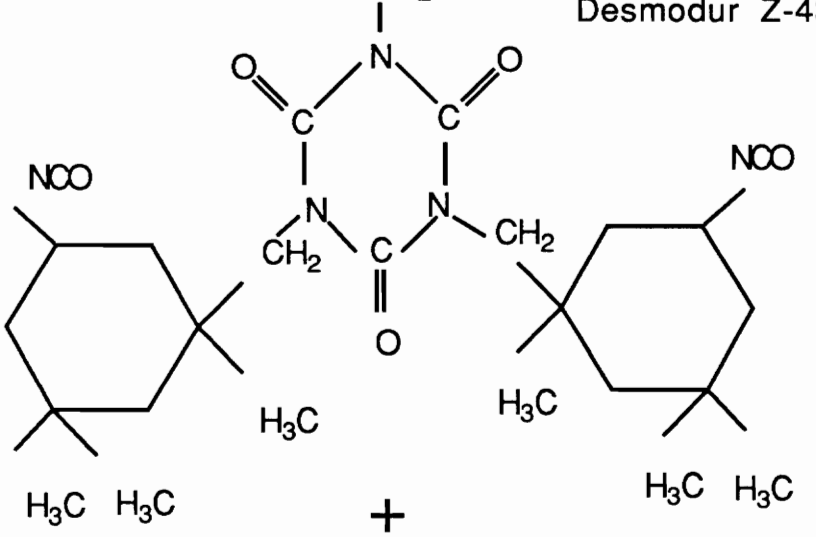

+

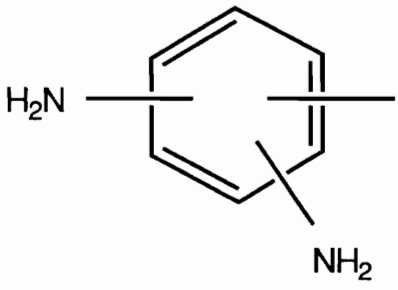

Alkylated Aromatic Diamine

DT

Figure 2.8

Starting materials for polyurea films.

mass/density. The densities used were: polymer-1.15 g/cm^3, iron-7 g/cm^3; and aluminum-2.7 g/cm^3. There were also two batches of aluminum paste used , one had 85% solids, while the old batch had 79% solids.

2.3.2 *Instrumentation*

2.3.2.1 Thermogravimetry/Differential Scanning Calorimetry

Thermogravimetry and differential scanning calorimetry was TA Instruments Thermal Analyst 2100 computer connected to a 951 Thermogravimetric Analyzer, a 912 Differential Scanning Calorimeter, or a 953 Dynamic Mechanical Analyzer. These were used in either sweep temperature or isothermal modes. The software provided with the instrument was used to evaluate total weight loss at any given temperature or time.

2.3.2.2 Thermogravimetry-Mass Spectroscopy

Thermogravimetry-Mass Spectral (TG-MS) analysis was done with a Perkin Elmer TAS 2 TGA connected by a capillary transfer line to a Hewlett Packard mass selective detector. A heating rate of 40°C/min was used so the volatiles would desorb rapidly from the sample. Helium, at a pressure of 40 psi was used as a carrier gas.

2.3.2.3 Dielectric Analysis by Parallel Plates

The room temperature dielectric analysis for solutions of bisphenol A compounds was done on a parallel plate system. The parallel plate dielectric measurements were taken on a 3" diameter micrometer controlled attachment with a guard ring to reduce fringing fields. This was coaxially connected to a Wayne Kerr bridge. The frequency range with the least noise was used from 1 to 100 kHz, with 1 V applied across the electrodes with a

minimum of 100 pf capacitance. The data were collected on a Hewlett Packard model 84 controller.

2.3.2.4 Dielectric Analysis at 2.45 GHz

The dielectric thermal analysis for solutions and the poly(amide-imide) were done by a cavity perturbation technique at a single frequency at 2.45 GHz in a WR 430 waveguide. A shift in resonant frequency relative to the empty cavity was related to a change of ε', Equation 2.12 and a shift in cavity Q compared to the unfilled cavity was related to ε'' Equation 2.13. The Q and resonant frequency values were obtained from a Hewlett Packard 8510 Network analyzer and manipulated on Hewlett Packard hardware and in-house designed software. The temperature was controlled by blowing nitrogen through a heated sand bath and passing it around the sample, which was contained within a Teflon® tube.

Figure 2.9a is a block diagram illustrating the arrangement of the experimental apparatus used for determining ε', ε'' vs. temperature for the poly(amide-imide) rod. The same system without the heating mechanism was used for determining dielectric properties of the bisphenol A solutions. A specialized waveguide cavity was constructed to perform these measurements. Figure 2.9b shows a cross-sectional view of the rectangular cavity (largely magnifying the sample compartment) and the placement of the sample. A one-port rectangular cavity was resonated in the TE103 mode. The cavity was made out of brass WR-130 waveguide with a sliding short

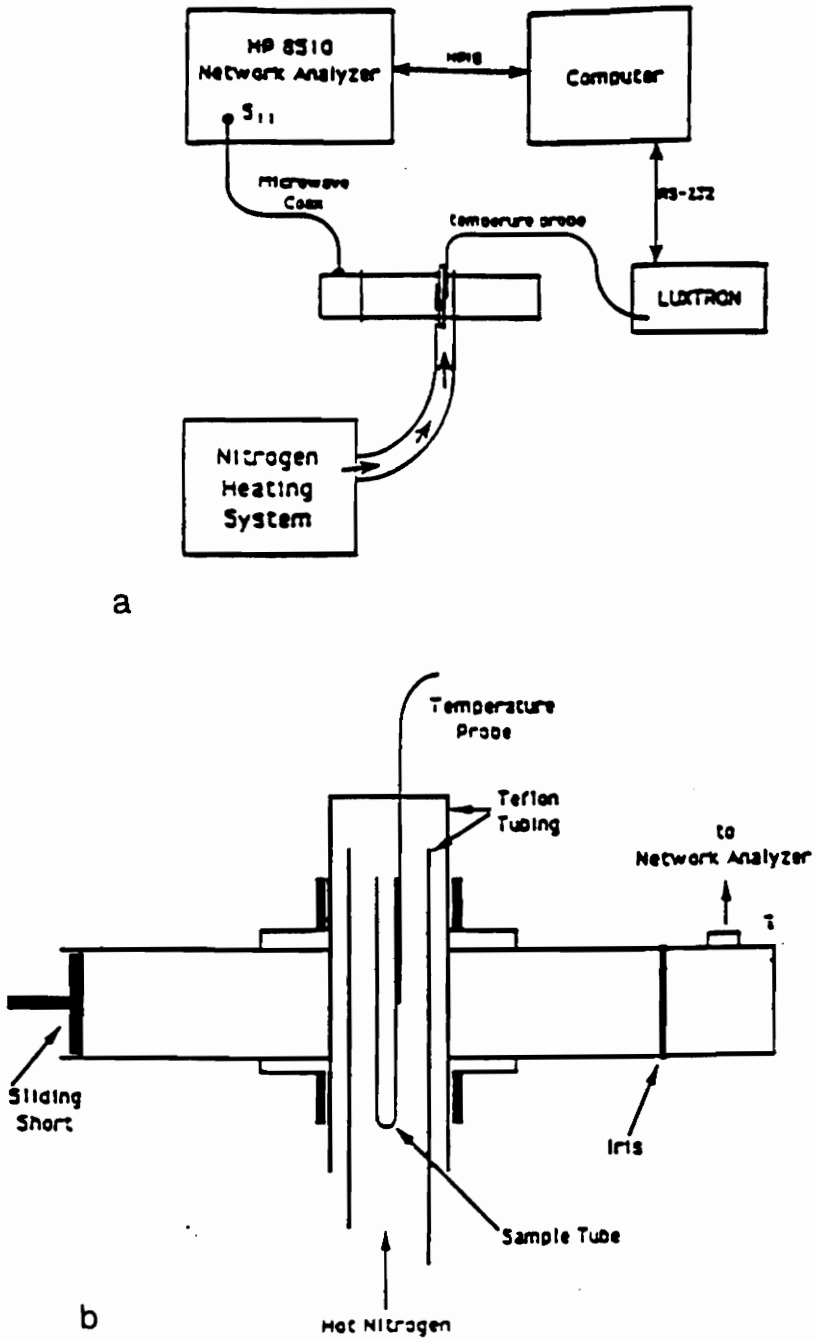

Figure 2.9

a. A schematic of experimental arrangement of dielectric measurements on solutions and poly(amide-imide) rod; b. A cross-sectional view of the microwave cavity with magnified sample compartment

terminating one end, and the input coupled to the network analyzer via an inductive iris. The waveguide was modified, top and bottom, with the addition of a shorted radial transmission line in combination with a one inch long circular waveguide to minimize the effects of the 7/16" diameter hole. The hole permits sample insertion and the introduction of hot nitrogen for thermal heating.

The temperature of the sample was monitored via a Luxtron model 750 fluoroptic probe in all experiments. The temperature of the N_2 gas was controlled by a gas flow rate and the settings on a Techne Fluidised Bath SBL-1 through which the gas was circulated. The nitrogen gas passed around the sample twice; first by the inner wall, then by the outer wall of the Teflon® tubing, to minimize any temperature gradients along the sample. Temperature gradients have been measured to be less than 3°C inside the cavity.

The complex dielectric constant, $\varepsilon^* = \varepsilon' + j\varepsilon''$, was measured using a cavity perturbation technique [62]. The geometry of the cavity in combination with the particular electromagnetic field mode (TE103) determined the resonant frequency and the Q of a particular cavity. The cavity Q was a measure of the energy losses that exist in the cavity. The cavity perturbation technique assumes that the introduction of the sample into a resonant cavity causes a small perturbation in the fields inside. Perturbations in the electromagnetic fields can be sensed by measurements of the resonant frequency and Q, assuming the cavity dimensions are constant. Thus, to determine the dielectric storage and loss both the resonant frequency and Q were measured. The dielectric storage is related to the resonant frequency, while the dielectric loss was related to the cavity Q. The theory for deriving values of dielectric constant from changes in the resonant frequency and Q is well developed [62]. It should

be pointed out that the power input into the cavity for the purpose of dielectric measurement is less than 10 mW. This is at least 2 or 3 orders of magnitude smaller than the power necessary to actually cure the sample.

Using a Hewlett-Packard 5810 Vector Network Analyzer under computer control, a sweep was made of frequency and the input reflection coefficient was measured. When the sweep was completed, the coefficients were transferred to the computer. There, they were processed to derive the resonant frequency and the Q. Then the sample was introduced into the cavity in the case of the poly(amide-imide) rod, and the resonant frequency and Q were measured again. For the solutions an empty 5 mm NMR tube was placed in the cavity as the reference and then the solution in the NMR tube was introduced as the sample. With this information ε', ε'' were calculated using the following Equations: 2.12 and 2.13:

$$\varepsilon' = 1 + \frac{1(\omega_0 - \omega_s)\, V_{cav}}{2\,\omega_0\, V_{sam}} \qquad \text{Eq. 2.12}$$

$$\varepsilon'' = \frac{1}{4}\left(\frac{1}{Q_0} - \frac{1}{Q_s}\right)\frac{V_{cav}}{V_{sam}} \qquad \text{Eq. 2.13}$$

where:
- ε' = the real part of the dielectric constant
- ε'' = the imaginary part of the dielectric constant
- ω_0 = resonant frequency of the empty cavity
- ω_s = resonant frequency of the perturbed cavity
- Q_0 = Q of the empty cavity
- Q_s = Q of the perturbed cavity
- V_{cav} = volume of the cavity
- V_{sam} = volume of the sample

In summary, first the cavity was calibrated. Then, for the solutions, an empty NMR

tube without the Teflon® tube heating system, was placed in the cavity; or for the poly(amide-imide) rod the Teflon® tube heating system was used and brought to the desired temperature. The system began by measuring the "empty cavity" approximately 22 times and calculated the resonant frequency and average Q. These average values of the "empty cavity" were remeasured at each temperature. The system then waits so the sample can be added to the cavity. The experiment continued by first measuring the temperature and then immediately the dielectric constant in the manner described above. This process takes approximately seven seconds. Approximately six measurements were made and averaged at each temperature.

2.3.2.5 Dielectric Measurements with Microwave Cure

Combined microwave cure and measurement of the complex dielectric constant were carried out using the experimental set-up shown in Figure 2.10. The microwaves were generated by a Raytheon Microwave Power Generator model PGM-10X1 operating at a nominal frequency of 2.45 GHZ. Using a coaxial cable, the source was connected to an isolator consisting of the circulator and dummy load 1. The isolator prevents any reflected power from damaging the source, and was connected directly to a 20 dB directional coupler arrangement. The coupler, attenuators, and Hewlett-Packard 435B power meters permit the transmitted and reflected power to be monitored. The output of the directional coupler was connected to switch (S1) via coaxial cable. S1 and S2 were Narda SEM123D RF coaxial switches connected via a one inch section of semi-rigid coaxial cable. This circuit eliminates the possibility of applying high power radiation to the front-end of the NA whose maximum input was 100 mW. The same cavity previously described was used. The switches alternatively attach the network analyzer to the cavity to make a dielectric constant measurement and then connect the high

powered microwave source to perform curing during the wait periods between dielectric constant measurements. The temperature of the sample was preset and held constant by the computer. S1 and S2 were used selectively to direct the microwave power to enter the cavity or direct the power to the dummy load 2. The experiment was simply a modification of the experiment that measured the dielectric constant Feedback from the fluoroptic thermometer to the computer initiates control of the switches. The variation in the sample temperature remains within ±1°C. The fluoroptic thermometer supplies a temperature measurement to the computer every 0.4 seconds. Thus, the shortest pulse of microwave energy would be 0.4 seconds, given that the computer supplied microwave energy to the sample and then immediately decided to remove it after receiving the next temperature update. This was not typically the case. The power applied to the cavity was approximately 20 W or less in all of these experiments.

2.3.2.6 7" Cylindrical Cavity for Microwave Processing

The 7" cylindrical cavity applicator shown schematically in Figure 2.11 was used to study the processing of 0.5" and 0.4" poly(amide-imide) balls. The 7" cylindrical cavity was designed and constructed by researchers at Michigan State University. The design of the cavity is described in a master's thesis by Bill Manring [63], and applications to polymer processing are noted in a dissertation by Jinder Jow [64]. A description of the cavity and microwave circuit follows, along with some empty cavity diagnostics.

The microwave cavity has a 7" internal diameter. It consists of a section of circular brass waveguide with shorting plates on either end that are perpendicular to the waveguide axis. The bottom shorting plate is removable for sample insertion, while the

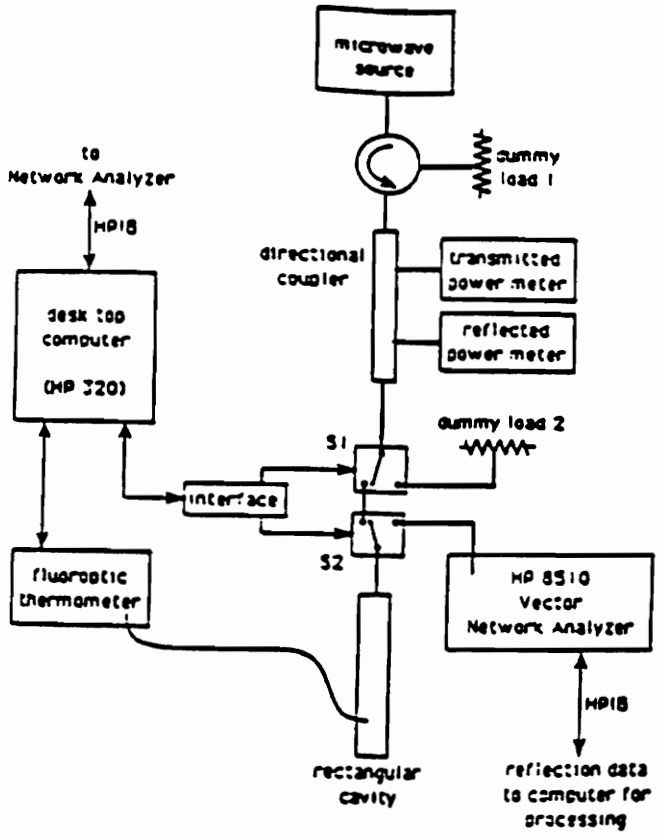

Figure 2.10

Experimental arrangement for combined microwave cure and measurement of the complex dielectric constant.

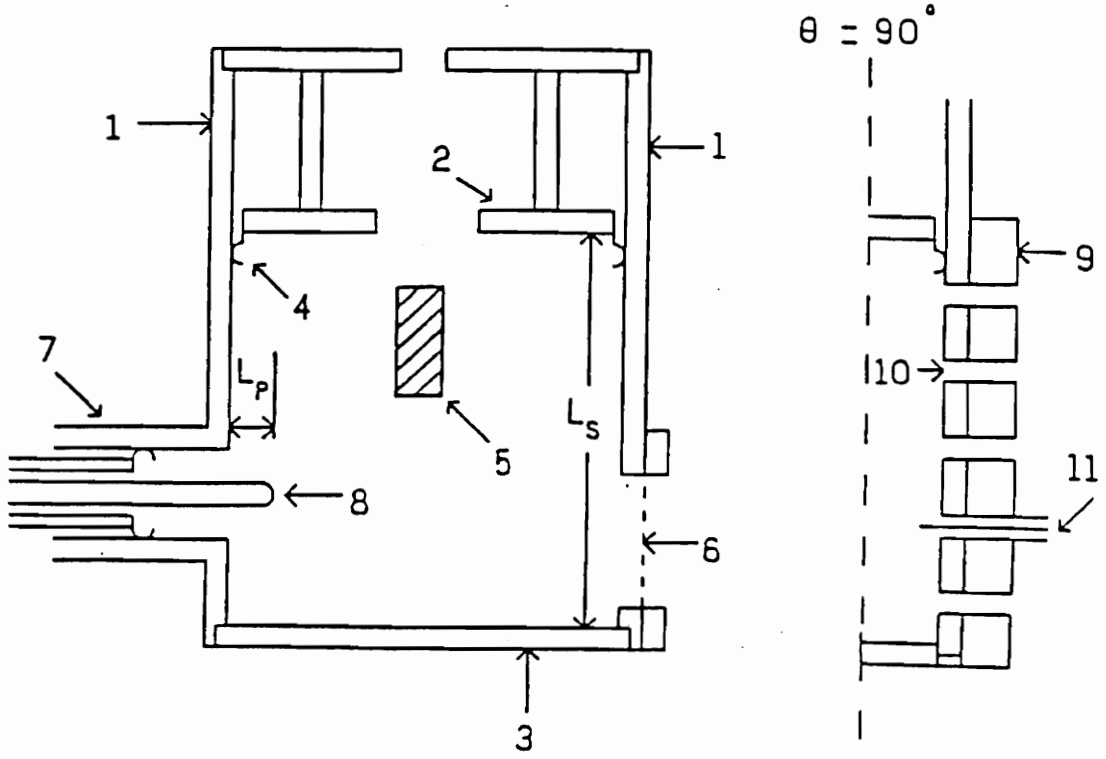

Figure 2.11

Cross-sectional view of a cylindrical cavity. Full cross-section is the $\Theta = 0$ plane passing through the input probe. Partial cross-section $1\Theta = 90$ displays the microcoaxial inputs. The numbered pieces are: (1) conducting cylindrical shell, (2) sliding short, (3) end plate, (4) silver finger stock, (5) process material, (6) screened viewing port, (7) coaxial input port, (8) adjustable coupling probe, (9) brass microcoaxial probe holder, (10) daignostic holes, and (11) microcoaxial electric field probe. [65].

top plate or sliding short is adjustable. The sliding short has a three inch long 3/4" internal diameter cut-off to reduce electric field leakage through the top. The hole in the top was used for insertion of the fluoroptic temperature probe.

To couple energy into the cavity, a 50 ohm coaxial transmission system was connected perpendicular to the circular surface. Its location was 1/4 wavelength above the bottom surface to excite the four lowest modes in the cavity. The lowest (or TE_{111}) mode was used and its field pattern is shown in Figure 2.12. The theoretical height of the sliding short is 6.69 cm for the empty cavity. This field pattern has planar electric fields and was appropriate for processing both disks and spheres. The choice of field patterns must match the geometry of the part. The electric field lines should be primarily tangential to the part surface.

The cavity wall has a diagnostic window through which to view the sample. The window was covered with a brass screen to contain the electric field. At 90 degrees to the incoming probe are several diagnostic ports. They are axially located and large enough for a 2 mm copper microcoaxial E-field probe. This diagnostic probe has only a very small inner-conductor depth, so that the electric field was detectable and essentially undisturbed. The E-field probe was inserted into the holes after the cavity was brought into resonance, and the electric field strength at the wall was determined as a function of location. The field strength at the wall for the TE_{111} mode should be semicircular or a maximum in strength at the middle of the cavity height. This was an analytical technique used to diagnose whether the correct mode was chosen and whether the cavity was working correctly.

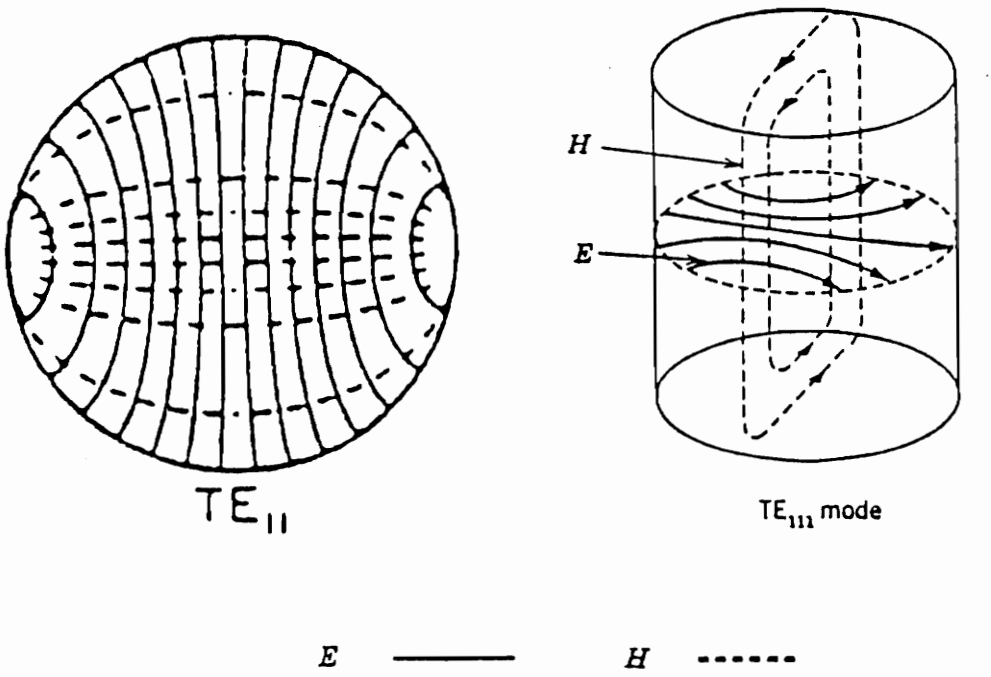

TE_{11} field distribution for a circular waveguide.

TE_{111} field distribution for a cylindrical cavity.

Figure 2.12

Figure 2.12a field lines for two-dimensional TE_{11} mode and Figure 2.12b three dimensional TE_{111} mode. The location of the 50 ohm coaxial probe for the TE_{11} mode would be at the bottom of the Figure. 2.12a.

2.3.2.6.1 Diagnostics on 7" Cylindrical Cavity

Three diagnostic techniques were utilized to characterize the empty cavity in the TE_{111} mode. One was the power at the wall, the second was a frequency vs. reflected power sweep, and the third was the cavity Q. The power at the wall and the frequency sweep are shown in Figures 2.13a and b. Together they show that there are two resonances around the TE_{111} region. The frequency sweep shows two peaks. The first one produced the low electric field at the wall, while the second one produced the high electric field at the wall. Locating the second resonance was accomplished only by increasing the depth of the incoming coaxial probe by a few thousandths of an inch from the zero position and adjusting the sliding short by a lesser distance. A qualitative method to externally monitor the different resonances was used by watching the reflected power go to zero. The first resonance results in a reflected power 5 - 10% of maximum reflected power, while the second resonance makes the reflected power go to zero.

The cavity Q_u (unloaded) is a measure of the ratio of the energy stored in the cavity electromagnetic fields per unit time to the energy lost in the cavity walls per unit time. It is a measure of the strength of the fields inside the cavity relative to the amount of power coupled into the cavity. The measurement of the cavity quality factor Q_u is done indirectly by measuring Q loaded (Q_l). The relationship between Q_l and Q_u when the cavity is critically coupled is given in Equation 2.14:

$$Q_u = 2Q_l \qquad \text{Eq. 2.14}$$

Q_l is obtained from the frequency spectrum of the circuit. Q_l is given in Equation 2.15.

$$Q_l = f_o/\Delta f \qquad \text{Eq. 2.15}$$

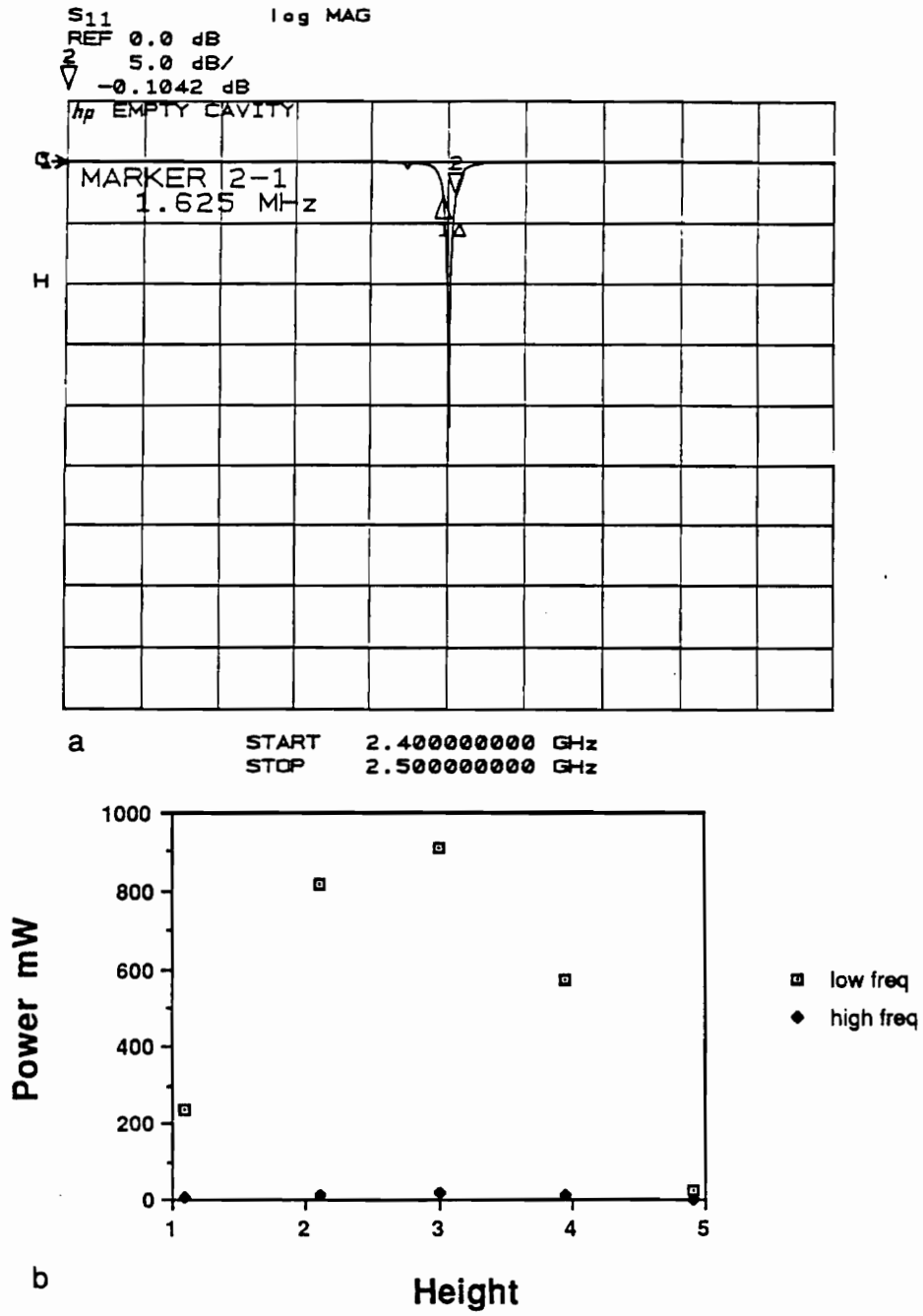

Figure 2.13

a. Reflected power vs. frequency sweep; b. Relative power vs. axial position plot for the two peaks in (a).

where f_o is the resonant frequency and Δf is the half power bandwidth of the experimental power absorption curve. The Q_u values for a cleaned cavity with new finger stock was ~6200. Values significantly lower than that indicated something was electrically incorrect about the cavity.

2.3.2.7 Open Coaxial Technique

An open coaxial technique was used to sweep frequency from 0.045 to 20 GHz for the solutions. The theory was initially described by Somlo [66], Bussey [67], and also reviewed by Stuchley [68]. Applications to biomaterials are described in the following papers [69-77]. The temperature of the solutions was controlled by placing each solution in a temperature bath.

2.3.2.8 Waveguide for Heating Bisphenol Solutions

The high power heating of the solutions was done in a rectangular waveguide in the transmission mode, described elsewhere [78]. Six millileters of solution were put in a Teflon® container in the same location within the waveguide. The power was turned on and the temperature recorded. The temperature was monitored by a Luxtron 750 fluoroptic system.

2.3.2.9 Coaxial Transmission Line

The measurements of (ε', ε'', μ', μ'') for the filled polyurea films were done with a 3 cm long coaxial transmission line, with doughnut shaped films 14 mm O.D. and 1.3 mm I.D, from 0.4 to 1.15 mm thick. One edge of the film was flush with the reference plane. The coaxial airline was coaxially connected to a Hewlett Packard 8510T Network Analyzer. The analyzer monitors voltage ratios by a two-port method the (ε', ε'', μ', μ'') are a

function of the ratios. The relationship between these ratios and the measured properties was explained in the Hewlett Packard Technical Note [79]. The frequency range covered was 0.5 GHz to 10.5 GHz. Only the results for 2.5 GHz are reported. The single decade in frequency covered in these measurements was insufficient to provide mechanistic information.

2.3.2.10 Scanning Electron Microscopy

The images of the poly(amide-imide) balls and iron and aluminum filled films were obtained on an ISI SX 40 scanning electron microscope (SEM). The machine was operated at 10 KV and 1000 X magnification. The polyurea filled samples were cut from large sections; two pieces were cut. One was placed flat on the sample mount and the other was placed at 90°. They were adhered to the SEM mount with two sided sticky tape. In this way, edge and surface pictures could be obtained. The samples were gold sputtered for 2 minutes in a Edwards model S150B sputter coater. The poly(amide-imide) balls had to have silver paint applied at the base to insure electrical contact from the surface of the sample to the mount.

2.4 Ionic Conductivity 0.1 - 100 kHz

2.4.1 Results

The dielectric properties as a function of chemistry, bisphenol A and diglycidylether of bisphenol A solutions in tetrahydrofuran or toluene were determined as a function of frequency 1-100 kHz and concentration 0 - 0.8 M. The plot of tan delta as a function of concentration are shown in Figure 2.14. This revealed that there was a linear relationship between tan delta at 100kHz and concentration in the bisphenol A

compounds, though each slope was different. The bisphenol A in tetrahydrofuran was highest, 0.07 ± .002, the diglycidylether of bisphenol A in tetrahydrofuran was lower value of 0.03 ± 0.02, but near Epon 828 in toluene, which had a value of 0.04 ± 0.004. The nature of the loss mechanism was not identified until plots of log ε" were plotted against log frequency for 0.4 M Epon 828 in toluene or tetrahydrofuran. Tan delta (ε"/ε') was assumed to be directly related to ε". This was shown in Figure 2.15a. A slope of -1 was obtained. Dipolar and conductive contributions can be determined by plots of ε"f vs. f shown in Figure 2.15b. The slope was related to the dipolar contribution and the intercept was related to the conductive contributions, Equation 2.4. Figure 2.15b is a plot of ε"f vs. f for 0.0402 M bisphenol A in tetrahydrofuran has a slope of essentially 0 and an intercept of 2990.

2.4.2 Discussion

Simply because linear relationships were obtained with addition of a bisphenol A compound does not necessarily mean it was the structure of that compound that was influencing the dielectric properties. Figure 2.15a reveals conclusively by a slope of minus1 that the losses were conductive. Figure 2.15b is a plot related to equation 2.4. The figure reveals from a slope of zero that there were no dipolar contributions. Conductive losses in liquids at these frequencies have been shown by Kienle [37], Whitehead [38], and Senturia [48]. The identification of ionic conductivity is important in the interpretation of dielectric spectra of polymeric systems. The frequencies between 1 - 100 kHz are similar to the ones used for dielectric analysis of polymers. Whenever there is a continuous or

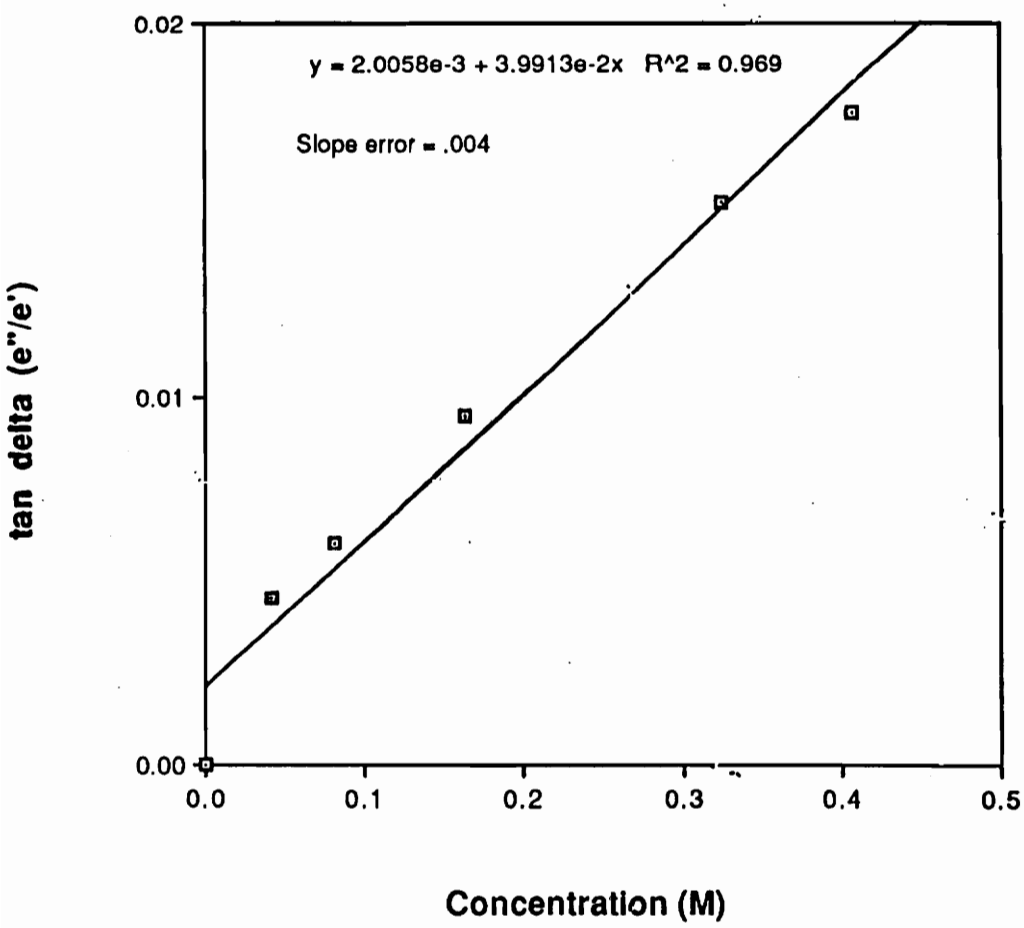

Figure 2.14

A plot of tan delta vs. concentration for Epon 828 in toluene.

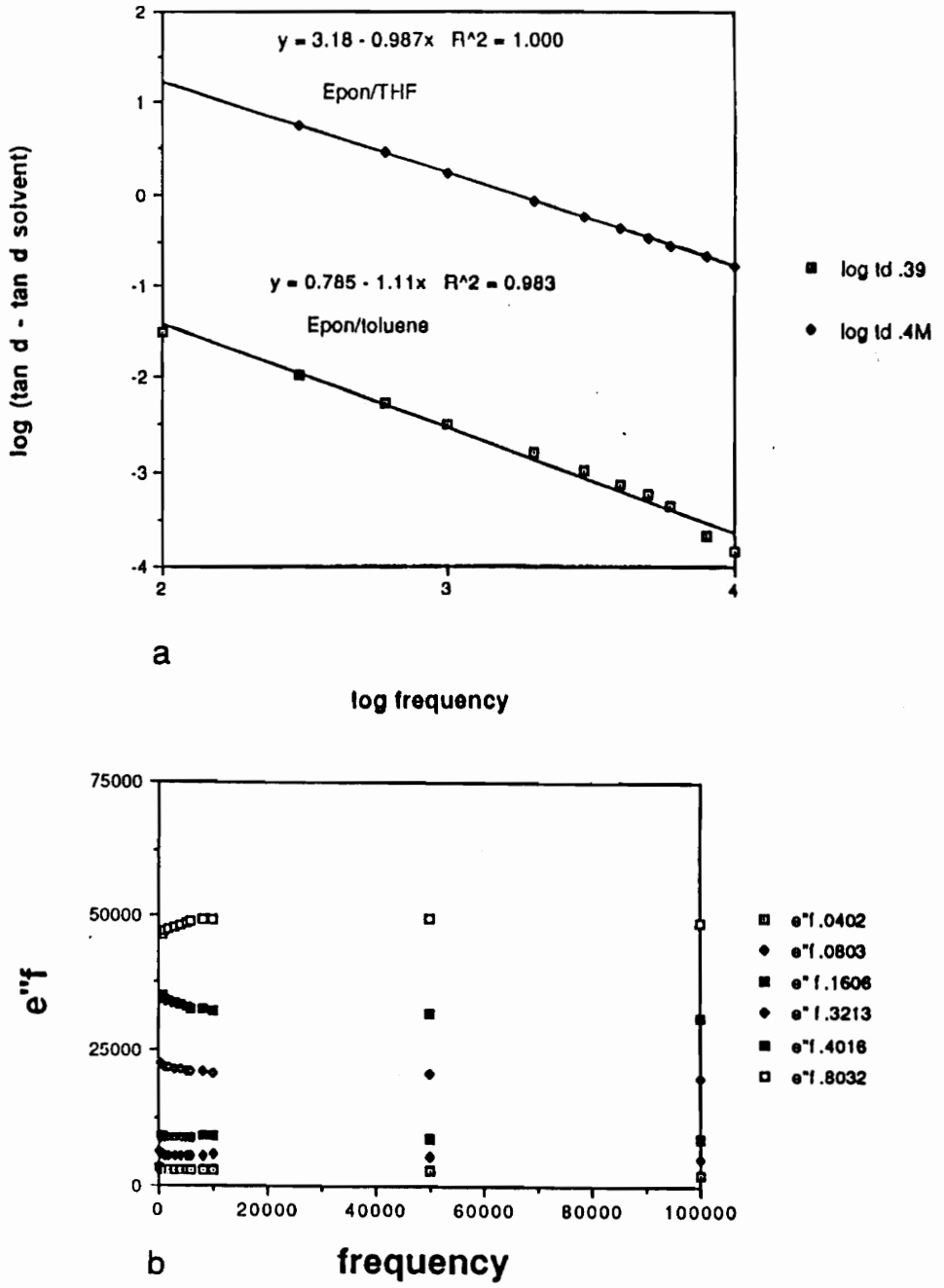

Figure 2.15

a. A plot of log ε" vs. log frequency for 0.4 M Epon 828 in toluene or tetrahydrofuran. A slope of -1 means the loss mechanism is totally conductive. b. A plot of ε"f vs. f for DGEBA in THF the slope is related to dipolar losses and the intercept is related to the other losses.

isolated region of liquid polymer, ionic conductivity effects the loss. This can occur when a polymer is on the liquidus side of its glass transition temperature. An example would be when a partially cured thermoset is heated through its Tg and becomes liquid or rubber-like. The conductivity can be seen in the multi-frequency spectra by a decrease in loss with increasing frequency [48][49].

The influence of solvent on tan delta was demonstrated by comparing the slopes of the lines for Epon 828 in tetrahydrofuran and toluene. The loss occurs from the energy loss of migrating ions to their local environment. The tetrahydrofuran causes much higher conductive losses than toluene. This could possibly be from the increased interaction of the tetrahydrofuran dipole with the ions than toluene. The relationships for the slope of the bisphenol A in tetrahydrofuran being higher than diglycidylether of bisphenol A was merely fortuitous, because the concentration and type of ions were not known to make an accurate comparison.

2.4.3 Conclusions

Ionic conductivity dominates the loss mechanism for the bisphenol A compounds at frequencies from 1 to 100 kHz and concentrations from 0 to 0.8 M solutions. It has been graphically determined that there was no dipolar contribution at these frequencies and concentrations. Changing the solvent from tetrahydrofuran to toluene increases the tan delta for Epon 828 solutions by two orders of magnitude. The trends seen for Epon 828 were representative of the other bisphenol solutions.

2.5 Dielectric Thermal Analysis of Bisphenol A Solutions at 2.45 GHz

2.5.1 Results

Figure 2.16 shows (ε', ε") vs. concentration for bisphenol A in tetrahydrofuran. Two distinct concentration regions were identified. In Region 1 dielectric loss scaled linearly with the number of dipoles. In Region 2 the dielectric loss does not scale linearly with concentration. At the transition between Region 1 and Region 2 a critical concentration ~1.2 M was observed. All three solutions showed similar trends. A lest squared fit to the data in Region 1 was used to compare the lines. The Region 1 values are tabulated in Table 2.1 for dielectric loss per mole and heating rate per mole. The heating rates were obtained from temperature vs. time plots for a series of solutions at different concentrations. The electromagnetic energy was applied in a 280 rectangular waveguide at 2.45 GHz.

2.5.2 Discussion

The slope of Region 1, which has units of ε"/M, will be used to compare the solutions. The value obtained from the linear regions of for diglycidylether of bisphenol A in tetrahydrofuran was 0.86 ± 0.03 ε"/M. Diglycidylether of bisphenol A in toluene has an initial slope of 0.53 ± 0.06 ε"/M and the critical concentration has shifted to a higher value of 2 M. The values for slope and critical concentration of bisphenol A in tetrahydrofuran, from Figure 2.16, were 1.15 ± 0.05 ε"/M, and the critical concentration has decreased to 1 M. This shows the influence of chemistry upon the dielectric loss per mole and critical concentration. This correlates well to the slope of the heating rates as a function of concentration (dT/dt)/M. The slope of the (dT/dt)/M of diglycidylether of bisphenol A in toluene was 0.114 ± 0.003 and diglycidylether of

bisphenol A in THF was 0.09. The (dT/dt)/M for bisphenol A in tetrahydrofuran was 0.143 ± 0.002. A possible reason for the (dT/dt)/M and for diglycidylether of bisphenol A in THF and toluene not matching the ε"/M values is that the THF has a higher dielectric constant then toluene, which would cause a higher reflection coffecient at the THF/air boundry then the toluene/air. Thus, more energy could penetrate into the toluene solutions resulting in higher energy dissipation and higher (dT/dt)/M.

The speculated reason for the critical concentration was that the dipoles reach a concentration where they interact with each other, Figure 2.1b, thus lowering their relaxation time and shifting it away from the 2.45 GHz measurement frequency. This was supported by the shift of dielectric values with concentration in all three cases. This is discussed in the next section.

2.5.3 Conclusions

The effect of changing molecular architecture shows that bisphenol A has a higher loss per mole than diglycidylether of bisphenol A in tetrahydrofuran. Thus, epoxy groups were less lossy than phenoxy groups at this frequency. The influence of local environment around the dipoles shows that the diglycidylether of bisphenol A in tetrahydrofuran has a higher dielectric loss per mole than the diglycidylether of bisphenol A in toluene. This was due to increased interactions of the epoxy in the tetrahydrofuran solvent. The values of ε"/M and (dT/dt)/M shows good agreements between high and low power experiments.

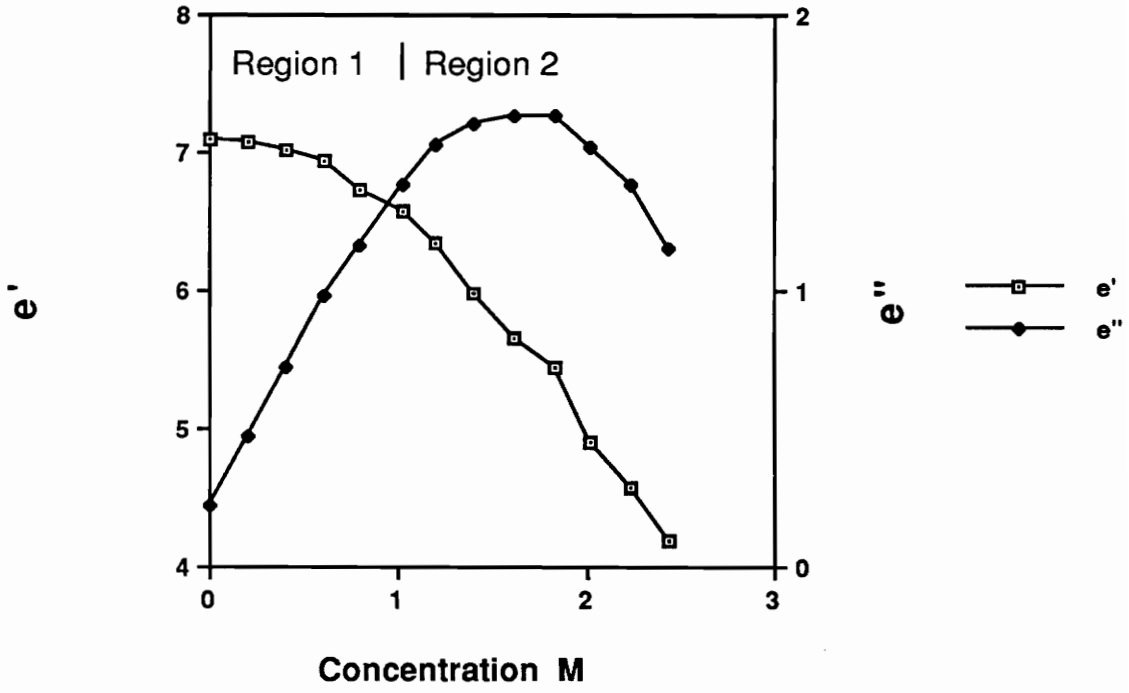

Figure 2.16

Dielectric storage (e') and dielectric loss (e") vs. concentration (M) for bishenol A in THF at 2.45 GHz.

Table 2.1

A Comparison Between ε''/M and $(dT/dt)/M$ for bisphenol A Solutions

	ε''/M	$(dT/dt)/M$
Bisphenol A/THF	1.15 ± 0.05	0.143 ± 0.002
DGEBA/THF	0.86 ± 0.03	0.09
DGEBA/toluene	0.53 ± 0.06	0.114 ± 0.003

2.6 Dielectric Measurements Between 0.045 to 20 GHz

2.6.1 Diglycidylether of Bisphenol A in Tetrahydrofuran

2.6.1.1 Results

The shift of the relaxation with temperature (-50 - 50°C) and concentration (0 - 1.5 M) has been confirmed by using an open coaxial sweep frequency technique from 0.045 to 20 GHz. An example of the influence of temperature is shown in Figure 2.17. The peak to the left-hand side for diglycidylehter of bisphenol A shifts to lower frequencies with decreased temperature. The temperature of -45°C shifts the relaxation off the left-hand edge of the graph. An increase in concentration shows the peak for diglycidylether of bisphenol A increasing in size, though the peak does not shift to lower frequencies. This was because the maximum concentration does not exceed the critical concentration.

2.6.1.2 Discussion

The ε" vs. frequency and temperature for diglycidylether of bisphenol A in tetrahydrofuran shows that the relaxation does shift to lower frequencies as temperature was decreased. This means the dipole motion was slowed as the temperature decreased. The ε" vs. frequency for a series of concentrations was also obtained, but the concentration was not above the critical concentration. Over the linear concentration range the peak did increase in size without a change in the location of the peak maximum with respect to frequency. This corresponds to the single frequency data from Figure 2.16.

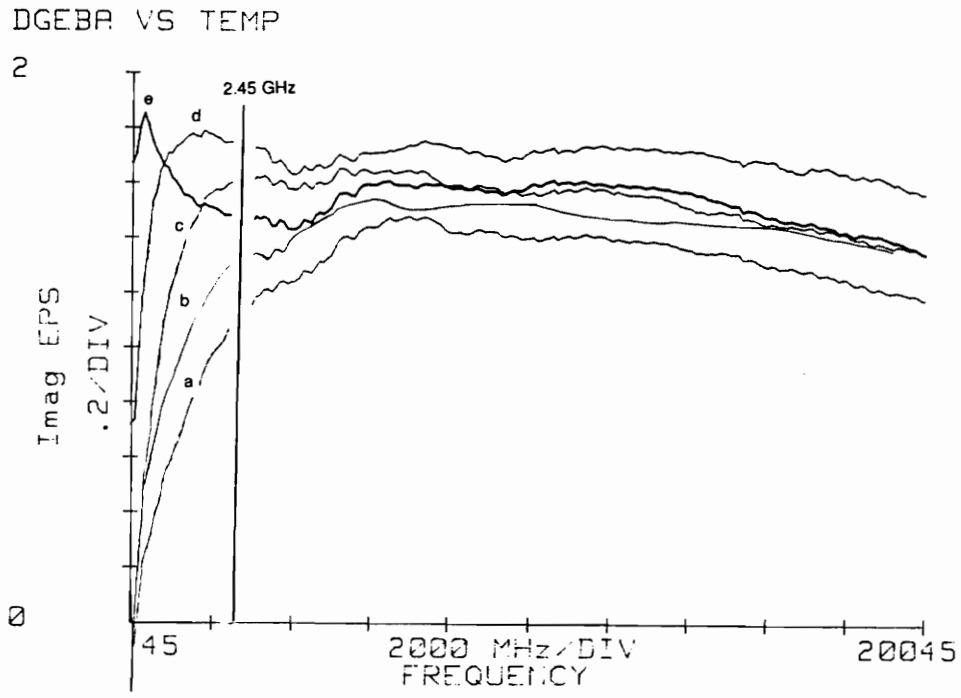

Figure 2.17

Dielectric loss (ε") vs. frequency from 0.045 to 20 GHz for DGEBA in THF for a series of temperatures from 50 to -50°C; a. 50, b 23, c -19, d -25, e -50°C.

2.6.1.3 Conclusions

The low power experiments have again given fundamental insight into the response of dielectric loss as a function of concentration, local environment, and molecular architecture. Thus, a simple additivity of functional groups can not be used to predict the dielectric loss over all concentrations, especially in the melt or resin form. Increased losses were obtained by changing a dipole's interaction with its local environment and changing chemistry from epoxy to phenoxy.

2.6.2 Bisphenol A in Tetrahydrofuran

2.6.2.1 Results

Dielectric storage and loss values were obtained at frequencies from 0.045 to 12 GHz by an open coaxial technique. The change in dielectric properties was examined as a function of temperature from -50 to 50°C and concentration from 0.0 to 2.4 M. Figures 2.18a and 2.18b show ε', ε'' as a function of frequency for concentrations from 0 to 2.4 M at room temperature Both storage and loss values increase through a maximum with concentration at 2.45 GHz. Figures 2.19a and 2.19b are examples of how ε', ε'' change as a function of temperature for 1 M bisphenol A in tetrahydrofuran. Thus, as temperature was increased ε', ε'' decrease across the frequency range examined. Dielectric properties were obtained for all concentrations, though only 1 M was shown because they all follow similar trends.

2.6.2.2 Discussion

The response ε', ε'' for bisphenol A in tetrahydrofuran to frequency was relatively flat compared to diglycidylether of bisphenol A in tetrahydrofuran as shown in Figure 2.17. The effect of concentration causes the lower frequency range of ε', ε'' to increase, while

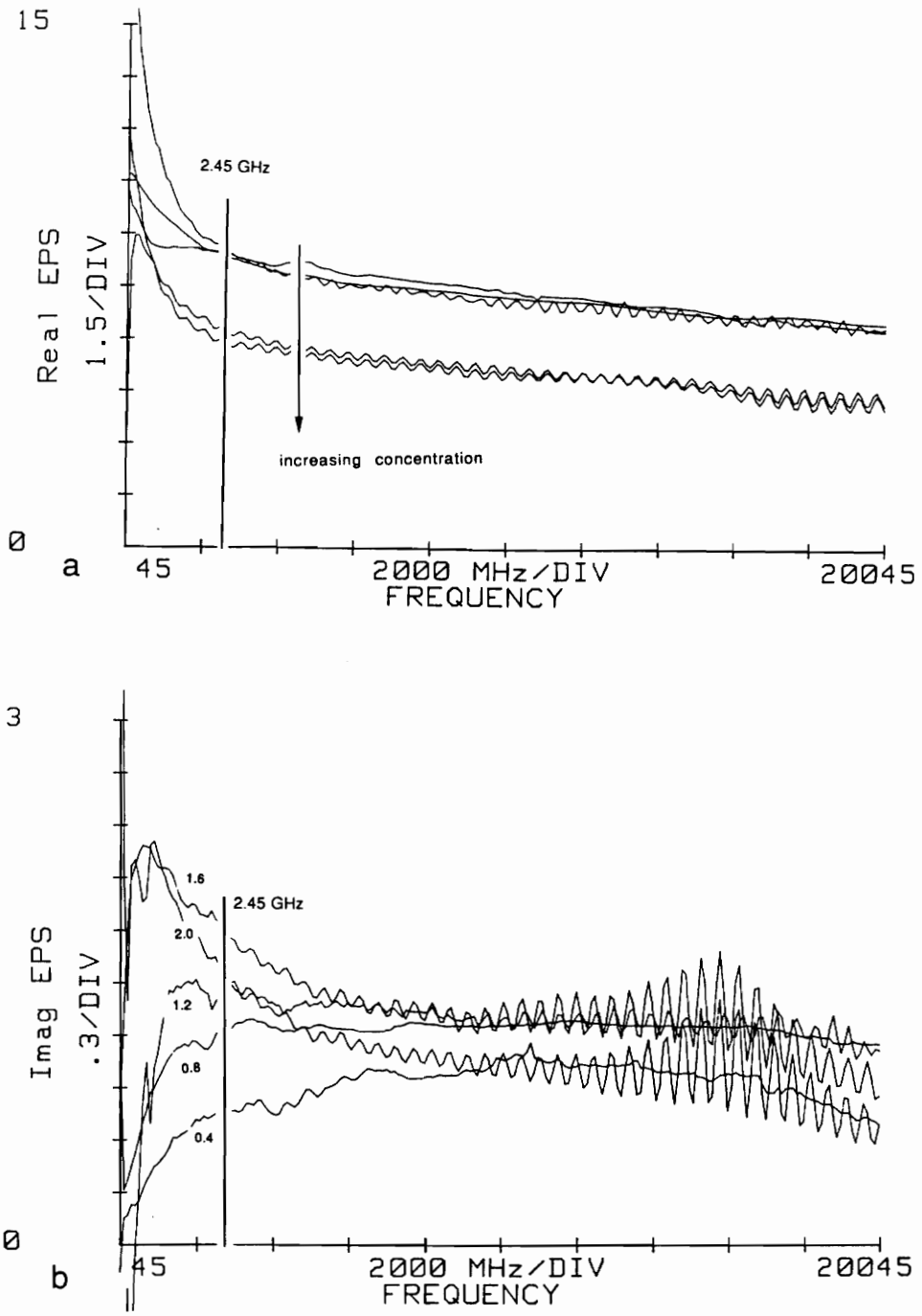

Figure 2.18

A plot of (a) ε' vs. frequency and a plot of (b) ε" vs. frequency for bisphenol A in THF for concentrations of; a 0.4, b 0.8, c 1.2, d 1.6, and e 2.0 M. Increasing concentration causes ε' to decrease and ε" to go through a maximum at 2.45 GHz.

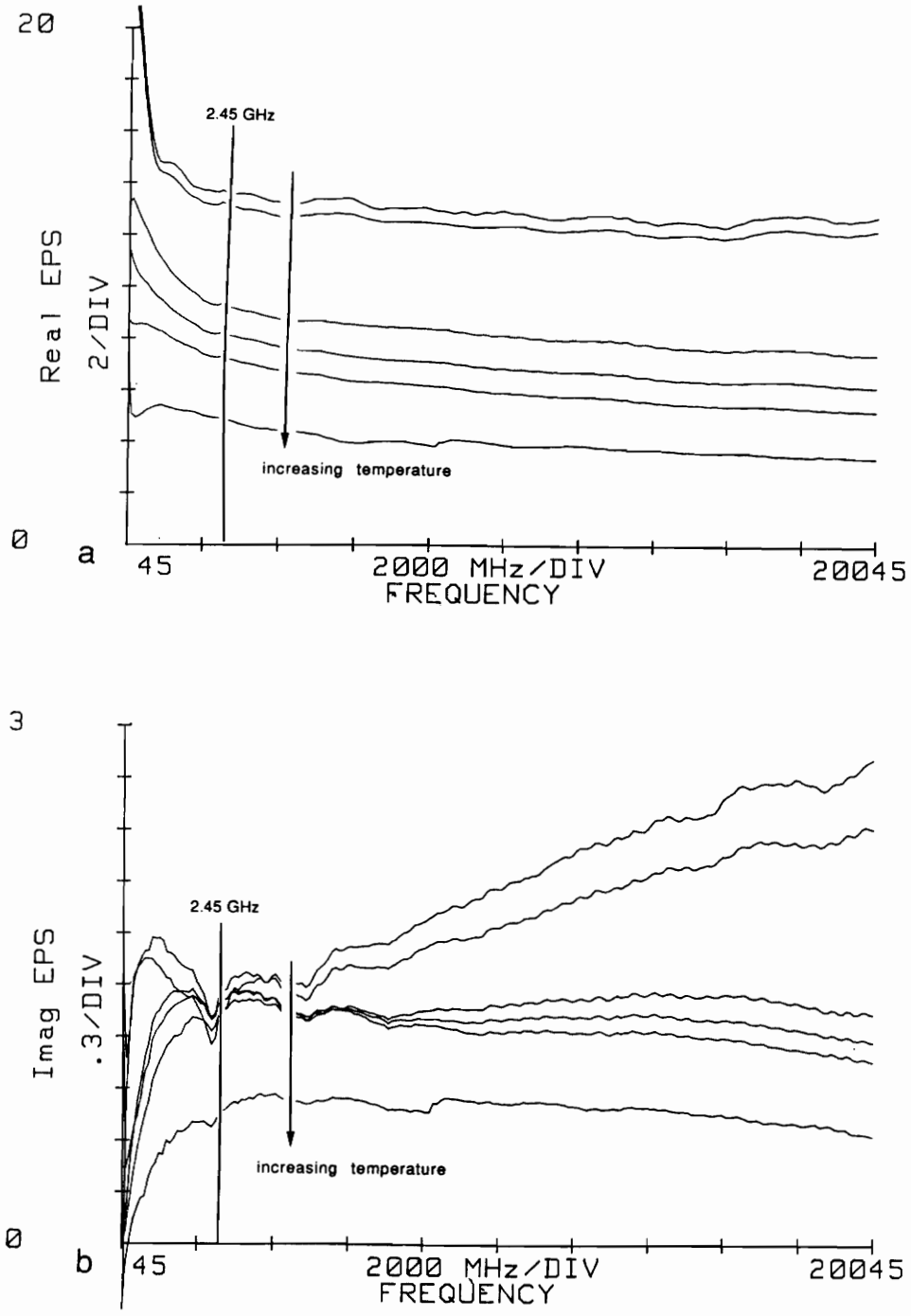

Figure 2.19

A plot of (a) ε' vs. frequency and (b) ε" vs. frequency for bisphenol A in THF at 1 M for a series of temperatures ranging from -40 - 40°C. Increasing temperature causes the dielectric values to decrease at 2.45 GHz.

the middle frequency region goes through a maximum. The values at 2.45 GHz from the sweep frequency technique compare well to those obtained by the single frequency cavity perturbation technique. The effect of increasing temperature was to decrease ε', ε'' at 2.45 GHz

There were some physical limits to the experiments that placed temperature bounds on the experiment. At low temperatures and high concentrations the bisphenol A would precipitate from solution. It could be quickly dissolved with increasing temperature. At the upper temperature region bubbles would form at the open coaxial face. The bubbles were visible dielectrically because they caused ripples in the dielectric values. The bisphenol solutions were assumed to be made of independent molecules in solution. NMR will be used to more accurately identify the structure in solution.

2.6.2.3 Conclusions

The response of ε', ε'' as function of frequency 0.045 - 12 GHz supported the single frequency data in Figure 2.16. The influence of decreasing temperature was to increase the dielectric storage and loss values for the 1 M bisphenol A solution. Increasing concentration increases the dielectric values at 2.45 GHz until the critical concentration, where they decrease.

2.7 NMR of Bisphenol A in d-acetone

2.7.1 Results

The NMR of bisphenol A in d-acetone was obtained as a function of temperature from minus 20 to 25°C at a concentration of 0.1M. The purpose was to identify the system in

solution and correlate these results to dielectric data. NMR of 0.1 M bisphenol A in d-acetone at room temperature is shown in Figure 2.20. The peaks were identified as follows: 8.1 ppm is due to the aromatic hydroxyl proton; the 7.04, 6.8 peaks were for aromatic protons the 7.04 peak was due to CH on the aromatic ring closest to OH. The peak at 3.09 ppm was due to H_2O. The one at 2.1 was for acetone. The peaks at 1.6 were the aliphatic protons on the isopropylidine group.

Since the focus was on the OH, a series of spectra as a function of temperature were obtained from 8 to 9 ppm. This series is shown in Figure 2.21 for 0.1 M. It was seen at low temperatures, below 5°C the two peaks were visible.

2.7.2 Discussion

Two possible proton interchange reactions exist, one between the aromatic hydroxyls and the other between water and the hydroxyls. The separation of the OH peak is possibly from an OH - OH associated dimer. The dimerization should deshield the OH and make the peak show up at higher ppm. The dimerization reaction is given by the following equilibrium constant, k, in Equation 2.16:

$$k = \frac{[A_2]}{[A][A]} \qquad \text{Eq. 2.16}$$

Increasing concentration will cause more A_2 to be present. An increase in concentration to 0.2 M causes only one peak to formed. Decreasing temperature causes more A_2 to appear, thus the formation of the peak at lower ppm with decreasing temperature. The average residence time (in seconds τ) for a proton at one site is given by Equation 2.7,

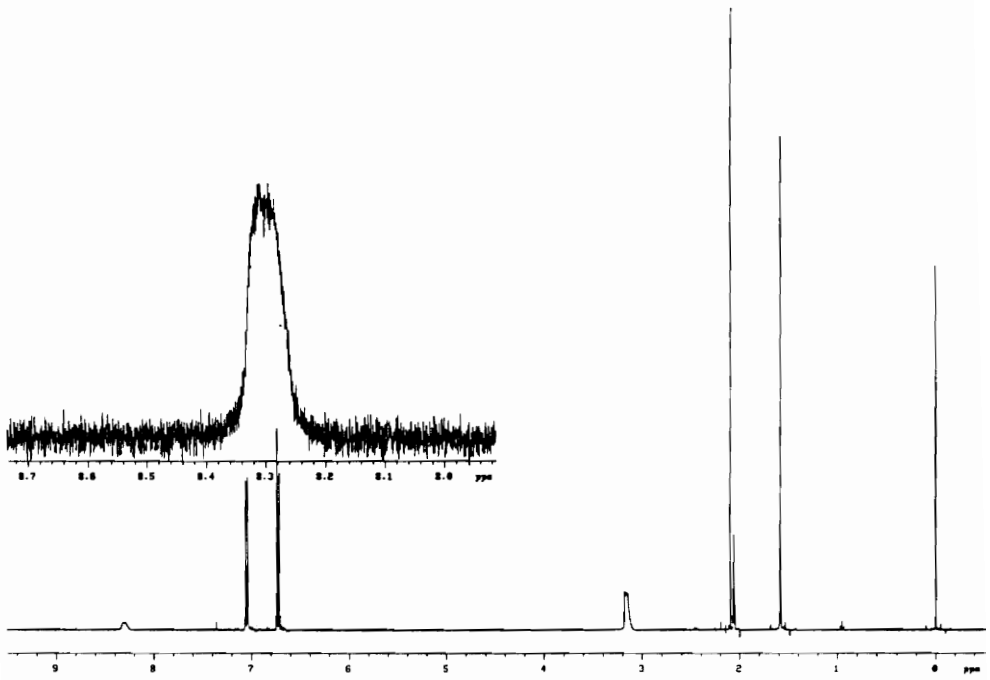

Figure 2.20

NMR spectra of bisphenol A in d-Acetone

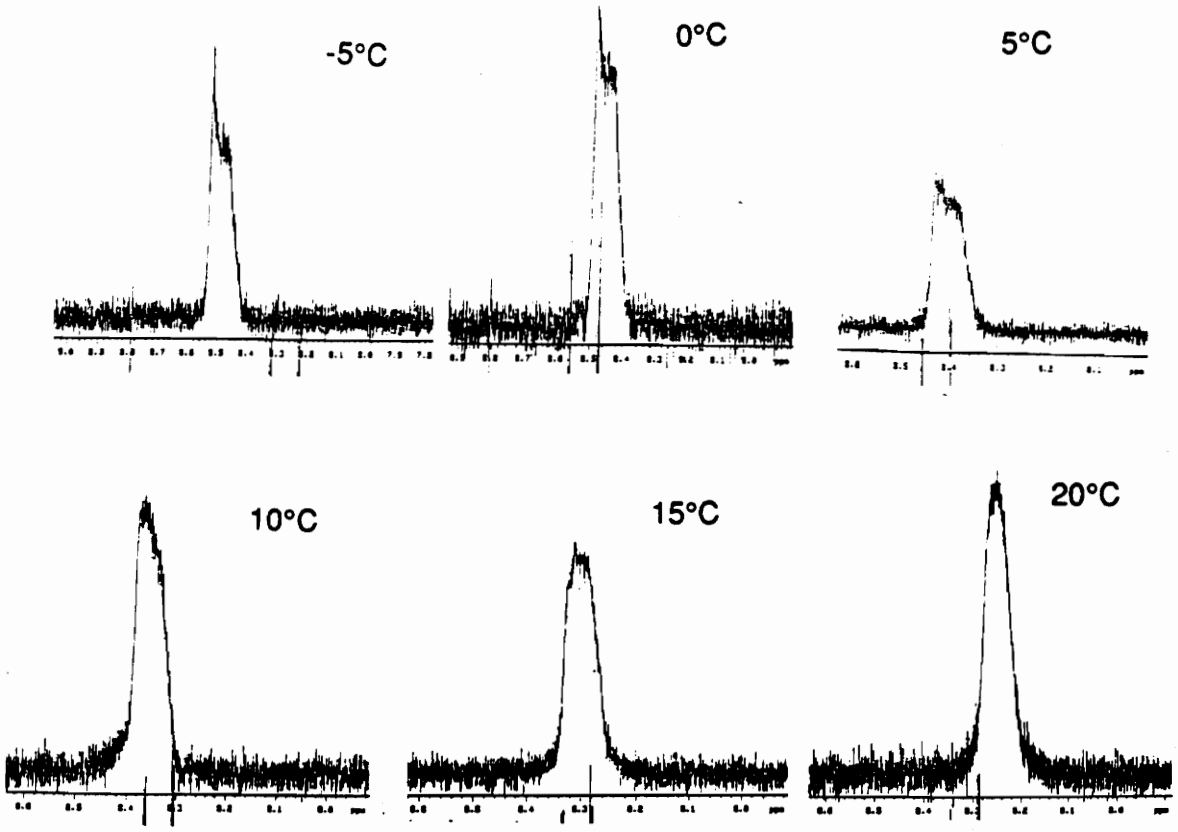

Figure 2.21

A series of NMR spectra of bisphenol A in d-acetone vs. temperature from 9 to 8 ppm.

where k is the separation of the peaks in Hz [80].

$$\tau = \frac{\sqrt{2}}{\pi k} \qquad \text{Eq. 2.17}$$

The τ was the rate of interchange between the two species. From the -5°C experiment the rate of interchange was ~80 Hz. This is the correct order of magnitude for proton interchange; an example is ethanol, which exchanges at 11 Hz. Compared to the sampling time of GHz or 10^{-9} seconds this means the dimer lasts long enough to be sampled by the dielectric experiments. The interaction with water cannot be confidently identified by these experiments. If another run were made with D_20 that resulted in a decrease of the OH peak size, this would suggest that there was also some water hydroxyl interchange. Thus, bisphenol A may be in solution in tetrahydrofuran but it does not stay as an independent dipole. The dimer should have a lower resonant frequency due to its increased mass. This will cause a ε" signal at lower frequencies to be added to the dipolar signal, thus showing a flat ε" vs. frequency response. Therefore, the linear response of ε" vs. concentration as shown in Figure 2.16 was fortuitous since the relative number of dimer and monomers in solution changes with increasing concentration.

These results for bisphenol A in d-acetone were extended to bisphenol A in tetrahydrofuran as they have similar solubility parameters, which were 9.1 for tetrahydrofuran and 9.9 [cal/cm^3]. The low concentrations were chosen to show the separation of the OH signal and identify the lowest concentration where the dimer was present; therefore at higher concentrations used for dielectric measurements more dimer will be formed.

2.7.3 Conclusions

At concentrations greater than 0.1 M bisphenol A in d-Acetone and temperatures greater than -20°C, the solution contains bisphenol A as well as another structure. One exchange rate was from 40 to 100 Hz, which was long enough to exist on the GHz time scale. This may cause the ε" vs. frequency signal to be flat.

2.8 Heating Rate vs. T for Polyhydroxyether

2.8.1 Results

A film of polyhydroxyether, a polymer derived from diglycidylether of bisphenol A and bisphenol A, described in Section 2.3.1.2, was coated between two 1" square quartz plates. The plates were spaced by 0.002" glass fibers. A hole was drilled in one quartz plate for a fluoroptic temperature probe. The assembly was placed on a 3 cm long, 2.5 cm diameter Teflon® rod and centered in a 7" cylindrical cavity. The cavity was brought into resonance or the reflected power brought to a minimum for each run, once for the system with the film and again for only the quartz plates. A comparison of the temperature time profiles is shown in Figure 2.22a.

A dT/dt vs. T plot was obtained for a 0.008" thick disk of polyhydroxyether film. These data were obtained in the 7" cylindrical cavity at 18 W of power. The curve is shown in Figure 2.22b. The onset of heating occurs at 125°C. The peak occurs at 150°C. The high temperature minimum occurs at 200°C.

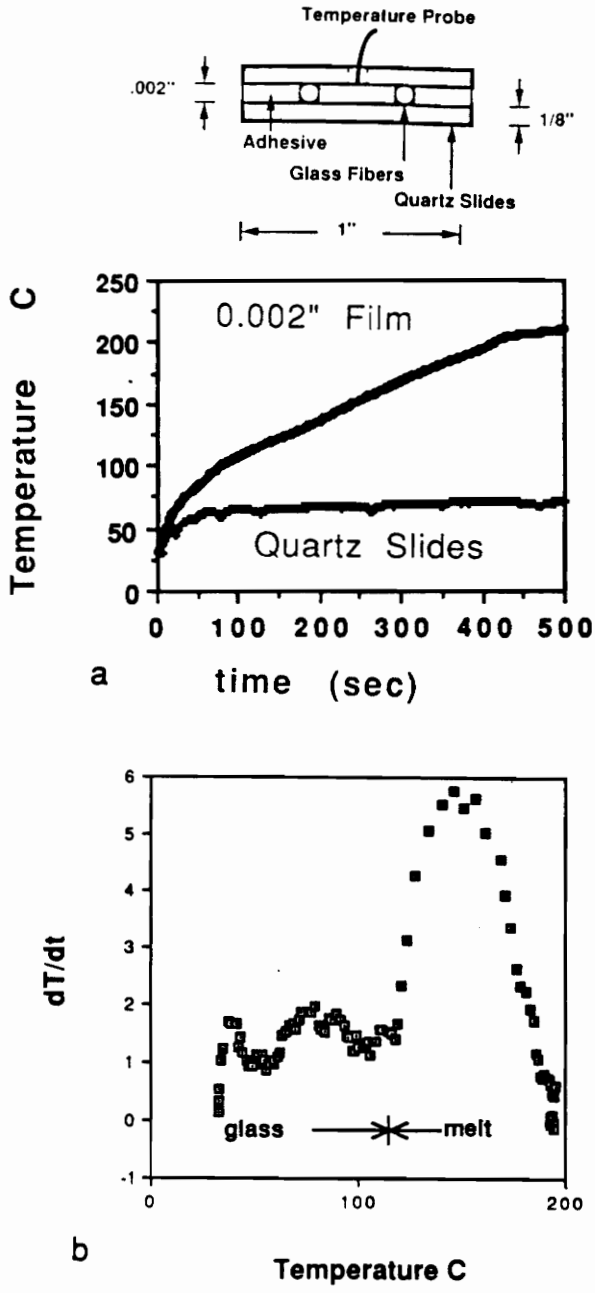

Figure 2.22

a. A plot comparing temperature vs. time for a 0.002" bipshenol A-quartz plate sandwich too just the quartz plates. b. A plot of dT/dt vs. temperature for an 0.008" thick polyhydroxyether film.

2.8.2 Discussion

The reason for obtaining the dT/dt vs. temperature plot was that dT/dt is proportional to ε" under adiabatic conditions. It is essentially a temperature plane through the distribution of dielectric relaxations for the polymer. Thus, the dT/dt vs. temperature curve is similar to a ε" vs. temmperature plot at 2.45 GHz. The peak maximum is analogous to the ε" peak maximum obtained at 2.45 GHz. Coupled with data from other frequencies gives an indication of the activation energy for motion for large scale macromolecular motion [78]. Due to sample preparation problems or lack of proper instrumentation the dielectric spectra at 2.45 GHz may not be obtainable, but this technique is simple to use and works on a variety of sample sizes. The information is useful when trying to anticipate proper processing conditions and prevent thermal runaway.

2.8.3 Conclusions

Thin 0.002" films can be heated in a 7" cylindrical cavity. The film was selectively heated and not the quartz plates. The dT/dt vs. temperature plots for the 0.008" polyhydroxyether film showed the onset of increased heating rate. This onset occurs ~125°C, which was similar to the Tg as obtained by DSC at 10°C/min. The peak in the curve occurs at ~150°C and the high temperature minimum occurs at 200°C.

2.9 Thermogravimetry of the poly(amide-imide)

2.9.1 Results

The weight percent vs. temperature data of uncured as received poly(amide-imide) show ~2.3 % weight loss (volatiles) between 40 to 320°C as shown in Figure 2.23. A peak in the derivative curve occurs around 245°C; this was near the sample's glass transition temperature of 260°C as measured by DSC. Weight loss due to material degradation did not begin until 350°C and continued to 750°C with 60% char under N_2 atmosphere. A more in-depth look at the chemistry of the volatiles and their desorbtion rate is discussed in Chapter 3. The volatiles were shown in Figure 3.7 to be NMP and water. The volatile desorbtion was shown to be mostly first order between 145 to 165°C by log - log plots of weight percent vs. time.

2.9.2 Discussion

The isothermal and sweep temperature thermogravimetry confirm that a few percent of volatiles remain from processing or are reabsorbed while exposed to the atmosphere. These volatiles have been shown to be NMP and water Figure 3.7. Recalling that water has a high dielectric constant and loss, from room temperature and above, will help one to understand why as received poly(amide-imide) has such a high loss value compared to the dried material, discussed in Section 2.10. For the weight loss vs. temperature profile for the TG-MS, a sharp drop in the weight percent occurs at the Tg. At the Tg large scale molecular motion commences and volatiles can escape from the glassy matrix more easily. From the TG-MS experiments in Figure 3.7a water seems to come off just before Tg and NMP afterward, though, their precise desorbtion times cannot be guaranteed as the residence time of each compound in the transfer line was not known.

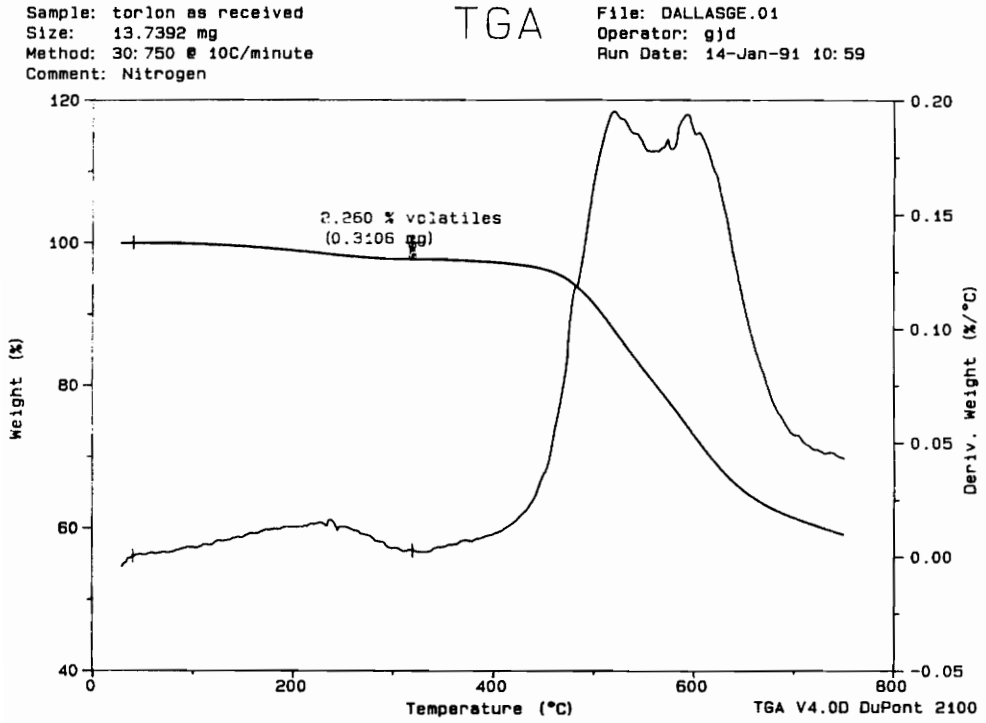

Figure 2.23

Weight loss vs. temperature for <u>as received</u> poly(amide-imide).

2.9.3 Conclusions

Uncured poly(amide-imide) has 2 - 2.5% volatiles as received. A maximum in weight loss occurred near the Tg of 260 as measured by DSC for 0.6 mm sheet. The volatiles were from NMP and water. The isothermal runs above 155°C in Figure 3.5 showed almost total elimination of volatiles, though it was not known whether NMP was completely gone after drying at isothermal temperatures as high as 165°C.

2.10 Dielectric Analysis vs. Temperature of a Poly(amide-imide) at 2.45 GHz

2.10.1 Results

The dielectric loss and storage (ε', ε") at 2.45 GHz were obtained for poly(amide-imide) rod as a function of temperature from room temperature to ~285°C. Figures 2.24a and b are a plot of ε', ε" for poly(amide-imide) uncured as received and dried and poly(amide-imide) full cured which had been out in a normal room environment for 20 days. Focusing on the ε" of poly(amide-imide) uncured, the values increase slightly until ~260°C, where the ε" increases more significantly with temperature. The full cure dried 20 days before shows slightly more ε" than the uncured poly(amide-imide) dried. Its ε" values increased with temperature until it reaches its Tg; afterwards the ε" increased much more rapidly. The uncured as received has significantly more ε" at all temperatures than the dried one. At Tg the ε" drops dramatically and follows the previous two. The ε' as a function of temperature showed a similar ordering with respect to volatile content and a slight increase near Tg.

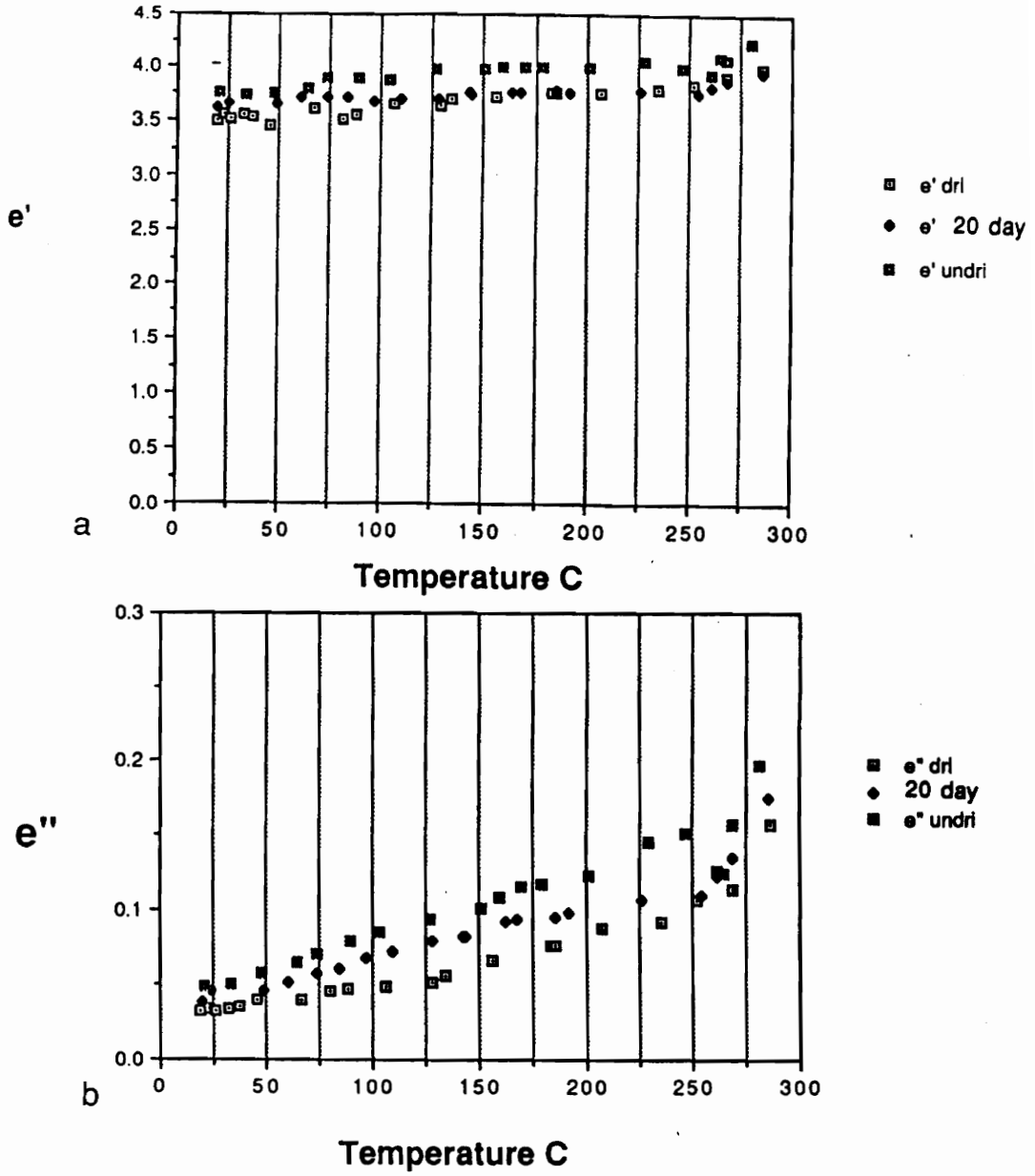

Figure 2.24

A plot of (a) ε' vs. temperature and (b) ε" vs. temperature for poly(amide-imide) uncured as received, full cured dried; and a full cured sample that had been on the bench for 20 days.

2.10.1 Discussion

The temperature sweep measurements indicate that the water significantly contributes to ε" and ε' below Tg for the as received poly(amide-imide), while above the glass transition temperature of 265°C dipole mobility increases ε" and ε' After going through glass transition temperature, the dielectric values of the as received poly(amide-imide) retraced the dried values upon cooling. The 20 day sample was included because it was assumed to have intermediate percent of water absorbed. Equilibrium water uptake took 200 days at room temp and moderate humidities. Transient dielectric effects were examined in Section 3.9. The dielectric values came from an average of six points, taken one every ten seconds for one minute. At temperatures above 150°C the water would desorb and change the dielectric values slightly within the one minute time span. Each one of these isothermal readings was taken at least 20 minutes after increasing to the next temperature setting. This was the time needed for both the sand bath and the waveguide to become isothermal. The resonant frequency of the waveguide was sensitive to the length of the waveguide. The resonant frequency would change with changing temperature. Thus, isothermal conditions must be met to insure accurate dielectric measurements.

2.10.3 Conclusions

The dielectric properties of the poly(amide-imide) as a function of temperature were significantly increased by the addition of 2 to 2.5% volatiles. Two and a half percent volatiles causes almost a 50% increase in ε" at 150°C. The volatiles desorbed rapidly near Tg. Drying the sample reduced the volatiles and the dielectric values. The ε" or ε' as a function of temperature increased steadily until Tg, where they increased more rapidly

as a function of temperature.

2.11 Polypropylene Filled with Carbon Black

2.11.1 *Results*

The dielectric loss and storage values were plotted vs. volume fraction of carbon black in Figure 2.25. The values were obtained at room temperature by the single frequency technique in a WR430 waveguide. The dielectric loss indicates a critical percolation point Φ_c of 0.2. The dielectric storage indicates steady increase until after 0.3 volume fraction.

2.11.2 *Discussion*

The dielectric loss behavior of the filled polypropylene shows percolation response. The critical volume fraction was 0.2 and the scaling exponent for this was 5. This value was much higher than exponents derived from computer models. This value is unexplainable at the present time. According to the development of connectivity for percolation, the connectivity occurred by connectivity with nearest neighbors. In this system there could be long range connectivity that was occurring thus causing a much higher scaling exponent. The reason for the decrease in dielectric storage above 0.3 volume fraction also is not known. The value was checked with different samples of the same batch and they remained the same.

2.11.3 Conclusions

The polypropylene system showed nonlinear response of ε'' with volume fraction carbon black. A critical volume fraction of 0.2 and a scaling exponent of 5 were obtained.

2.12 Polyurea Filled with Iron and Aluminum

2.12.1 *Results*

Figure 2.26 is a three dimensional plot of ε' over the aluminum volume fraction (Φ_{Al}), iron volume fraction (Φ_{Fe}) matrix. A non-planar surface was observed. The ε' values increased with the addition of either aluminum flake or iron particles. Figure 2.27 is a plot of μ'' vs. volume fraction of iron. The solid dots are for iron alone. The doughnuts are for aluminum/iron mixtures. A critical volume fraction of ~0.25 was observed. The addition of aluminum flake above 0.4 volume fraction iron decreases μ''. The critical volume fraction and scaling exponents for the three systems were compared to those derived by the percolation model in Table 2.2.

2.12.2 *Discussion*

Second order type transitions were observed for μ'' with Φ_{Fe} and ε'' with Φ_{Al}. The experimental transitions occured from 0.11 to 0.25 volume fraction filler. A log-log plot of the data above a volume fraction of 0.25 shows a slope of ~1.4, which would be expected for the percolation response of randomly ordered spherical particles [51]. The scaling value of 1.1 for aluminum flake was similar to the value of 1.1 calculated theoretically for two-dimensional growth [53]. In Figure 2.27 the μ'' values to ~0.3 Φ_{Fe} were not effected by addition of aluminum flake, but at ~0.4 Φ_{Fe} the addition of aluminum flake decreases the these values.

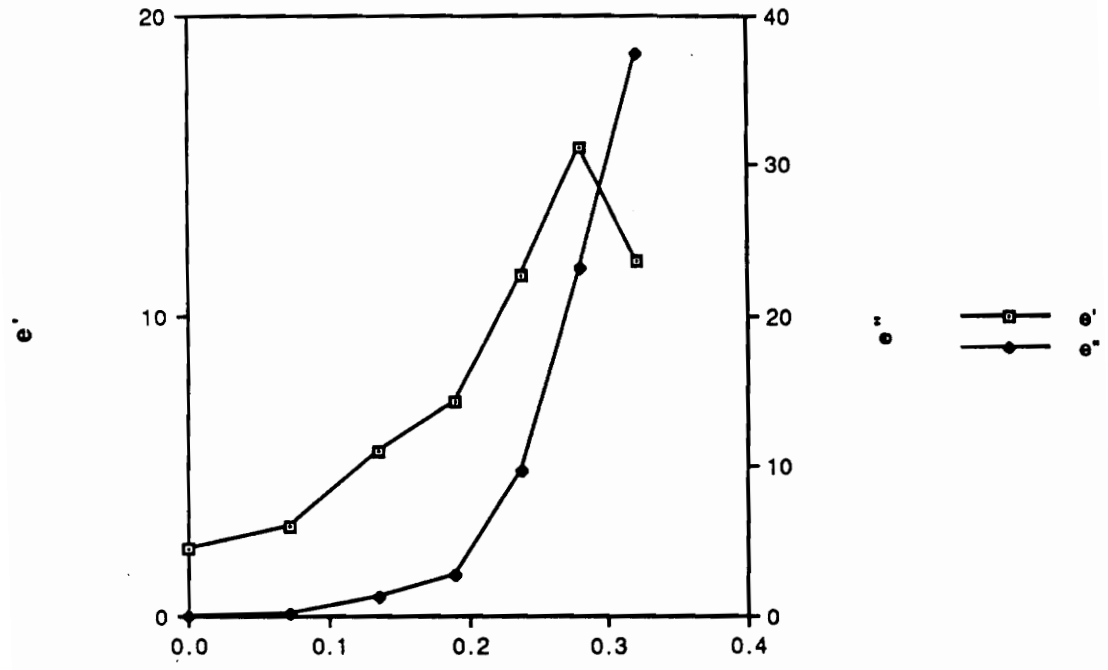

Figure 2.25

Dielectric loss and storage vs. volume fraction carbon black in polypropylene.

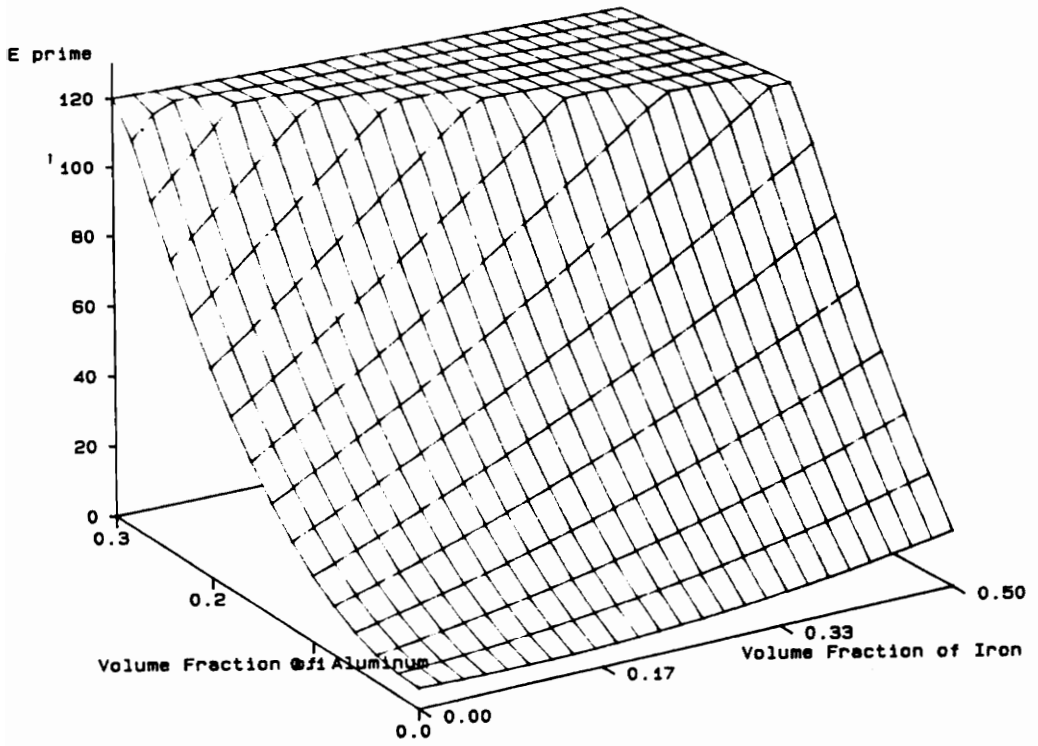

Figure 2.26

Dielectric storage (ε') at 2.5 GHz vs. volume fraction aluminum flake and volume fraction iron.

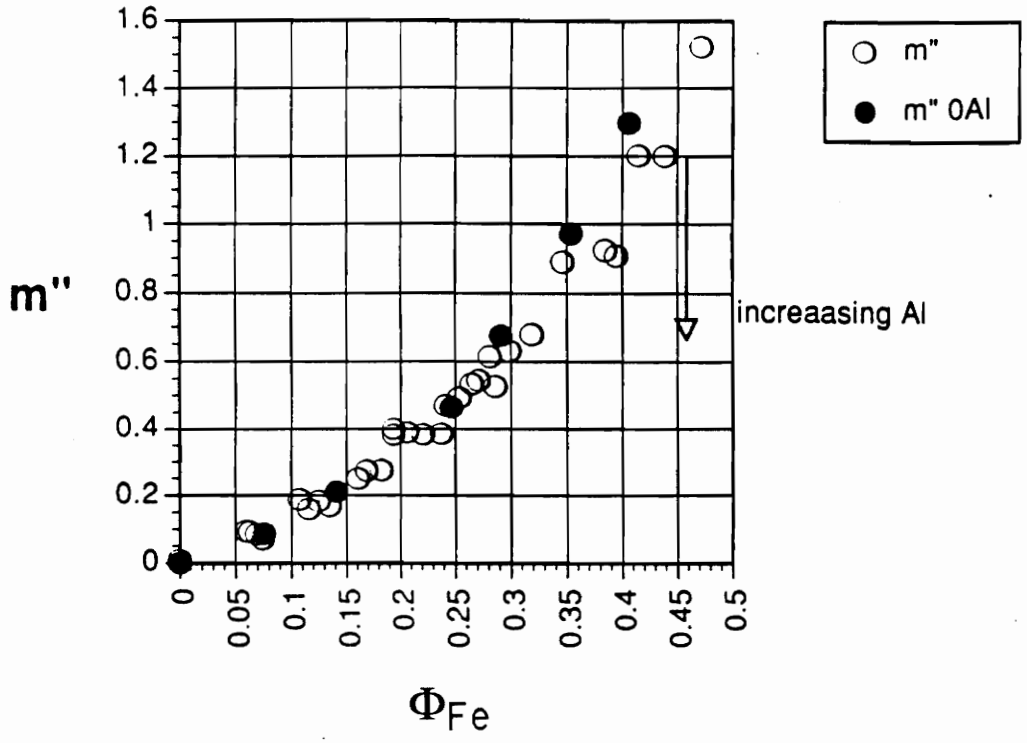

Figure 2.27

Magnetic loss (μ") vs. volume fraction iron (Φ_{Fe}) for iron and iron/aluminum flake mixtures.

Table 2.2

Comparison of Critical Volume Fraction (Φ_c) and Scaling Behavior from Theory and Experiment

	Experiment		Theory[50-53]	
Material	(Φ_c)	Scaling	(Φ_c)	Scaling
Polypropylene/ Carbon Black	0.2 ± 0.05	5	0.15 - 0.25	1.5
Aluminum Flake	0.11 ±0.05*	1.1	0.15 - 0.25	1.1/2d
1.65/3d				
Iron	0.25 ± 0.05	1.4	0.15 - 0.25	1.5 - 1.6

* Transition difficult to identify due to small differences in slopes

The scaling value of 1.1 for aluminum flake implies that the connectivity that developed was primarily two dimensional. This was examined by scanning electron microscopy in Section 2.14. The aluminum structure that developed above critical volume fraction shows planar arrangement of flakes in long veins, supporting the observed scaling value.

The effect of increased dielectric and magnetic filler caused the wave traveling through the material to be compressed. The addition of aluminum and iron reduced the 2.5 GHz wave from 7 cm for polyurea to less then 1 cm as shown in Figure 2.28. The wavelength in the material λ_m relative to the free space wavelength λ_o was calculated by using Equation 2.18.

$$\lambda_m = \frac{\lambda_0}{(a^2 + b^2)^{1/4} \cos(1/2\tan^{-1}(-b/a))}$$

$$a = \varepsilon'\mu' - \mu''\varepsilon''$$

$$b = \varepsilon''\mu' + \varepsilon'\mu''$$

Eq. 2.18

Table 2.2 summarizes the scaling and critical exponent data for the carbon black, aluminum flake, and iron data. Most scaling exponents and critical volume fractions agree with percolation theory. Thus, for these filled systems where the particles interact, critical volume fraction and scaling concepts are useful for predicting dielectric and magnetic values.

2.12.3 *Conclusions*

A nonlinear response of the measured dielectric properties with volume fraction aluminum and iron has been observed. Above ~0.25 the measured properties showed percolation behavior. The addition of aluminum and iron above 0.4 volume fraction iron decreases μ". The scaling of aluminum or iron fits theory, while the fifth power scaling of carbon black in polypropylene does not fit any known theory. The effective medium wavelength of the films can be reduced from 7 cm to less than 1 cm by blending aluminum and iron fillers.

2.13 Magnetization of Iron/Aluminum Films

2.13.1 Results

The magnetization (B) vs. applied magnetic field strength (H) was obtained for all the iron films and one iron/aluminum mixture that caused a decrease in μ" with aluminum. The applied magnetic field was cycled between ± 3000 Oe. A typical B vs. H plot is shown in Figure 2.29. The intercept with the B axis is the remnant magnetization, while the intersection of the curve with the -H axis is the coercivity. Both of these values were essentially zero within experimental error. The magnetization values at 3000 Oe were used to obtain plots of normalized magnetization (Gauss) vs. volume fraction iron as shown in Figure 2.30.

2.13.2 Discussion

The same characteristic shape for μ" vs. volume fraction is shown Figure 2.27 is also seen as normalized magnetization vs. volume fraction iron in Figure 2.30. A critical volume fraction around 0.25 also was apparent. The mixed system shows a lower value of Gauss. Though the exact reason for the decreased normalized magnetization value was not known. It could be the aluminum disrupting the magnetic structure or simply a

not known. It could be the aluminum disrupting the magnetic structure or simply a decrease in X because of dilution of the iron with aluminum since the system was near phase inversion. This will be examined by microscopy in the next section.

2.13.3 Conclusions

Magnetization vs. applied magnetic field shows that there was no remnant magnetization or coercivity for the polyurea iron films. The normalized magnetization vs. volume fraction iron Figure 2.30 shows a similar curve as μ" vs. volume fraction iron as shown in Figure 2.27. A critical volume fraction of 0.25 also was observed. Thus, the high magnetic field strength experiment results in data similar to that of the low field strength.

2.14 Scanning Electron Microscopy of Filled Films

2.14.1 Results

2.14.1.1 Films of Aluminum Flake

The scanning electron microscopy for the filled films was done to monitor structural changes as a function of composition. Four different types of systems were observed. The changes in structure associated with pure aluminum flake, pure iron, mixtures of the two and the change in surface smoothness as a function of total volume fraction filler were obtained. The photographs were taken with a 90 degree orientation to a cut side. Most of the films were cut with scissors, while two of the films with the highest concentrations of aluminum flake were freeze fractured. In the photographs the film surfaces are at the top and bottom of the picture; the length of the film goes

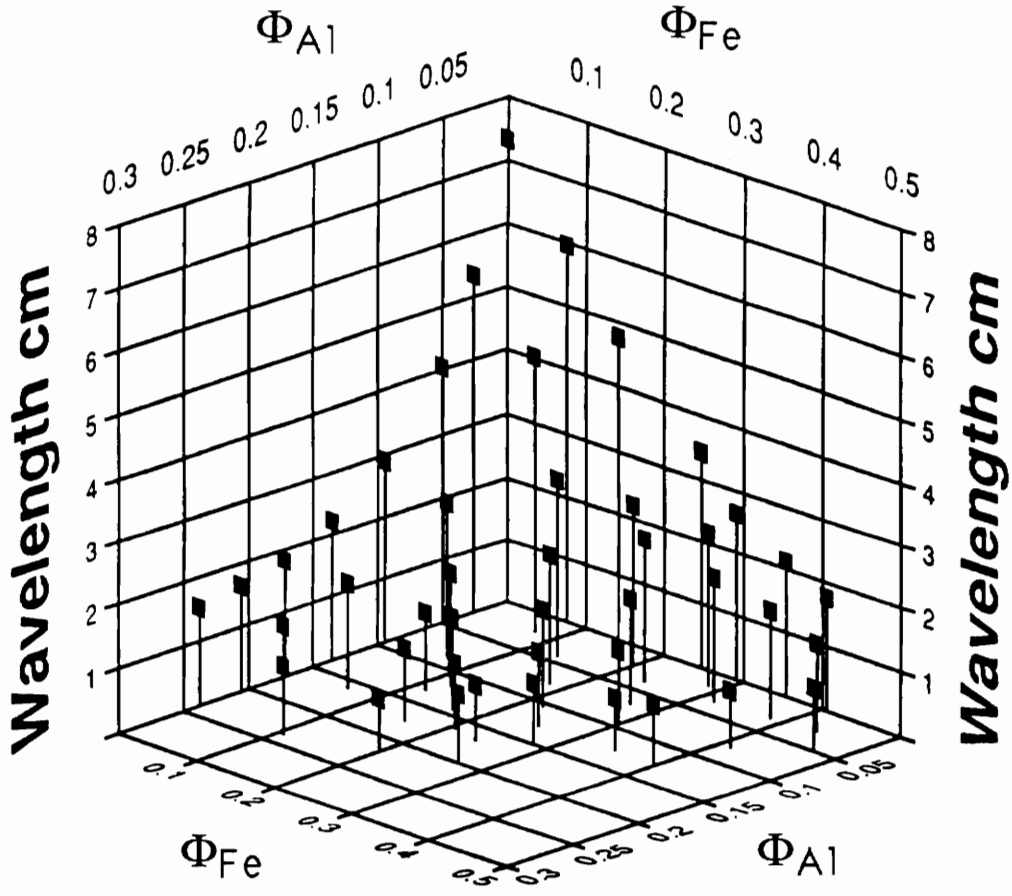

Figure 2.28

Calculated wavelength vs. volume fraction aluminum (Φ_{Al}) and iron (Φ_{Fe}) for an initial wave of 2.45 GHz.

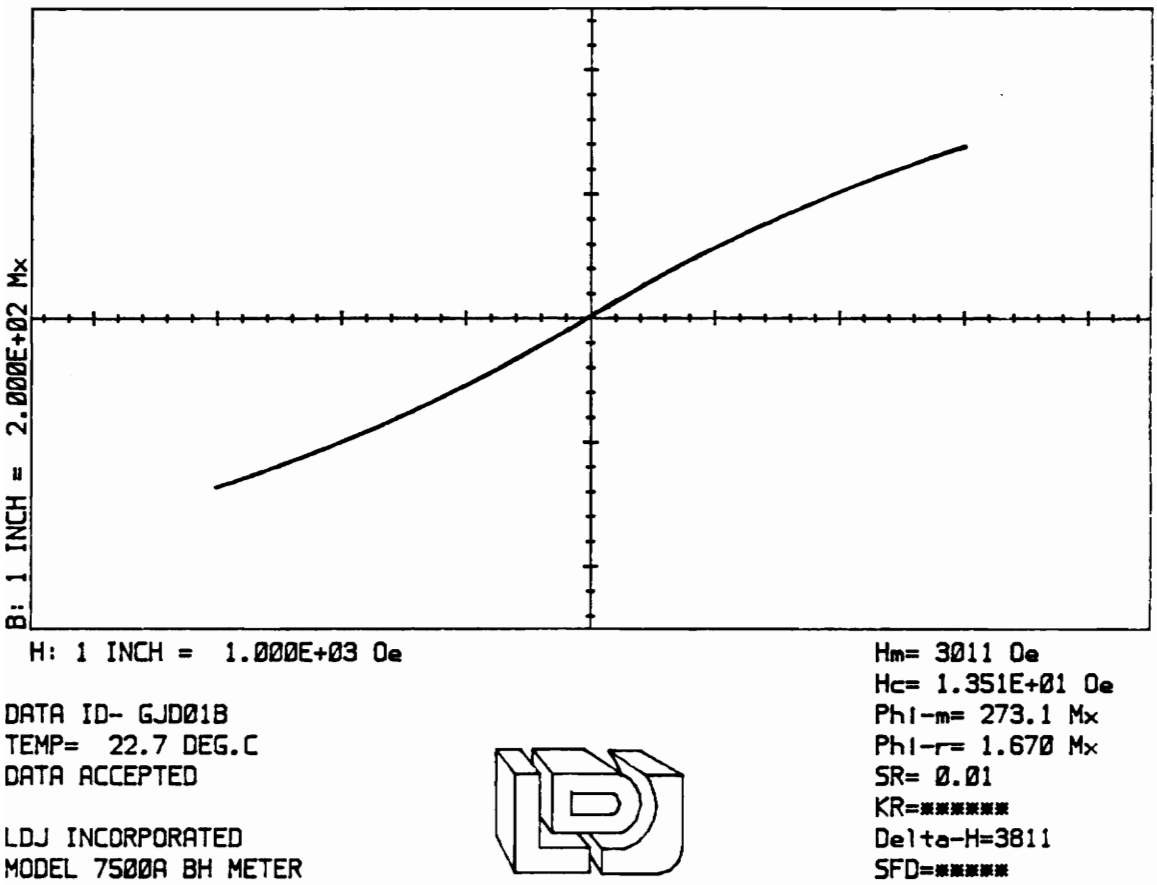

Figure 2.29

A plot of magnetization (B) vs. applied magnetic field (H) ± 3000 Oe for a film containing 0.132 volume fraction iron.

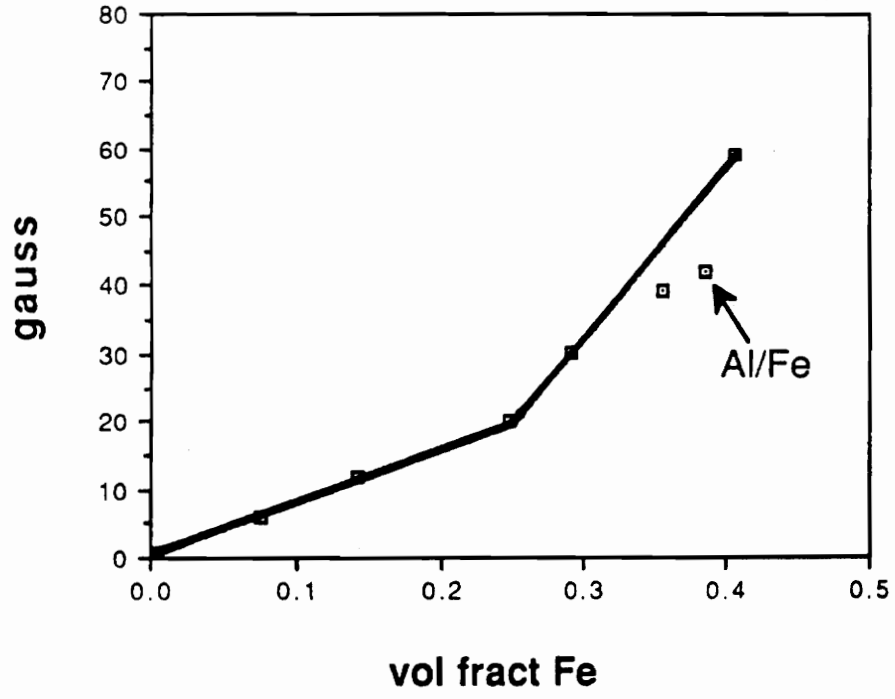

Figure 2.30

A plot of normalized magnetization (Gauss) vs. volume fraction iron and an aluminum/iron mixture.

from left to right. The magnification was 1000 X and the scale bar was ~10 microns. Before the high magnification pictures were taken a low magnification photo of the edge of the film was shown in Figure 2.31. The circles in the film were bubbles, approximately 75 - 125 microns in diameter.

Figures 2.32 a, b, c, and d are a series of photos for aluminum flake in polyurea matrix. The volume fractions are 0.025, 0.092, 0.132, 0.202 aluminum, respectively. The aluminum flake was seen in Figure 2.32a to exist as independent particles, well bonded to the matrix and separated by approximately 20 microns. The flakes have an average orientation planar to the top and bottom surfaces. In Figure 2.32b, 0.092 volume fraction aluminum there was a higher density of particles and occasionally a small planar cluster of flakes; they were separated by 5 - 10 microns. The flakes exist parallel to the surface. There was slight separation of the flakes with the matrix. The 0.132 volume fraction aluminum was freeze fractured and shows 10 to 15 micron veins of aluminum flake running lengthwise. The flakes in the veins were separated by a few microns. The veins were separated by 20 to 30 microns. The 0.202 volume fraction aluminum shown in Figure 2.32d shows 20 - 30 micron veins of aluminum flake. The veins were separated by 10 microns and the flakes were separated by ~1 micron. The flakes in Figures 2.32c and 2.32d were well bonded to the matrix.

2.14.1.2 Films With Iron Particles

Figures 2.33a, b, c,and d are a series of photos for iron particles in polyurea film. The volume fractions are 0.132, 0.233, 0.328, and 0.449 respectively. The series of iron particles starts with the low concentrations, Figure 2.33a, which showed the iron particles well dispersed in the matrix; clusters of several particles also existed. The

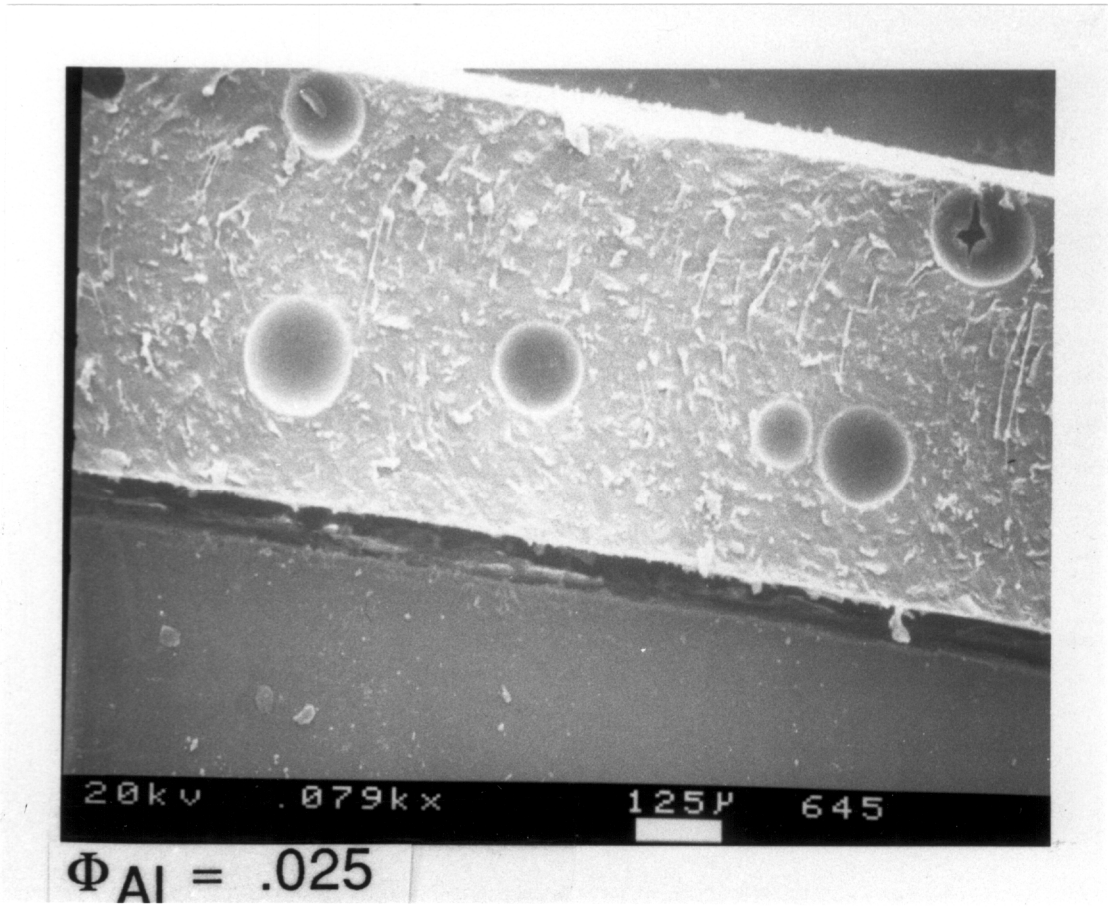

Figure 2.31

A low magnification picture of the edge of a film. The hemispheres are from bubbles.

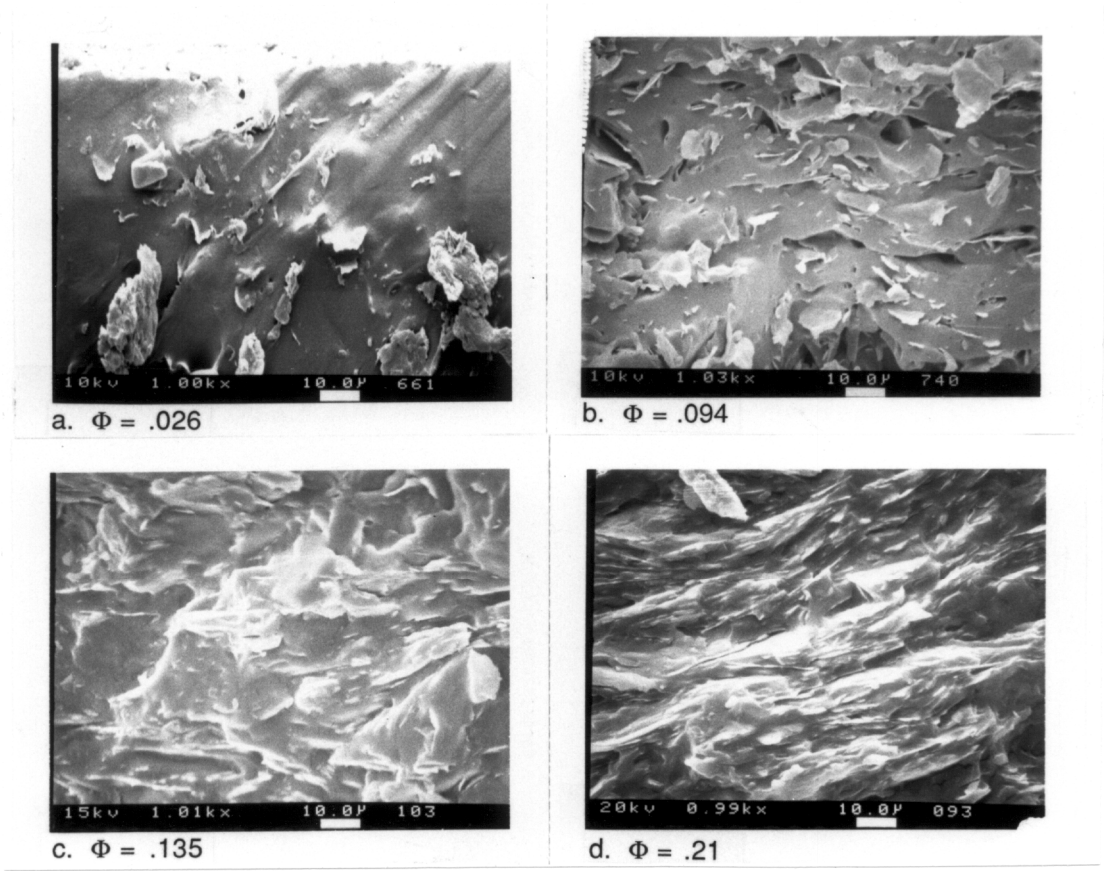

Figure 2.32

A series of scanning electron micrographs showing the development of with increasing volume fraction aluminum flake in polyurea binder: a. 0.025, b. 0.092, c. 0.132, d. 0.202.

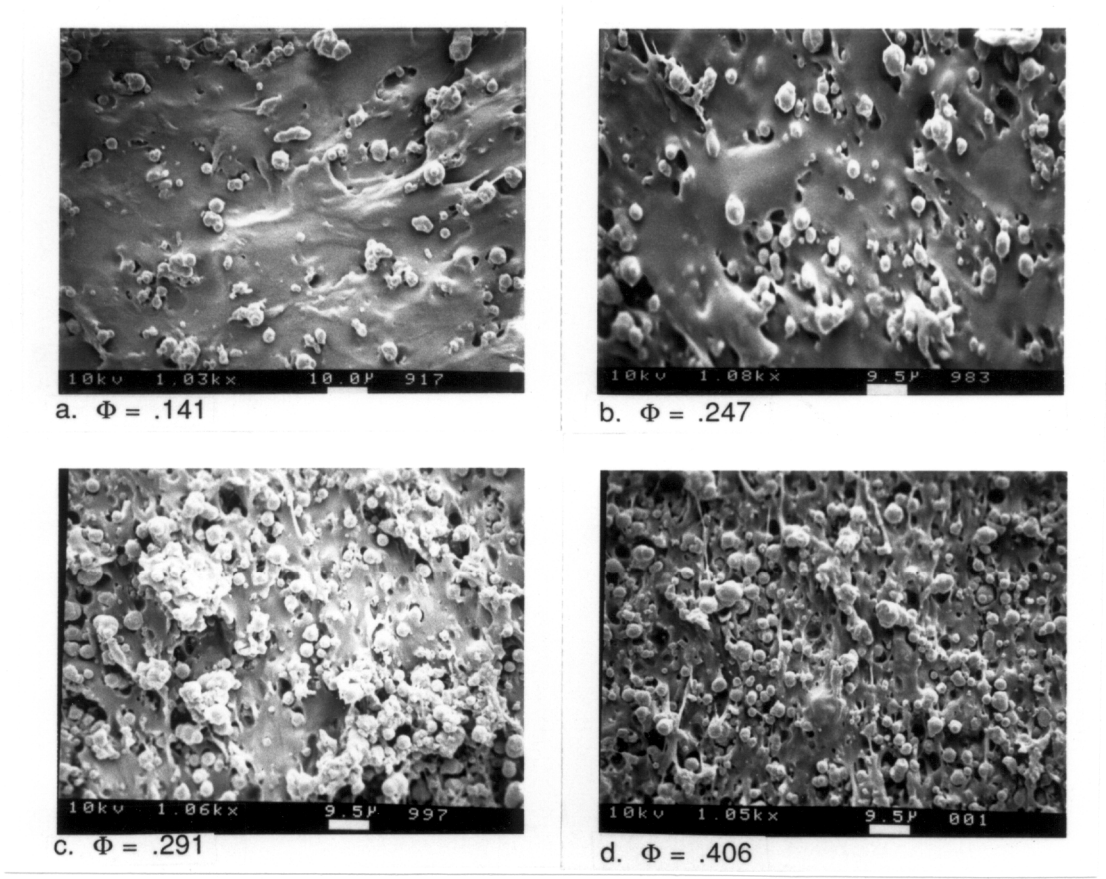

Figure 2.33

A series of scanning electron micrographs showing the development of connectivity with increasing volume fraction iron in polyurea binder: a. 0.132, b. 0.233, c. 0.328, d. 0.449.

independent particles were more than 10 microns apart from their nearest neighbor. These were a few particle diameters. The clusters were at least one cluster diameter apart. In Figure 2.33b the 0.233 volume fraction iron shows clusters of 10 to 20 particles. The dispersion within the binder showed voids near the individual particles or clusters. The intercluster spacing has decreased to about one cluster diameter. In Figure 2.33c, at 0.328 volume fraction, continuous veins of iron particles consisting of particles within one particle diameter exist. The cluster size was about 50 microns. Smaller clusters of iron spheres existed in the areas between the large clusters. In Figure 2.33d, the highest volume fraction 0.449, larger 40 - 60 micron veins of iron particles existed and fewer individual or independent clusters existed, compared to the 0.328 volume fraction iron. The size of the veins was determined by examining a surface photograph.

2.14.1.3 Films with Aluminum Flake and Iron Particles

The mixtures of aluminum flake and iron particles begin at compositions below 0.4 volume fraction iron. The second composition was one where the volume fraction of aluminum was high enough to decrease the μ'' value at the 0.4 volume fraction. These are shown in Figures 2.34a and b. In Figure 2.34a, the aluminum flake was located randomly within the iron network 10 - 15 microns apart. Figure 2.32b shows a wall of iron particles with aluminum horizontally positioned and regularly spaced in the iron matrix. The aluminum was in either independent flakes or small plate-like clusters. The spacing of the flakes was about 5 microns apart in both the horizontal and vertical directions.

Figures 2.35a, b, and c showed the progression of phase inversion with total volume fraction from a surface perspective. The total volume fractions were 0.34, 0.446,

0.502. The separate volume fractions were (Al/Fe) 0.0338/0.304, 0.028/0.418, and 0.126/0.376 for Figures 2.35a, b, and c respectively. In Figure 2.34a 0.34 volume fraction filler shows a somewhat smooth surface with some iron spheres deforming the surface. The 0.446 volume fraction indicates regions of smooth surface with rough scaly regions of aluminum flake. Finally, the 0.502 volume fraction shows complete phase inversion where the particles were not contained within a matrix but bonded together by the polymer.

2.14.2 *Discussion*

Bubbles appeared inside sprayed polyurea films, perhaps produced by the solvent trying to escape, while the rubbery network was forming around them. The bubbles were sometimes seen in the films below the 0.2 total volume fraction filler range. The maximum bubble content appearing in these films would account for less than 3% error in total volume. The error was determined by a two-dimensional approximation, assuming the surface area contained by the bubbles was equal to the volume contained by the bubbles within the matrix 12 bubbles with 2 mm radius on a surface of 2500 mm^2. After the 0.2 volume fraction range, voids could be observed in the iron films. This was due to less than perfect packing of the matrix and filler, though the films were tough. There was no way to qualitatively estimate the error caused in volume fraction calculations by the voids. Assuming the error due to voids was significant in the volume fraction calculations above 0.2 volume fraction would lead one to overestimate the volume fraction of filler and thus critical volume fraction to percolation should be shifted to lower values.

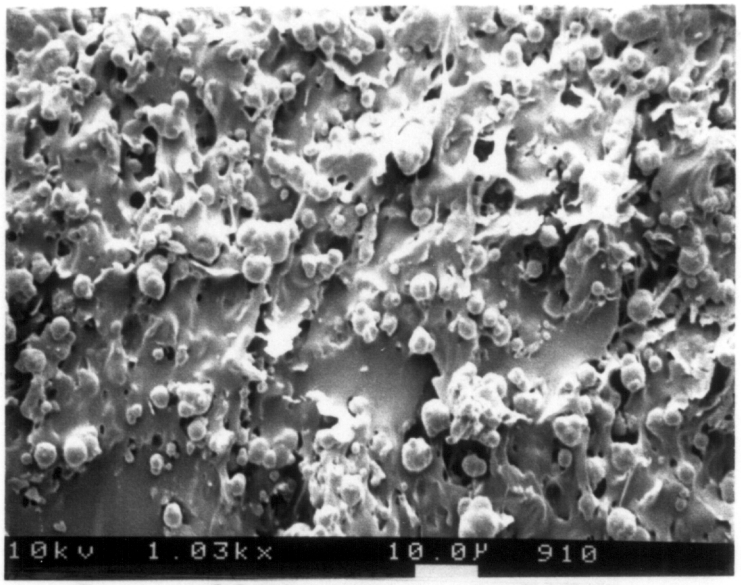

a. $\Phi_{Al} = .0336$ $\Phi_{Fe} = .319$

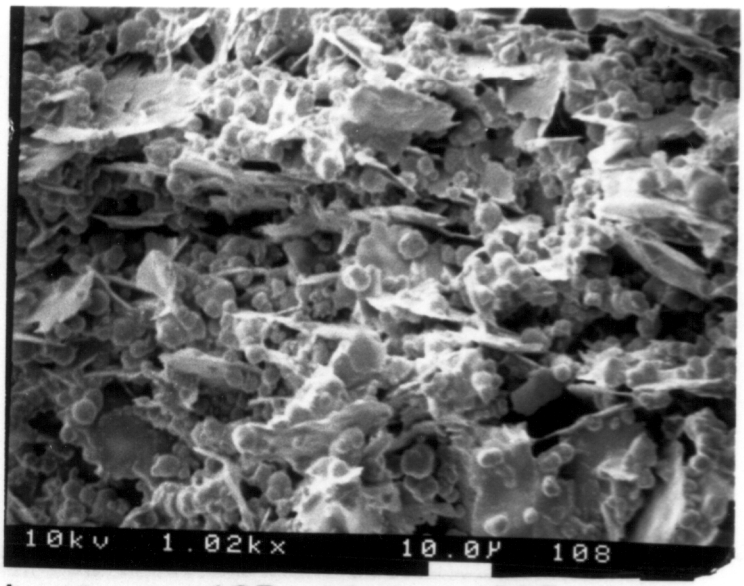

b. $\Phi_{Al} = .125$ $\Phi_{Fe} = .395$

Figure 2.34

Scanning electron micrographs of aluminum/iron mixtures (a) below and (b) above the volume fractions necessary to cause the μ" to decrease with addition of aluminum.

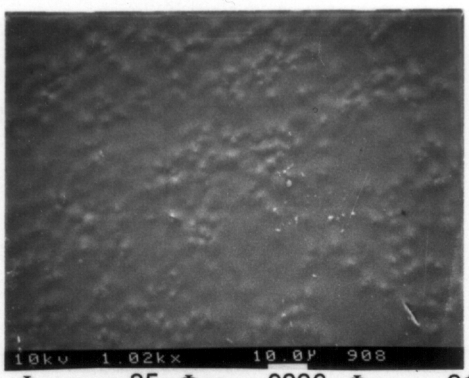

a. $\Phi_{total} = .35$ $\Phi_{Al} = .0336$ $\Phi_{Fe} = .319$

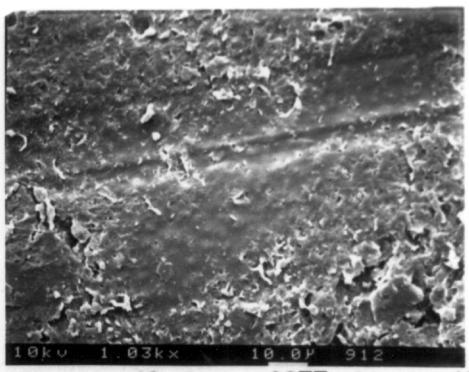

b. $\Phi_{total} = .46$ $\Phi_{Al} = .0277$ $\Phi_{Fe} = .439$

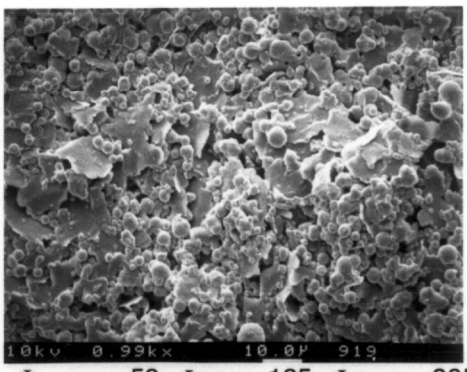

c. $\Phi_{total} = .53$ $\Phi_{Al} = .125$ $\Phi_{Fe} = .395$

Figure 2.35

Scanning electron micrographs of the surfaces of aluminum/iron films. The purpose is to show phase inversion was seen with respect to total volume fraction filler, which are a. 0.35, b. 0.46, and c. 0.53.

The growth of iron and aluminum structure with volume fraction filler follows the proposed growth mechanism by percolation. At low volume fractions there were mostly independent particles or small clusters more than a few structural diameters apart. Approaching the percolation point, these clusters grow in size and become closer together. Above percolation large veins of material appear to exist from one edge to another. The spacing was calculated for the critical volume fraction 0.2 by Equation 2.7 is ~8 μm, which agrees well to the spacing seen in the photograph in Figure 2.33b. The growth of the aluminum structures forms a more two-dimensional structure compared to the iron spheres, though three different concentration regions appear to exist. At low volume fraction 0.026 shown in Figure 2.32a the flakes were independent and horizontally oriented within the matrix. The 0.094 volume fraction shown in Figure 2.32b shows preferential orientation of the flakes parallel to the film surfaces, though the flakes appear randomly dispersed within each plane. The separation of the flakes from the polymer film was probably caused by the scissors used to cut the film. At higher volume fraction filler this did not occur as a freeze fracture technique was used to prepare the samples. The higher volume fractions showed veins of aluminum flake, which increase in thickness with increasing volume fraction aluminum.

The purpose of the mixture series was to try to explain why μ" decreases with increasing flake content at 0.4 volume fraction iron. The 0.35 volume fraction shown in Figure 2.34a was above percolation but below 0.4 volume fraction iron. This photo shows continuous veins of iron with aluminum randomly dispersed within the iron network ~15 microns apart. The 0.395 volume fraction iron with 0.125 aluminum shown in Figure 2.34b shows layers where aluminum flake was preferentially aligned with either surface. This ordering and layering of the aluminum may degrade the iron

network. The iron particles must communicate with each other to generate the measured μ", and the aluminum flake was disrupting this. A simpler explanation exists for the influence of aluminum flake at 0.4 volume fraction iron on the decrease in μ". Comparing the visual information from the iron mixtures and the surface photographs indicates that there was a phase inversion between the filler and the binder around the 0.45 total volume fraction region. Therefore, above phase inversion, the aluminum will dilute the iron concentration and reduce μ". Lastly, remembering that scanning electron micrographs were two dimensional images and cannot be used for quantitative structural determination with this three dimensional network, though the images do appear useful in identifying the relationship between structure and measured properties.

2.14.3 Conclusions

The SEM photographs reveal how filler structure develops as its volume fraction increases. The iron system shows the three regions of structure; Region 1 contains independent particles and clusters, Region 2 contains large clusters and individual particles within one structural diameter of each other, Region 3, at or above percolation, shows continuous veins of iron within the matrix. The mixtures indicate that either the ordering of the aluminum within the iron network must be responsible for the decrease in μ" with increasing aluminum at 0.4 volume fraction of iron, or the dilution of the mixture above phase inversion decreases μ". The aluminum also shows three distinct regions, though a planar structure develops with orientation of the flakes parallel to the film surfaces. At the critical percolation point, veins of aluminum flakes transverse along the length of the film. Finally, phase inversion occurs at approximately 0.45 volume fraction filler. The process of manufacturing the films

generates bubbles in the films at volume fractions less than 0.2 filler; above this value voids were formed in the mixtures. Both will decrease the calculated values of volume fraction filler present.

2.15 Summary of Chapter 2

Anticipating reflection and absorption characteristics of a material or electromagnetic processing of materials can be visualized by focusing on the total ε', ε'', μ', μ''. These values increase with volume fraction filler. The increase has been shown to be a function of material type, geometry, and critical volume fraction. The critical volume fractions occurred from 0.15 - 0.25. The critical volume fractions showed good agreement with theory Table 2.2. The critical concentrations for the solutions was less predictable and varied with solvent and chemistry. The low power findings correlated well with high power experiments. The low power experiments were used to identify the loss caused by the molecular motions. The loss mechanisms for the materials examined were ionic conductive, electronic conductive, and electronic and magnetic dipolar. These losses were dependent upon:

- Molecular architecture
- Concentration or volume fraction
- Temperature
- Frequency
- Solvent or local environment

It was hoped that, insights have been gained into how dielectric (ε', ε''), magnetic (μ',

μ") properties behave as a function of the above variables, which will lead to the ability to calculate the reflection and absorption characteristics from the sum of the constituents.

References

1. Stonier, R.A., *Stealth Aircraft and Technology from World War II to the Gulf.* SAMPE Journal, 1991. **27**(4): p. 9-17.

2. Smyth, C.P., *Static Dielectric Constant and Dipole Moment,* in *Dielectric Behavior and Structure.* 1955, Mcgraw-Hill: New York. p. 23-51.

3. von Hippel, A.R., *Dielectrics and Waves.* 1954, New York: John Wiley and Sons.

4. Lekner, J., *The Theory of Reflection.* 1986, . 1 - 10.

5. Knott, E.F., J.f. Shaeffer, and M.T. Tuley, *Radar Cross Section.* 1985, Dedham, MA: Artech House.

6. Onsager, L., Journal of the American Chemical Society, 1936. **58**: p. 1486.

7. Debye, P., *Polar Molecules.* 1929, New York: Chemical Catolog Company.

8. Van Krevelen, D.W., *Properties of Polymers.* 3 rd ed. 1990, Amsterdam: Elsevier.

9. Akhadov, Y.Y., *Dielectric Properties of Binary Solutions.* 1981, Oxford: Pergamon Press.

10. Mansfield, M.L., *Mean Square Dipole Moment of Excluded Volume Polymers.* Macromolecules, 1986. **19**: p. 1427-1430.

11. von Hippel, A. and W.B. Westphal. *Contributions to the Molecular Dielectric Analysis of Polar Liquids.* Lab. for Insulation Res. MIT. Dec. NIH-5-P01-HL14322-03

12. Kauzmann, W., *Dielectric Relaxation as a Chemical Rate Process.* Reviews of Modern Phsyics, 1942. **14**: p. 12-44.

13. Adachi, K. and T. Kotaka, *Dielectric Normal Mode Process in Semidilute and Concentrated Solutions of cis-Polyisoprene.* Macromolecules, 1988. **21**: p. 157-164.

14. Tveekrem, J.L., S.C. Greer, and D.T. Jacobs, *The Dielectric Constant Near the Liquid-Liquid Critical Point for Polystyrene in Diethyl Malonate.* Macromolecules, 1988. **27**(21): p. 147 - 153.

15. Phillips, P.J. and A.M. North, *Comparisons of the Dielectric and Viscoelastic Relaxations in Dilute Solutions of Some Acrylic Polymers.* Transactions of the Faraday Society, 1967. **63**: p. 1537 - 1545.

16. Phillips, P.J. and A.M. North, *Dielectric Properties of Poly-(N-vinlycarbazole) Solutions.* Chemical Communications, 1968. : p. 1340 - 1341.

17. Phillips, P.J. and A.M. North, *Dielectric Relaxation in Solutions of Poly(p-*

methoxyphenylacetylene) and Poly(p-chlorophenylacetylene). Transactions of the Faraday Society. 1968. **64**: p. 3235 - 3241.

18. Phillips, P.J. and G. Singh, *Dielectric Relaxation in Concentrated solutions of Poly(methyl Methacrylate).* Journal of Polymer Science: Polymer Physics Edition. 1975. **13**: p. 1377-1386.

19. Adachi, K., *et al., Dielectric Study of the Concentration Dependence of the End-to End Distance and Normal-Mode Relaxation Time of Polyisoprene in Moderately Good Solvents.* Macromolecules. 1989. **22**: p. 2391-2395.

20. Ying, Q. and B. Chu, *Overlap Concentration of Macromolecules in Solution.* Macromolecules. 1987. **20**: p. 362-366.

21. De Gennes, P.G., *Dynamics of Entangled Polymer Solutions I. The Rouse Model.* Macromolecules. 1976. **9**(4): p. 587-598.

22. De Gennes, P.G., *Dynamics of Entangeld Polymer Solutions II. Inclusion of Hydrodynamic Interactions.* Macromolecules. 1976. **9**(4): p. 594-598.

23. Doi, M. and S.F. Edwards, *Dynamics of Concentrated Polymer Solutions.* Journal of the Chemical Society Faraday Transactions 2. 1978. **74**: p. 1789-1801.

24. De Gennes, P.G. and F. Brochard, *Polymer-Polymer Interdiffusion.* Europhysics Letters. 1986. **1**(5): p. 221-224.

25. Composto, R.J., E.J. Kramer, and D.M. White, *Mutual Diffusion in the Miscible Polymer Blend Polystyrene/Poly(xylenyl ether).* Macromolecules. 1988. **21**: p. 2580-2588.

26. Palmstrom, C.J., P. Green, and E.J. Kramer, *Interdiffusion and Marker Movements in Concentrated Polymer-Polymer Diffusion Couples.* Polymer. 1984. **25**: p. 473-480.

27. Graessley, W.W., *Some Phenomenological Consequences of the Doi-Edwards Theory of Viscoelasticity.* Journal of Polymer Science: Polymer Physics Edition. 1980. **18**: p. 27-34.

28. Graessley, W.W. and M.J. Struglinski, *Effects of Polydispersity on the Linear Viscoelastic Properties of Entangled Polymers. 1. Experimental Observations for Binary Mixtures of Linear Polybutadiene.* Macromolecules. 1985. **18**: p. 2630-2643.

29. Graessley, W.W. and M.J. Struglinski, *Effects of Polydispersity on the Linear Viscoelastic Properties of Entalgled Polymers. 2. Comparison of Viscosity and Recoverable Compliance with Tube Model.* Macromolecules. 1986. **19**: p. 1754-1760.

30. Palmstrom, C.J., *et al., Limits of Reptation in Polymer Melts.* Physical Review Letters. 1984. **53**(22): p. 2145-2148.

31. Fowkes, F.M., *Attractive Forces at Interfaces.* Industrial and Engineering Chemistry, 1964. **56**(12): p. 40 - 53.

32. Fowkes, F.M. and R.L. Riddle, *Spectral Shifts in Acid-Base Chemistry. 1. Van der Walls Contributions to Acceptor Numbers.* Journal of Americal Chemical Society, 1990. **112**(9): p. 3259 - 3264.

33. Fowkes, F.M., *et al., Acid-Base Complexes of Polymers.* J. of Polymer Science: Polymer Chemistry Ed., 1984. **22**: p. 547 - 566.

34. van Oss, C.J., R.J. Good, and M.K. Chaudhury, *Additive and Nonadditive Surface Tension Components and Interpretation of Contact Angles.* Langmuir, 1988. **4**(4): p. 884 - 891.

35. Lifshitz, E.M., *The Theory of Molecular Attractive Forces Between Solids.* Soviet Physics, 1956. **2**(1): p. 73 - 83.

36. Barrow, *Physical Chemistry.* 3 ed. 1973, McGraw HIll. 617-625.

37. Kienle, R.H. and H.H. Race, *The Electrical, Chemical, and Physical Properties of Alkyd Resins.* Transactions of The Electrochemical Society, 1934. **35**: p. 87-107.

38. Whitehead, J.B., *Liquid Insulators.* Transactions of the Faraday Society, 1934. **65**: p. 35-46.

39. Rancourt, J.D. and L.T. Taylor, *Applications of Thermoelectrometry to Metal-Ion Modified Polyimide Films.* Journal of Thermal Analysis, 1986. **31**: p. 1131 - 1141.

40. Senturia, S., S.A. Bidstrup, and N.F. Sheppard. *Dielectric Analysis of the Cure of Thermosetting Epoxy/Amine Systems.* Massachusetts Institute of Technology. November 15,1986. NTIS. AD-A177 569

41. Senturia, S., W. Bidstrup, and N. Sheppard. *Monitoring of Laminate Cure with Microdielectrometry.* Massachusetts Institute of Technology. May 2, 1985. NTIS. AD-A150 863

42. Senturia, S.D. and N.F. Sheppard. *Chemical Interpretation of the Relaxed Permittivity During Epoxy Resin Cure.* Massachusetts Insistute of Technology. May 2, 1985. NTIS. AD-A150 955

43. Senturia, S. and N. Sheppard. *WLF Dependence of the Dielectric Properties of DGEBA Epoxy Resins.* Massachusetts Institute of Technology. August 23,1985. NTIS. AD-A159 224

44. Senturia, S., M.C.E. Coln, and N. Sheppard. *A Dielectric Study of the time-Temperature-Transformation (tTT) Diagram of DGEBA Epoxy Resins Cured with DDS.* in *29th National SAMPE Symposium.* 1984.

45. Senturia, S.D., N.F. Sheppart, and M.C.W. Coln. *A Dielectric Study of The time-Temperature-Transformation (tTT) Diegram of DGEBA Epoxy Resins Cured with DDS.*

Massachusetts Institute of Technology. December 14, 1983. NTIS. AD-A137 358

46. Senturia, S.D., *et al. Cure Monitoring and Control With Combined Dielectric/Temperature Probes.* Massachusetts Institute of Technology. Jananuary 10, 1983. NTIS. AD-A123 512

47. Senturia, S.D. *Understanding Dielectric Cure Monitoring.* Massachusetts Institute of Technology. October 5, 1982. NTIS. AD-A123 507

48. Senturia, S. and N.F. Sheppard, *Dielectric Analysis of Thermoset Cure.* Advances in Polymer Science, 1986. **80**: p. 1-47.

49. Pochan, J.M. and D.M. Pai, *Dielectric and Photoconductive Properties,* in *Plastics Polymer Science and Technology,* M.D. Baijal, Editor. 1982, John Wiley and Sons: New York.

50. Zallen, R., *The Physics of Amorphous Solids.* 1983, John Wiley and Sons, Inc.

51. Kirkpatrick, S., *Percolation and Conduction.* Reviews of Modern Physics, 1973. **45**(4): p. 574-588.

52. Kirkpatrick, S. and V.K.S. Shante, *An Introduction to Percolation Theory.* Advances in Physics, 1971. **20**: p. 325-355.

53. Zallen, R. and H. Scher, *Percolation on a Continuum and the Localization-Delocalization Transition in Amorphous Semiconductors.* Physical Review B, 1971. **4**(12): p. 4471-4479.

54. Fabish, T.J., *The Feasibility of Microwavable Foil-Based Container Stock.* 1990, Alcoa Laboratories:

55. Rizzi, P., *Microwave Engineering.* 1988, Prentice Hall.

56. Lederer, P.G. *An Introduction to Radar Absorbant Materials.* Royal Signals and Redar Establishment. 85016

57. Knott, E.F., *The Thickness Criterion for Single-Layer Radar Absorbents.* IEEE Transaction of Antennas and Propogation, 1979. **27**(5): p. 698 - 701.

58. Moore, R.L., A. MacDonald, and H.R. Moroz, *Permittivitty of Fiber-Polymer Composites: A Study to Determine the Effects of The Environment.* Microwave Journal, 1991. : p. 67-82.

59. Verbicky, J.W., *Polyimides,* in *Encyclopedia of Polymer Science,* H. Mark, *et al.*, Editor. John Wiley and Sons: New York. p. 364-383.

60. Odian, G., *Principles of Polymerization.* 2 ed. 1981, New York: John Wiley and Sons, Inc.

61. Chen, P., *et al., Recent Developments In Fluoro-containing Polyamideimides,* in

High Performance Polymers. 1990, p. 39-46.

62. Rzpecka, M.A., *A Cavity Perturbation Method for Routine Permittivity Measurement.* Journal of Microwave Power. 1973. **8**(1): p. 3 - 11.

63. Manring, E.B., *An Experimental Investigation of the Microwave Heating of Solid Non-Reactive Materials in a Circular Cylindrical Resonant Cavity.* 1988, MIchigan State Univeristy:

64. Jow, J., *et al., Microwave Processing and Diagnosis of Chemically Reacting Materials in a Single-Mode Cavity Applicator.* IEEE Transactions on Microwave Theory and Techniques. 1987. **35**(12): p. 1435 - 1443.

65. Jow, J., *Microwave Processing and Dielectric Diagnosis of Polymers and Composites Using a Single-Mode Resonant Cavity Technique.* 1988, Michigan State University:

66. Somlo, P.I. *The Discontinuity Capacitance and the Effective Position of a Shielded Open Circuit in a Coaxial Line.* in *Proceedings Institution of Radio and electronic Engineers.* 1967. Australia:

67. Bussey, H.E., *Dielectric Measurements in a Shielded Open Circuit Coaxial Line.* IEEE Transactionns on Instrumentation and Measurement. 1980. **29**(2): p. 120-124.

68. Stuchly, S.S. and G. Gajda, *The Equivalent Circuit of an Open-Ended Coaxial Line.* IEEE Transactions on Instrumentation and Measurement. 1983. **32**(4): p. 506 - 508.

69. Stuchly, M., *et al., Measurement of Radio Freqency Permittivity Biological Tissues with an Open-Ended Coaxial Line: Part II Experimental Results.* IEEE Transactions on Microwave Theory and Techniques. 1982. **30**(1): p. 87-92.

70. Stuchly, M., S.S. Stuchly, and T.W. Sthey, *Measurement of Radio Frequency Permittivity of Biological Tissues with an Open-ended Coacial Line: Part 1.* IEEE Transactions on Microwave Theory and Techniques. 1982. **30**(1): p. 82-86.

71. Stuchly, S.S., *et al., On the Measurement Accuracy of the Tissue Permittivity In Vivo.* IEEE Transactions on Instrumentation and Measurement. 1983. **32**(1): p. 37 - 42.

72. Stuchly, M.A. and S.S. Stuchly, ed. *A Six-Octive Experiment System for In-Vivo and In-Vitro Dielectrc Measurements.* Interactions Between Electromagnetic Fields and Cells, ed. A. Chiabrera, C. Nicolini, andH.P. Schwan. 1985, Plenum Pub.: New York. 117 - 129.

73. Stuchly, M.A., *et al., Dielectric Properties of Liposome Vesicles at the Phase Transition.* Physics in Medicine Biology. 1988. **33**(11): p. 1309 - 1324.

74. Stuchly, S.S., *et al., Dielectric Properties of Breast Carcinoma and the Surrounding Tissue.* IEEE Transactions of Biomedical Engineering. 1988. **35**(4): p. 257 - 263.

75. Stuchly, S.S. and K.P.A.P. Esselle, *Capacitive Sensors for In-Vivo Measurments fo the Dielectric Properties of Biological Materials.* IEEE Transactions on Instrumentation and Measurement, 1988. **37**(1): p. 101 - 105.

76. Stuchly, M., *et al., Dielectric Properties of Liposome Vessicles at the Phase Transition.* Physics in Medicine and Biology, 1988. **33**(11): p. 1309-1324.

77. Stuchly, S., *et al., Dielectric Properties fo Breast Carcinoma and the Surrounding Tissues.* IEEE Transactions on Biomedical Engineering, 1988. **35**(4): p. 257-263.

78. Chen, M., *Electromagnetic Radiation Calorimetry of Thermoplastics, Elastomer, and Composites Systems.* 1989, Virginia Polytechnic Institute and State University:

79. Hewlett Packard. *Measuring Dielectric Constant with the HP 8510 Network Analyzer.* Product Note. 8510-3

80. Dyer, J.r., *Applications of Absorption Spectroscopy of Organic Compounds.* 1965, Englewood Cliffs: Prentics-Hall.

Chapter 3

Volatiles in and Low Temperature Aging of a Poly(amide-imide)

3.1 Introduction

Optimizing microwave or thermal processing of the poly(amide-imide) requires a thorough knowledge of volatile content (water and n-methyl-2-pyrolidone). Reducing these volatiles resulted in improved temperature vs. time profiles and dimensional stability. Sample matrices of fully cured and uncured poly(amide-imide) were subjected to a series of dielectric and thermal characterization techniques. Both fully cured and uncured samples were tested in the varied conditions of dried, as received, and saturated-with-water. The techniques included dielectric analysis at 2.45 GHz, thermogravimetry (TG), thermogravimetry-mass spectrometry (TG-MS), thermomechanical analysis (TMA), and dynamic mechanical thermal analysis (DMTA). Most thermal characterization experiments were conducted in both the temperature and time domains.

The purpose of using these techniques was to examine the influence of water and low temperature aging from 20 to 50°C on either the dielectric or dynamic mechanical properties of a poly(amide-imide). Thermogravimetry was used to monitor weight percent loss of volatiles and the kinetics of their desorbtion. TG-MS was used to identify water and NMP as the volatiles desorbed during heating. Thermomechanical analysis was used to identify the point at which volatiles caused irreversible expansion of the poly(amide-imide) sheet. At heating rates of 20°C/min, this occurred below the glass transition temperature of 265°C at 235°C. Dynamic mechanical properties were shown to be a function of cure, volatiles content and low temperature aging. The activation

energies for the β transition were shown to be a function of the temperature and time of low temperature aging. This chapter is divided into characterization techniques and microwave and thermal processing with each section containing a Results, Discussion, and Conclusions section.

Low power dielectric analysis is essential to understanding the high power microwave processing of the poly(amide-imide) due to the proportionality between heating rate and ε". The dielectric properties were dependent upon volatiles content and glass transition temperature. Poly(amide-imide) balls were processed in both thermal and microwave environments. Their cross-sections were examined for structural differences by scanning electron microscopy (SEM). The pictures revealed, for the undried balls, that the thermally processed ones had a skin formation around the exterior that trapped the volatiles, causing a cell structure to occur. The microwaved balls produced no exterior skin and the escape of the volatiles proceeded through the surface-air interphase. Finally, removal of volatiles and a rapid thermal temperature-time profile were combined to show that 0.4" in diameter poly(amide-imide) balls could be brought to a high processing temperature of 275°C within three hours and dimensional stability maintained within 0.001" on either the seam or off seam axis as shown in Figure 3.3. Drying 0.3" in diameter rod at 180°C for 12 hours under vacuum allowed microwave processing at 290°C for eight hours. This advanced the core T_g 8°C, though the sample diameter of the rod increased 20%.

3.2 Literature Review

The ingression of water has significant influence on mechanical properties of glassy

polymers. It has been shown to effect modulus [1-4] and fatigue properties of nylons [5]. The water exists in a few different forms in polymers and appears to ingress into the polymer in a few stages. In the first stage the water ingresses into the free volume of the polymer and forms H-bonds [1, 6, 7]. The hydrogen bonding has been confirmed by infrared and NMR experiments [1, 6-12]. At higher percent water, the water forms clusters [1, 6, 8, 13, 14]. Gas phase water clusters have been shown to be stable by mass spectroscopy [15]. Water clustering has been shown to be a function of the amount of ions present in Nafion® polymers [16, 17]. Nafion is a perfluorosulfonic acid polymer. As the concentration of water increased, the magnitude of the β relaxation in the dynamic mechanical thermal analysis increased [18-20]. These data were complemented by water absorption studies [21], which indicated a temperature and time dependence of water absorption when fluctuating in temperatures above and below the β transition [19]. Impact resistance has been shown to be dependent upon the β transition [22]. The relationship between molecular motion and mechanical properties has been reviewed by Boyer [23-25], McCrum [26], Hunston [27], and Hadley [28].

The effect of water and other small molecules on the DMTA spectra has been observed by Mohajer [29] and Robeson [30]. In Gillham's work on water ingression into polyimides, he tabulates the type of polyimide and the maximum in water peak at low temperatures from -90 to -120°C at 1 Hz [31]. This peak in the dielectric region has been determined by Johnson [14] to be due to both clustered and H-bonded water. Increasing the amount of clustered water increases the magnitude of the peak as shown in Figure 3.1a. Figure 3.1a illustrates a plot of ε" vs. temperature at 1 kHz. The total percent water was the same though the percent of clustered water was varied. The threshold water concentration for cluster formation can be seen by DSC. Figure 3.1b is

a series of DSC scans for poly(vinylacetate) with increasing percents of water. The 4.6% water shows a melt transition after 0°C for clustered water, therefore, for polyvinylacetate the percent of water needed to form water clusters was greater than 4%.

From DMTA and DETA, hydrogen bonding activation energies can be determined. They can be compared to a table of hydrogen bonding energies found in the book entitled, The Hydrogen Bond by Pimentel [32] page 214 or in von Hippel's dielectric analysis of ice [33]. The values range from 15 to 30 kJ/(M of hydrogen bonds).

3.2.1 Physical Aging

Physical aging of glasses was associated with densification of the polymer below Tg. Experiments have been conducted by Struik [34] on creep behavior of many polymers and reviewed by Van Krevelen [35]. The physical aging has been modeled by Alkonis [36] for both expansion and contraction experiments. The volume temperature response is shown in Figure 3.2a. The region where physical aging was proposed to occur was between Tg and the temperature of the highest secondary transition. One set of experiments conducted at the same aging time but at different Tg - T values, showed that increasing Tg - T slowed the rate of creep. The relationship between relaxation time and Tg - T is illustrated in Figure 3.2b. Increasing Tg - T increases the relaxation times. Recent dilatometric measurements by Lee on atactic polystyrenes indicate that volume relaxation can occur below the β transition [37]. These data supported work done by Moraglio [38] and Bianchi [39] and Reed and Dean [40]. The low temperature aging will provide an alternative explanation for the temperature-time dependence for the

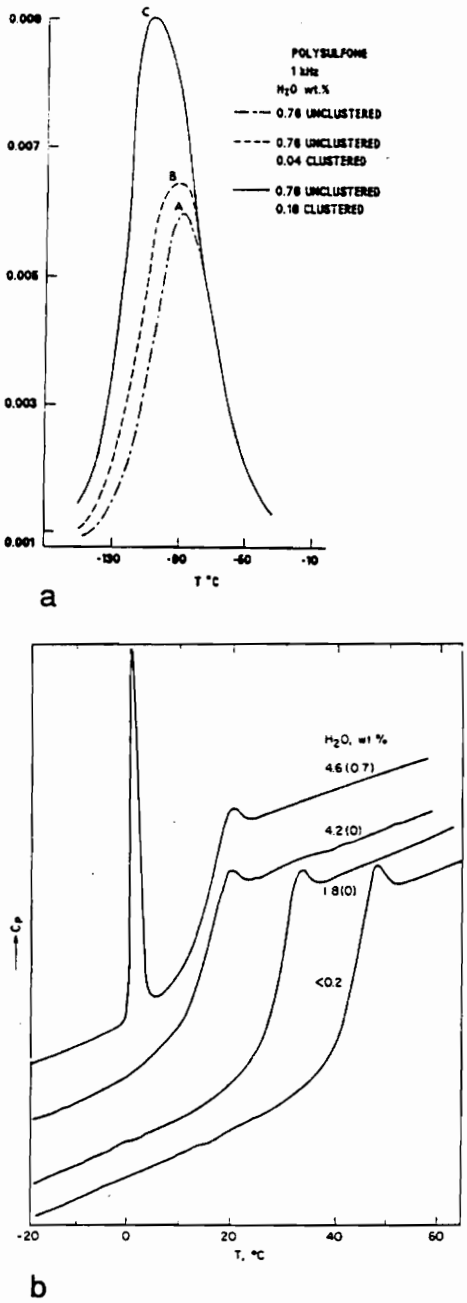

Figure 3.1

a. A plot of ε" vs. temperature, illustrating the effect of clustered water on the polysulfone β transition's dielectric response. b. DSC curves for polyvinylacetate as a function of total percent water content (clustered percent in parentheses) [14].

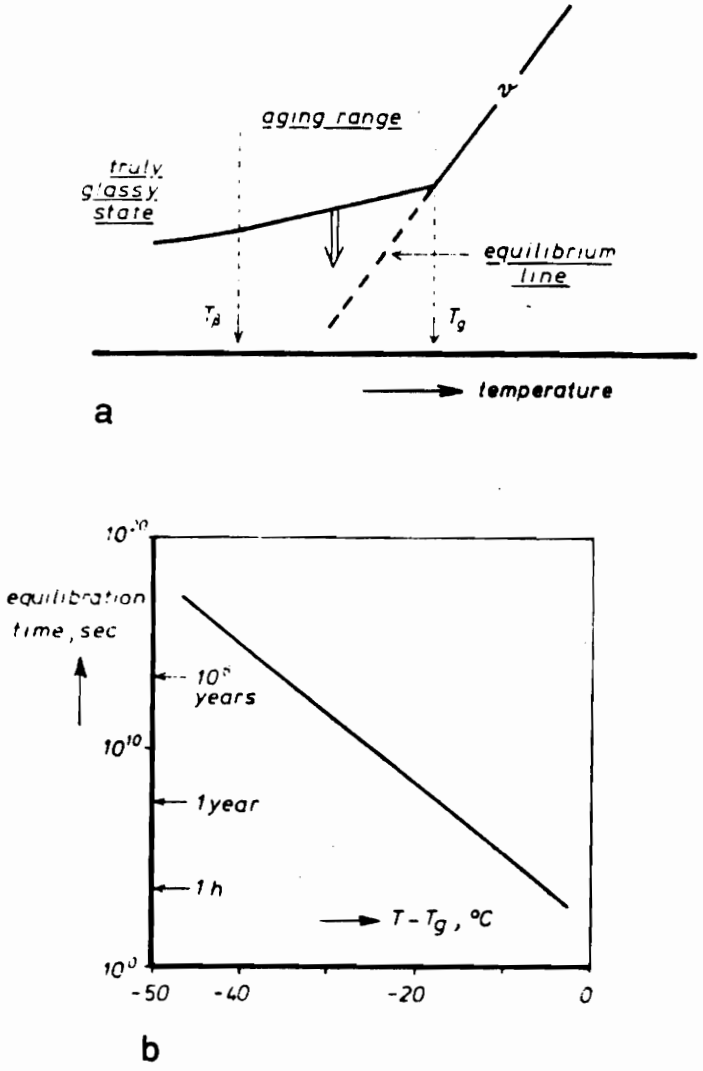

Figure 3.2

a. Specific volume vs. temperature plot, shows the origin of aging: Tg is the glass transition temperature, Tβ the temperature of the highest secondary transition. b. Illustrates the variation of relaxation time τ in the glassy state with temperature T - Tg [34].

water absorption studies.

3.2.2 Dynamic Mechanical Thermal Analysis

Dynamic mechanical thermal analysis (DMTA) is a forced oscillation experiment. The mechanical wave that is propagated through a sample can be either elastically stored or dissipated by small or large scale molecular motion. The stored energy is related to the storage modulus, E', while the dissipated energy is related to the loss modulus, E". The dissipation occurs when a mechanical motion within the polymer can couple with the applied frequency. DMTA actually measures a stiffness and phase angle shift from the applied and detected wave. E' and E" were converted from this through geometry constraints. A simplified version of the mechanical forced oscillation equation is given by Equation 3.1.

$$F_p \sin(\omega t) = \frac{M dx^2}{d^2 t} + b\frac{dx}{dt} + kx \qquad \text{Eq. 3.1}$$

where: Fp = peak force from vibrator
M = mass of vibrating system
b is proportional to viscous damping
ω = angular frequency $2\pi f$
x = axial displacement
t = time
k = complex stiffness of system

The complete equation and conversion to E' and E" are given in the Polymer Labs Instruction Manual.

At this point it is useful to compare this mechanical forced oscillation equation with the

electrical one in Equation 3.2. Equation 3.2 describes the motion of an electronic oscillator subjected to a driving force.

$$\frac{d^2z}{d^2t} + \frac{2\alpha dz}{dt} + \omega_0^2 z = \frac{e}{m} E' e^{i\omega t} \qquad \text{Eq. 3.2}$$

where z = location
t = time
ω_o = resonant frequency
m = mass of electron
e = charge of electron
E' = local electric field strength
2α = friction factor

There are similarities to these equations in that they are both forced oscillation experiments with similar variables. Their difference is that the propagating wave is a mechanical one for E' and E", while it is an electrical one for ε' and $\varepsilon"$. The loss mechanism for the electrical experiment is either ionic, electronic, dipolar, or atomic. These motions are orders of magnitude less in mass than that involved in the coupling of a β transition or the segmental motion of 5 to 20 repeat units associated with the glass transition.

To date many experimental techniques have been used to study the effect of water on polymers. These show that water exists in many forms within a polymer, either hydrogen bonded or in clusters. Its presence also has been correlated to an increase in magnitude of the β transition and a decrease in Tg. However, some questionable research has been done with improper drying of polymers. The drying was done only at temperatures of from 90 to 120°C, which was not high enough in temperature to

eliminate completely the water. Drying should be done above Tg or at least above the upper region of the β transition with a high Tg polymer. The second generalization should be complemented by thermogravimetry. Thus, the purpose of this work will be to reproduce some literature observations for thermal scans of DMTA and DETA and extend these experiments to transient behavior, along with observations on low temperature aging below the peak of the β transition.

3.3 Theory

3.3.1 First Order Events

The data from Thermogravimetry (TG) and Dynamic Mechanical Thermal Analysis (DMTA) were used in conjunction with theoretical models to evaluate the kinetics of volatile desorbtion and activation energies of mechanical motion for the β transition of poly(amide-imide). The isothermal plots of weight loss as a function of time could be plotted as the natural logarithm of the weight percent loss as a function of time to illustrate first order volatile desorbtion. For ~90% of the weight loss, the plots showed primarily first order behavior. This is supported by diluent desorbtion work conducted by Errede [41].

A first order reaction of A is given by Equation 3.3:

$$-\frac{d[A]}{dt} = k[A] \qquad \text{Eq. 3.3}$$

Equation 3.3 can be separated and integrated to give Equation 3.4:

$$\ln([A]_t/[A]_o) = -kt \qquad \text{Eq. 3.4}$$

A is the concentration of the species leaving initially (0) and at any time (t).

3.3.2 Graphical Methods to Determine Activation Energies

Graphical methods can be used to explore thermodynamic aspects of mechanical motion of the β transition. The Gibbs function of activation (ΔG^*) can be defined through Equation 3.5

$$-RT \ln k' = \Delta G^* \qquad \text{Eq. 3.5}$$

where R is the gas constant, T is temperature in degrees Kelvin, k' is the jump rate for the β transition, and ΔG^* is the molar free energy of activation.

Assuming ΔG^* is not temperature dependent, the slope of ln k' plotted against 1/T or d ln k'/d1/T will equal $-\Delta G^*/R$. Since $\Delta G = \Delta H - T\,\Delta S$, the right hand side of the equation can be substituted into Equation 3.5. The method of Kauzmann based upon transition state theory can be used to graphically determine the enthalpic and entropic values. The assumptions behind the Kauzmann method is that ΔG^* is not a function of T, and the transition that is occurring is a simple relaxation. The slope(s) obtained from the plot of ln τT (where τ is the relaxation time) against 1/T, is related to these quantities by Equation 3.6 and Equation 3.7:

$$\Delta H^* = 2.303Rs - RT \qquad \text{Eq. 3.6}$$

$$\Delta S^* = 2.303R(\log K' - \log kT/h + s/T) - R \qquad \text{Eq. 3.7}$$

h = Planck's constant 6.626 x 10 -34 J•s
k = Boltzman's constant 1.38 x 10 -23 J/K

Assuming that ΔG^* is temperature dependent, the value of the derivative is given by Equation 3.8.

$$\frac{d \ln k}{d 1/T} = - \frac{\Delta H}{R} \qquad \text{Eq. 3.8}$$

The derivation is given in Appendix 2.

3.4 Experimental

3.4.1 Thermal Analysis Equipment

The experimental section focuses on sample preparation and instrumentation used to evaluate or process the poly(amide-imide) samples. The samples were the poly(amide-imide) ~0.65 mm thick sheet, 1.5 mm in diameter rod, and 10 mm (0.4") or 13 mm (0.5") in diameter balls, and powder. The samples were analysed as as received, dried, or saturated with water. Each will be underlined throughout the text to help the reader identify each sample. Drying was done under vacuum in a National Appliance Company model 5831 vacuum oven at temperatures from 155 to 190°C from 3 to 24 hours. The curing of the poly(amide-imide) balls was done in a Fisher programmable oven or a Hewlett Packard model 5890A Gas Chromatography oven preheated to 288°C. To monitor the temperature of the poly(amide-imide) balls during isothermal curing, one poly(amide-imide) ball was drilled and a temperature probe placed inside it. The balls were held so their interior temperature was ~280°C for 900 seconds. The fully cured sheet and rod samples were obtained as received or cured in a nine day cure cycle in-house. For the in-house cure, temperature vs. time profile was chosen similar to that

house. For the in-house cure, temperature vs. time profile was chosen similar to that recommended in trade literature. The samples for DMTA were prepared by cutting the sheet with a razor blade, always in the same machine direction. The edges were sanded and their dimensions measured with calipers. The samples saturated with water were prepared by refluxing in water from 12 to 44 hours. Samples less than 10 mm in width were used because they saturated within 12 hours; larger ones (> 18 mm) took more than a day to become saturated. The diameter of the rod used, for dielectric measurement, was determined by averaging at least 10 measurements, five on each axis. The samples for thermogravimetry, which were cut from the poly(amide-imide), sheet weighed between 10 to 15 mg.

The thermogravimetry, differential scanning calorimetry, and dynamic mechanical analysis equipment included the TA instruments Thermal Analyst 2100 computer was connected to either a 951 Thermogravimetric Analyzer, a 912 Differential Scanning Calorimeter, or a 953 Dynamic Mechanical Analyzer. Perkin Elmer Thermal Mechanical Analyzer (TMA) and Thermogravimetric Analyzer (TG) were used to monitor dimensional changes and weight loss, respectively. These were connected to Perkin Elmer TAC7/PC for data collection and control. These instruments were used in either temperature sweep or isothermal modes. A Polymer Labs DMTA, with small frames in single cantilever mode, was used to evaluate the dynamic mechanical properties as a function of temperature and time. The frequencies chosen were from 0.03 to 30 Hz for the DMTA and from 0.1 to 2.5 for the DMA. The temperature range was from -140 to 300°C for the DMTA and from -75 to 230°C for the DMA. The starting point for the 150°C isothermal E" vs. time runs were determined from the temperature vs. time profile. It was the time at which the temperature first reaches 150°C. This starting

time was about seven to nine minutes after the start of the experiment.

3.4.2 Thermogravimetry-Mass Spectrometry

Thermogravimetry-Mass Spectral (TG-MS) analysis was done with a Perkin Elmer TAS 2 TGA connected by a capillary transfer line to a Hewlett Packard mass selective detector. A heating rate of 40°C/min was used so that the volatiles would rapidly desorb from the sample. Helium was used as a carrier gas at a pressure of 40 psi.

3.4.3 Thermomechanical Analysis

Thermomechanical analysis was undertaken in the penetration mode with 10 mN of force. The purge gas was nitrogen and the heating rate was typically 20°C/min. These experiments were run between 30 to 300°C. The onset of dimensional changes was determined by manufacturer supplied software.

3.4.4 Dielectric Thermal Analysis at 2.45 GHz

Dielectric thermal analysis was done by a cavity perturbation technique at a single frequency in a WR 430 waveguide. A shift in resonant frequency relative to the empty cavity was related to a change of ε' and a shift in cavity Q compared to the unfilled cavity was related to ε''. The Q and resonant frequency values were obtained from a Hewlett Packard 8510 Network Analyzer and manipulated on Hewlett Packard hardware and in-house designed software. The temperature was controlled by blowing nitrogen through a heated sand bath and passing it around the sample, which was contained within a Teflon®

tube.

3.4.4 7" Cylindrical Cavity

The microwave experiments were done in a 7" tuneable cylindrical cavity coaxially connected to an 85 W maximum power magnetron. The electric field mode selected for processing was TE_{111}. This mode has planar electric fields parallel to the bottom plate. The highest electric field strength is in the geometric center. The electric field pattern within the cavity is manipulated by adjusting a sliding short (top wall of the cavity) and the depth of a center conductor of coaxial airline into the cavity. The coaxial airline guides the power into the cavity. Adjusting these two pieces was how the reflected power was controlled to adjust the power vs. time profiles.

There were two types of sample shapes, disks and balls. The items were placed on a 1" round Teflon® rod ~3 cm off the bottom. The temperature was monitored by a Luxtron 750 fluoroptic probe. For the disks, two probes were put in direct contact. For the balls, a hole was drilled into its center and the temperature probe was inserted. It was protected by a glass capillary as shown in Figure 3.3.

3.5 Thermogravimetry

3.5.1 Results

The weight percent vs. temperature data of uncured as received poly(amide-imide) showed ~2.3% weight loss (volatiles) between 40 - 320°C as shown in Figure 3.4. Isothermal runs at 145°C, 155°C, and 165°C were done to obtain the rate of volatile

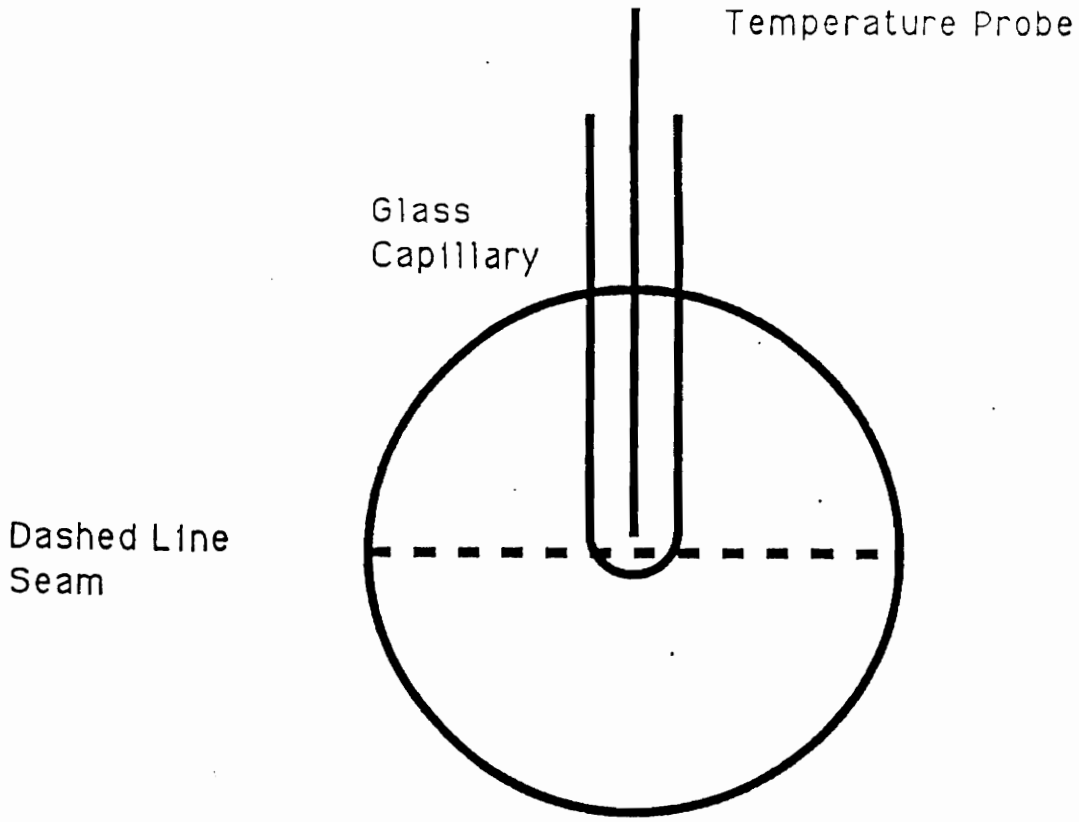

Figure 3.3

Poly(amide-imide) ball with temperature probe.

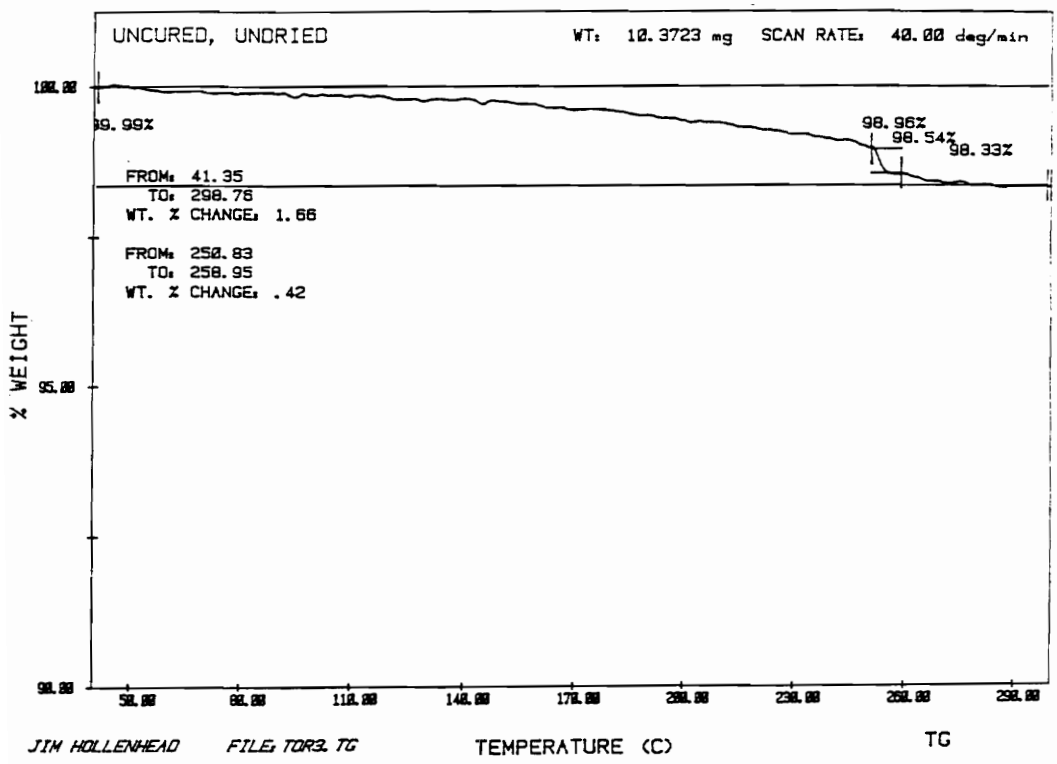

Figure 3.4

Weight percent vs. temperature for the poly(amide-imide) uncured as received.

desorbtion. A comparison of the 145°C, 155°C, and 165°C runs is shown in Figure 3.5. The desorbtion rate at 155°C was faster than at 145°C. The 155°C and 165°C runs were shown to be indistinguishable. The desorbtion rates proved to be primarily first order over ~90 % of the weight loss region. This was determined by a linear relationship between ln weight percent vs. time.

Identification of the volatiles was undertaken by TG-MS method. An example of the weight loss as a function of temperature for a heating rate of 40°C/min was similar to Figure 3.4. The T_g occurred at five minutes during the TGA-MS experiment. A 2 - 2.5% weight loss occurred at 255°C, near the 260°C T_g as measured by DSC. The composite mass-to-charge ratios are shown in Figure 3.6. The peak at 28 was due to N_2. The other peak at 18 was due to water and those at 44 and 96 were due to NMP. The peaks for NMP were confirmed by running an NMP blank and comparing the resulting spectrum to those in a library of spectra. The evolution of water (18) and NMP (96), as a function of time is shown in Figures 3.7 a and b. respectively. The water signal relative to the background spanned from two to nine minutes with a peak at 5.5 minutes. The NMP signal above background spanned from six to nine minutes with a peak at eight minutes.

3.5.2 Discussion

Thermogravimetry and thermogravimetry-mass spectroscopy confirm that from 2 to 2.5% volatiles remain from processing or were reabsorbed while exposed to the atmosphere. They were identified as water and n-methyl pyrolidone (NMP).

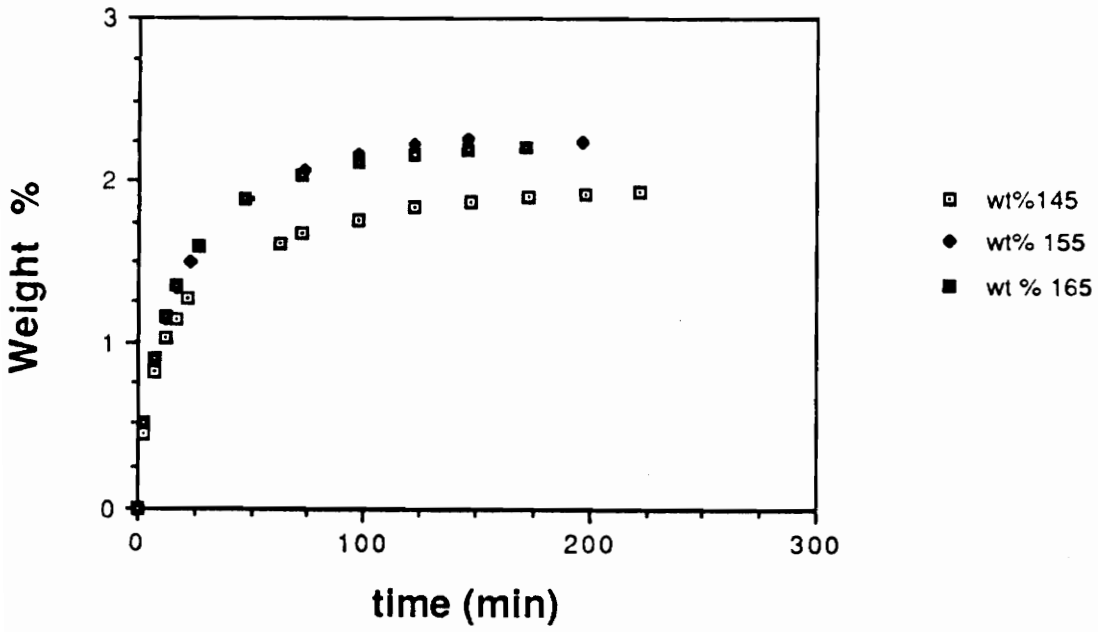

Figure 3.5

Weight percent volatiles evolved vs. time in minutes for 145°C 155°C, and 165°C isothermal experiments for the poly(amide-imide) uncured as received.

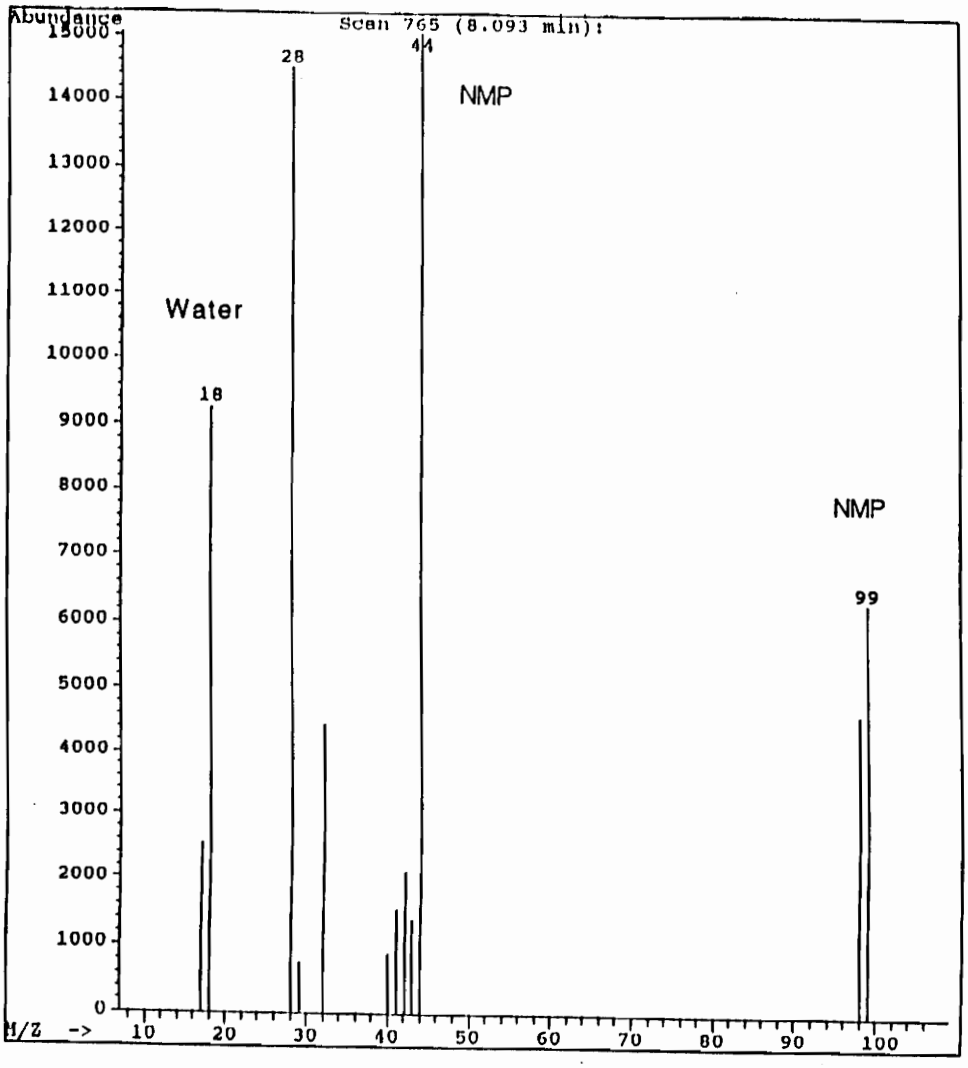

Figure 3.6

Abundance vs. mass to charge ratio for uncured poly(amide-imide) as received.

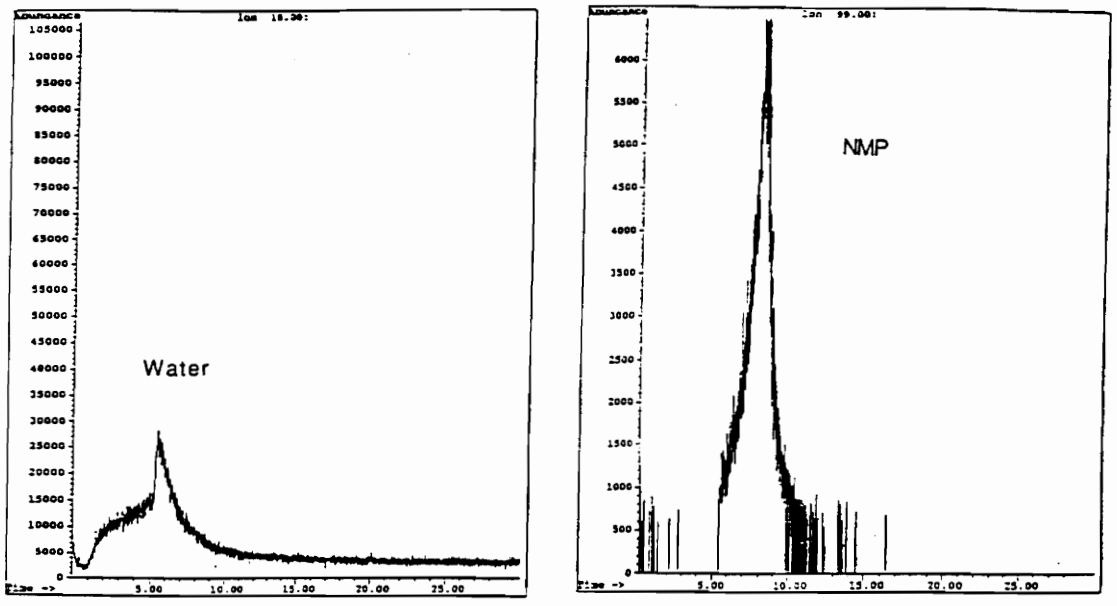

Figure 3.7

a. Water signal (18) as a function of time and (b) is NMP signal as a function of time for the poly(amide-imide) uncured as received.

The water was absorbed from the atmosphere, while the NMP stayed in the polymer from the synthesis. A heating rate of 40°C/min was chosen for the TG-MS experiment so that a large quantity of volatiles would evolve quickly. The detector was sensitive only to the higher concentration of volatiles and would not have been able to detect volatiles evolving under isothermal conditions. For the weight loss vs. temperature profile for the TG-MS a sharp drop in the weight percent occurs at the T_g. At the T_g large scale molecular motion commences and volatiles can escape from the glassy matrix more easily. Water seems to come off just before T_g, and NMP afterward. Their precise desorbtion times were not known since the residence time of each compound in the transfer line was not known.

The temperature vs. time profile chosen to simulate isothermal conditions for thermogravimetry includes a 40°C/min initial heating rate to reach the isothermal temperature. Thus, a start time of approximately three minutes was chosen as time equal to zero. The Dupont instrument produces a simulated weight gain or hump in the signal at the beginning of the experiment due to the expansion of the horizontal quartz weighing arm. The time to reach isothermal conditions, approximately the three-minute mark occurred after this hump. This made a real initial start time was difficult to define, which lead to errors of a few tenths of a percent of weight. Any irregularities in the isothermal runs could be due to different total uptakes of volatiles within each poly(amide-imide) sample. The overlap of 165°C and 155°C isothermal runs was confirmed a few times. This is unexplainable at this time.

3.5.3 Conclusions

Uncured poly(amide-imide) has 2 - 2.5% volatiles as received. This compares well to literature for poly(amide-imide) at 23°C and 30% relative humidity. The volatiles were NMP and water. An increase in isothermal drying temperature showed increased rate of volatile desorbtion for 0.6 mm sheet. The isothermal runs showed almost total elimination of volatiles though it was not known whether NMP was completely gone after these experiments.

3.6 Thermomechanical Analysis

3.6.1 Results

Thermomechanical analysis was done on as received and dried uncured poly(amide-imide). This comparison was undertaken to identify when irreversible expansion occurred in the poly(amide-imide) sheet. Figure 3.8a is the poly(amide-imide) uncured as received. Irreversible expansion occurs at ~235°C. Figure 3.8b shows a plot of linear dimensions vs. temperature for dried poly(amide-imide) uncured. Irreversible penetration does not occur until 265°C.

3.6.2 Discussion

The volatiles cause irreversible deformation of the sheet surface. This occurs at 235°C, when blisters were formed at the surface and a cell structure was formed in the interior. The drying seems to eliminate the expansion that occurs near Tg. This can be useful when processing since it was important to get above Tg to advance the cure. These dimensional changes occurred at a heating rate 20°C/min; no data was collected to examine the effects of varying heating rate.

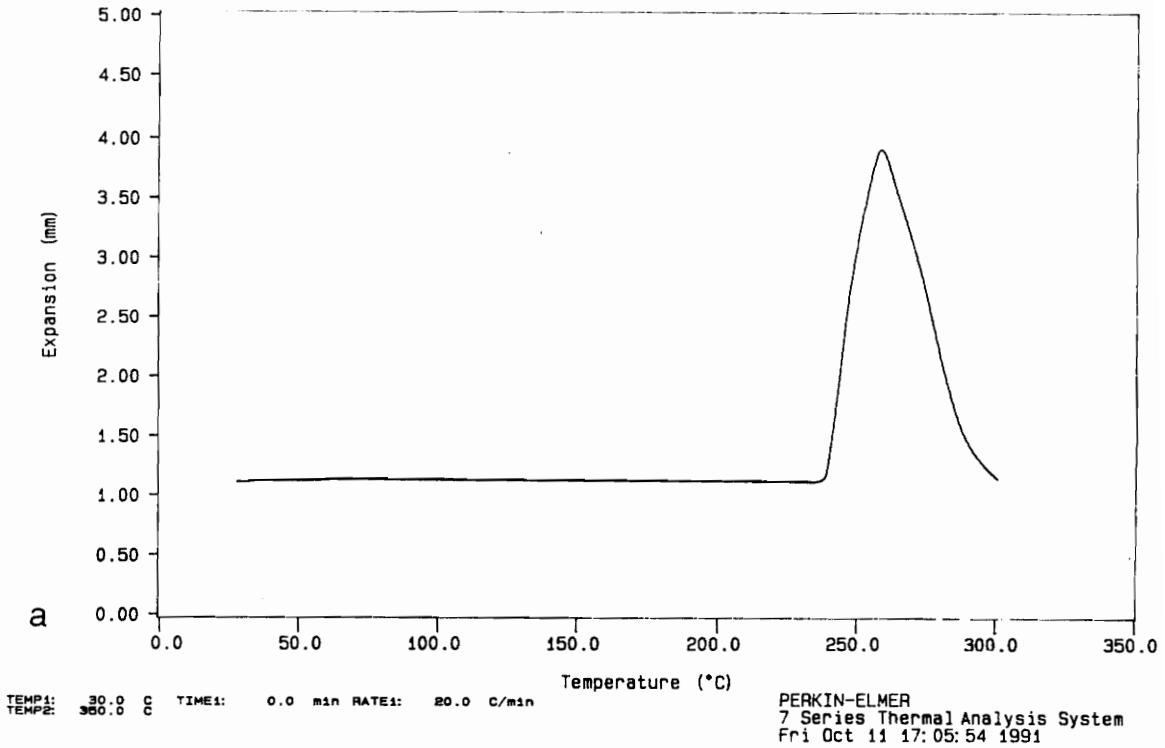

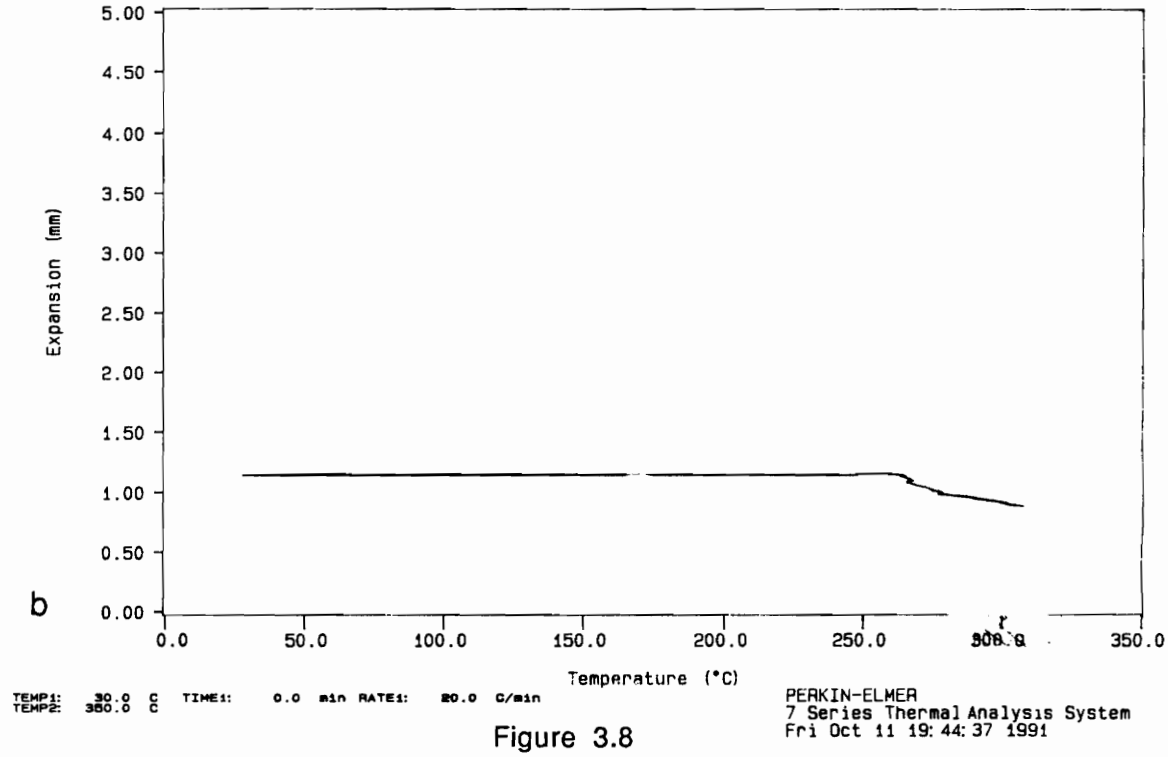

Figure 3.8

a. Dimensional changes vs. temperature for <u>as received</u> poly(amide-imide) uncured. b. Dimensional changes vs. temperature for <u>dried</u> poly(amide-imide) uncured.

Presumably, a slower heating rate might allow the volatiles to escape while heating so no expansion would occur.

3.6.3 Conclusions

Heating as received uncured poly(amide-imide) at 20°C/min causes irreversible expansion of the sheet at 235°C. Drying the sample at 190°C for 3 hours reduces the volatiles enough so that this does not occur; only penetration occurs at 265°C.

3.7 Dynamic Mechanical Thermal Analysis

3.7.1 Results

The influence of drying, aging time, and addition of water on mechanical properties were explored. The weight percentage of water in a sample saturated with water compared to the dried samples was between 4 to 4.5% as measured by weight gain. The extra weight from volatiles for as received poly(amide-imide) was between 2 to 2.5% when compared to the dried samples. The drying was done under vacuum with temperatures ranging from 160 to 190°C from 3 - 24 hours. The DMTA storage and loss modulus (E', E") for as received poly(amide-imide) uncured and fully cured are presented in Figures 3.9a and b. A difference in the Tg peak for E" was noticed between the fully cured and uncured systems. The fully cured has an average peak shift approximately 20°C greater than the uncured system. The β transition for the fully cured system was ~40°C less than the uncured system.

The E" vs. temperature of uncured as received and saturated with water are shown in Figures 3.10 a and b. The β transition was shown to be extremely sensitive to the

addition of water. A shift to higher temperatures of approximately 80°C was observed. Also, a broadening of the peaks was observed. The DMA was used to identify the breadth of the peaks as a function of temperature and confirm the findings of the DMTA. Another water relaxation can be identified in the low temperature range from -100 to -80°C of the E" vs. temperature spectra. Figures 3.11a and b illustrate a comparison between fully cured as received and fully cured dried. The dried and saturated samples of the fully cured system also were compared. A shift of ~70°C in the β transition from ~ 40 to 110°C was observed between the dried and saturated samples. Since the β transition showed such sensitivity to water, isothermal runs at 150°C were undertaken to compare the saturated with water to the dried samples. These were done at 0.2 Hz for 60 minutes.

Plots of E" vs. time for dried and water saturated uncured and fully cured systems are shown in Figures 3.12 a and b. The as received values were intermediate between the wet and dry curves. There was a progressively larger change in E" as the percent of volatiles increases. The maximum change in loss modulus for the uncured system was approximately 0.4 log modulus units. The reproducibility for the uncured data was confirmed by cycling the *same sample* between dried and saturated conditions. The E" of the fully cured system does not change as significantly with time compared to the uncured poly(amide-imide). The time scale of change for E" was similar in time scale to water desorbtion as determined by thermogravimetry as shown in Figure 3.5.

The physical aging of as received fully cured poly(amide-imide) below the β transition was determined dynamic-mechanically by running analogous experiments to those done for physical aging involving the α transition. The *same sample* was held at 190°C in a

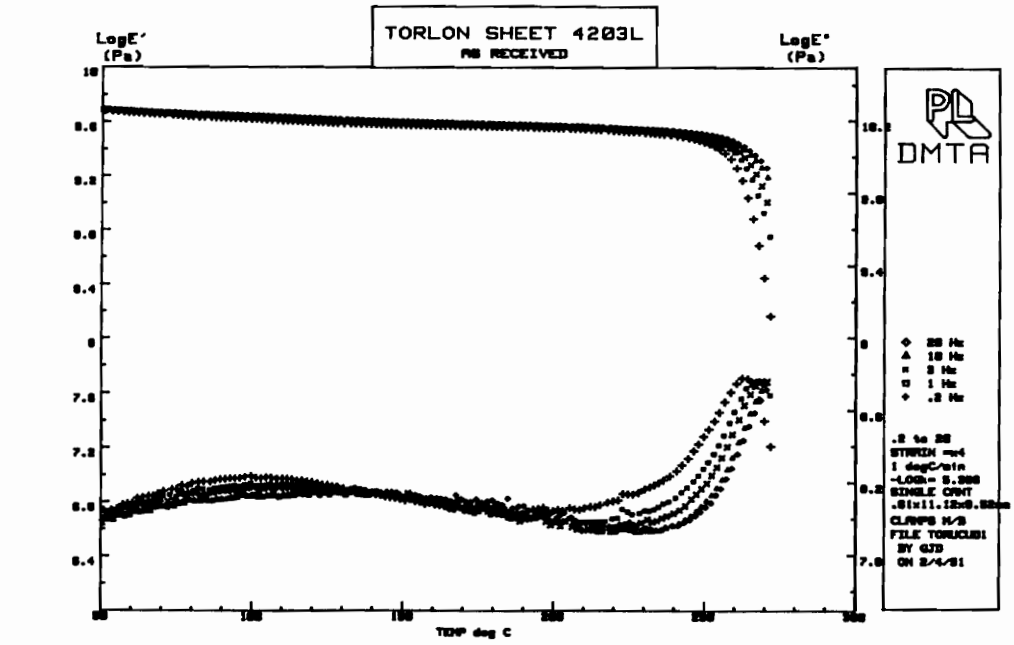

a

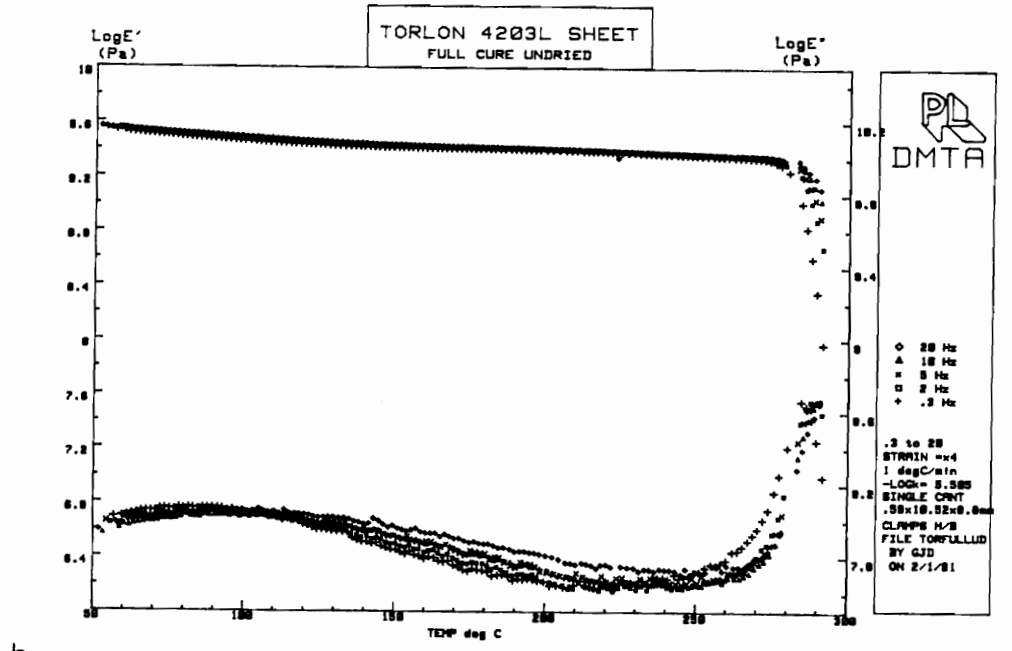

b

Figure 3.9

a. E', E" vs. temperature for the poly(amide-imide) uncured sheet as received; b. E', E" vs. temperature for the poly(amide-imide) fully cured as received.

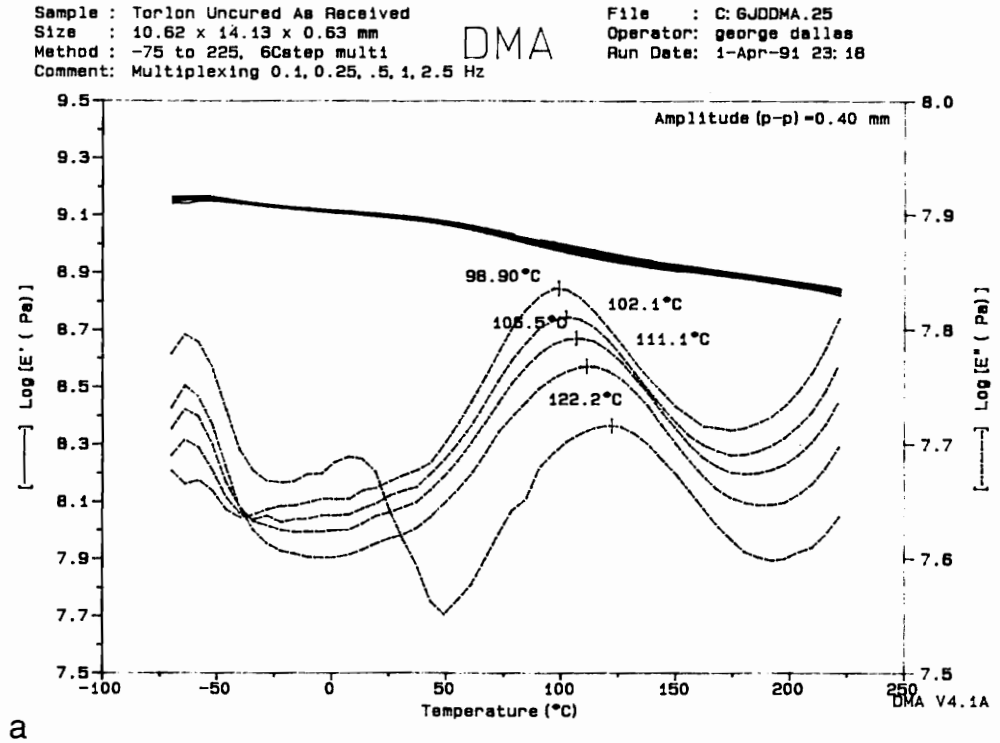

a

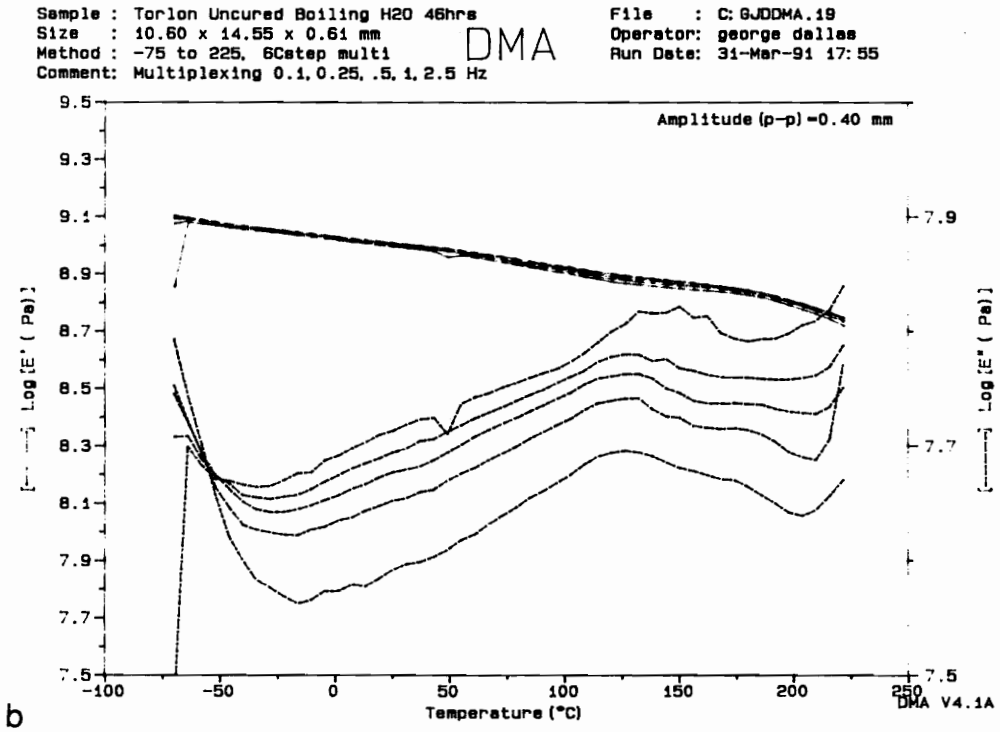

b

Figure 3.10

a. E', E" vs. temperature for the poly(amide-imide) uncured as received; b. E', E" vs. temperature for the poly(amide-imide) uncured saturated with water.

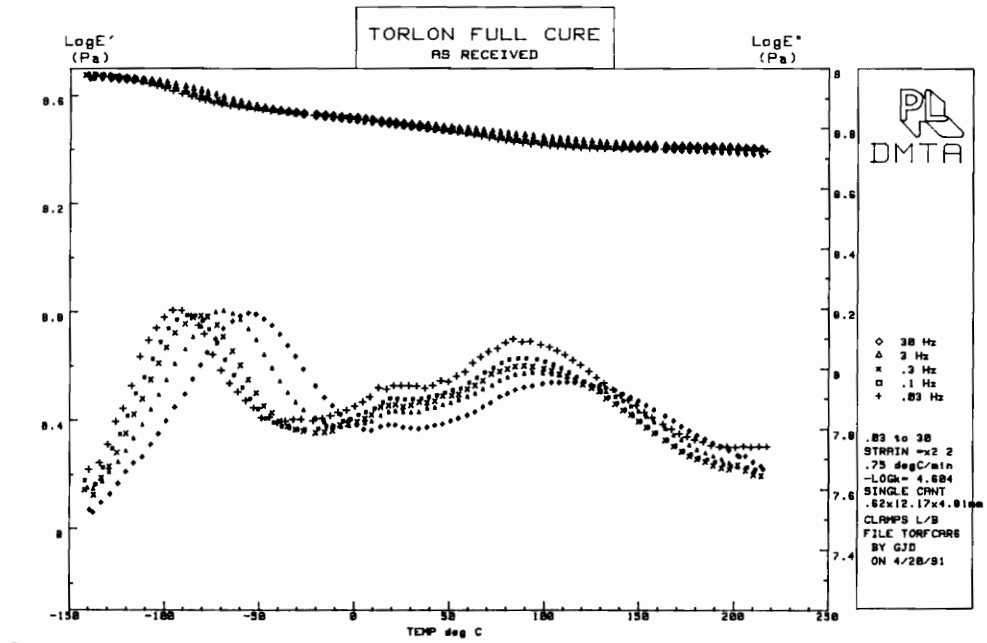

a

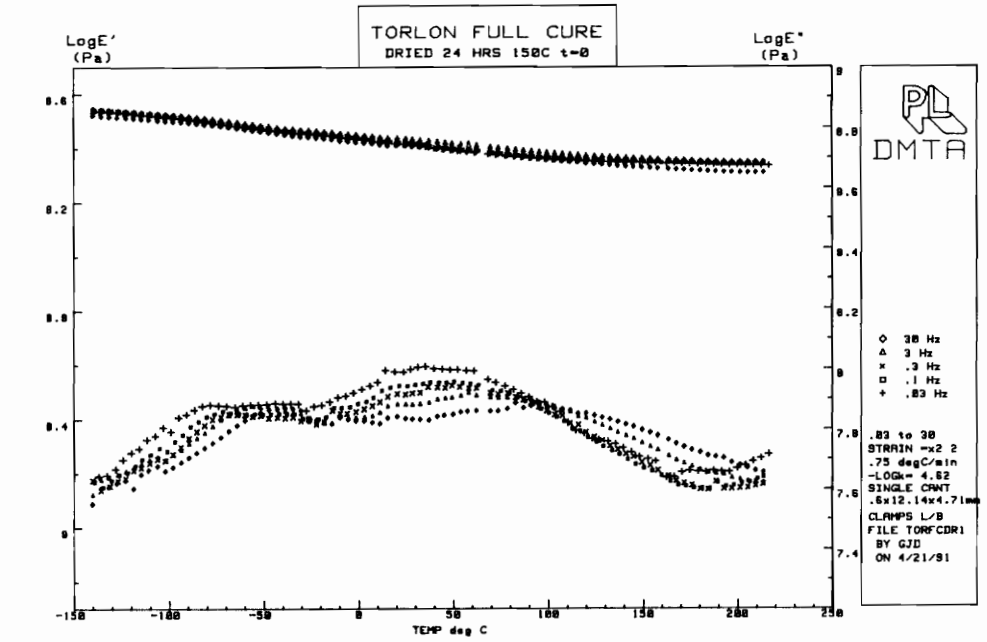

b

Figure 3.11

a. E" vs. temperature for the poly(amide-imide) fully cured as received; b. E" vs. temperature for the poly(amide-imide) fully cured dried.

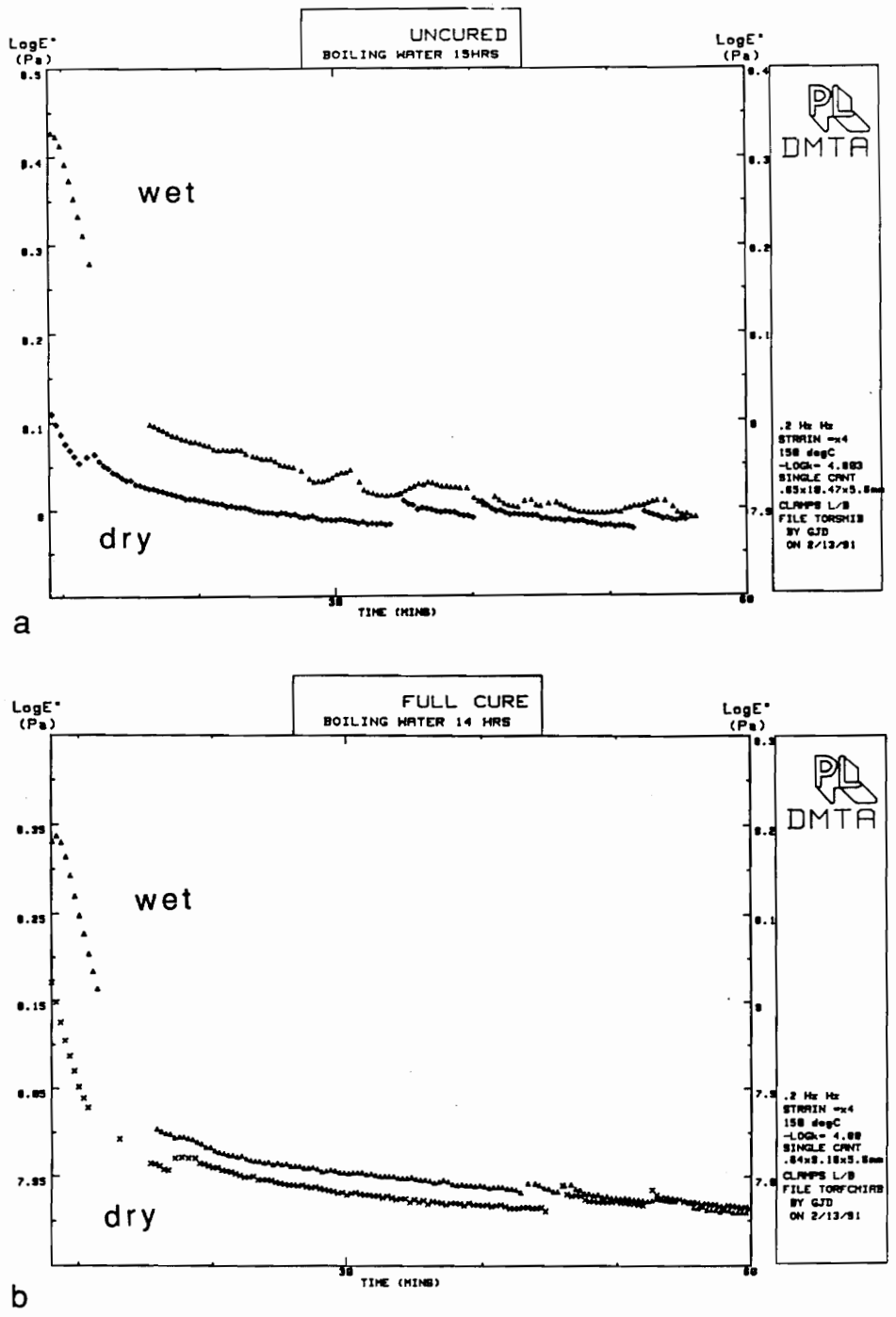

Figure 3.12

a. E" vs. time for the poly(amide-imide) uncured saturated with water (wet) and the poly(amide-imide) uncured dried; b. E" vs. time for the poly(amide-imide) fully cured saturated with water (wet) and the poly(amide imide) fully cured dried.

vacuum oven from 3 to 24 hours. This temperature was above the β transition, but below Tg. The sample was then quenched by placing it on a cool counter top at ~20°C. Aging was conducted at isothermal temperatures of 20°C, 35°C, and 60°C. The times at 20°C were zero days (Figure 3.13b) and 15 days, (Figure 3.14a). The time at 35°C was 4.5 days as shown in Figure 3.14b. The sample was also aged for 23 hours at 60°C (Figure 3.15). These experiments were conducted with two samples to show reproducibility. The DMTA was done at frequencies from 0.03 to 30 Hz. The E" vs. temperature results are shown in Figures 3.13a and b, Figure 3.14a and b, and Figure 3.15.

The reduction of the activation energy for the β transition from drying at time equal to 0 can be seen by comparing the as received E" vs. temperature values shown in Figure 3.13a to the dried values not aged values shown in Figure 3.13b. The effect of aging at 20 - 35°C on the β transition were to move the peaks to higher temperatures. This is illustrated by comparing Figure 3.13b to Figures 3.14a and b. The lower frequency peaks were more influenced by aging and were shifted more dramatically with temperature. The ΔH, ΔG and ΔS of activation for the β transition for the fully cured aged, dried and as received, and uncured dried, as received samples are shown in Table 3.1, along with the values for the low temperature water relaxation shown in Figure 3.11a. These values were calculated using the Kauzmann method [42].

3.7.2 Discussion

Dynamic Mechanical Thermal Analysis of the poly(amide-imide) sample matrix revealed distinct differences between the samples. Degree of cure, water content, and

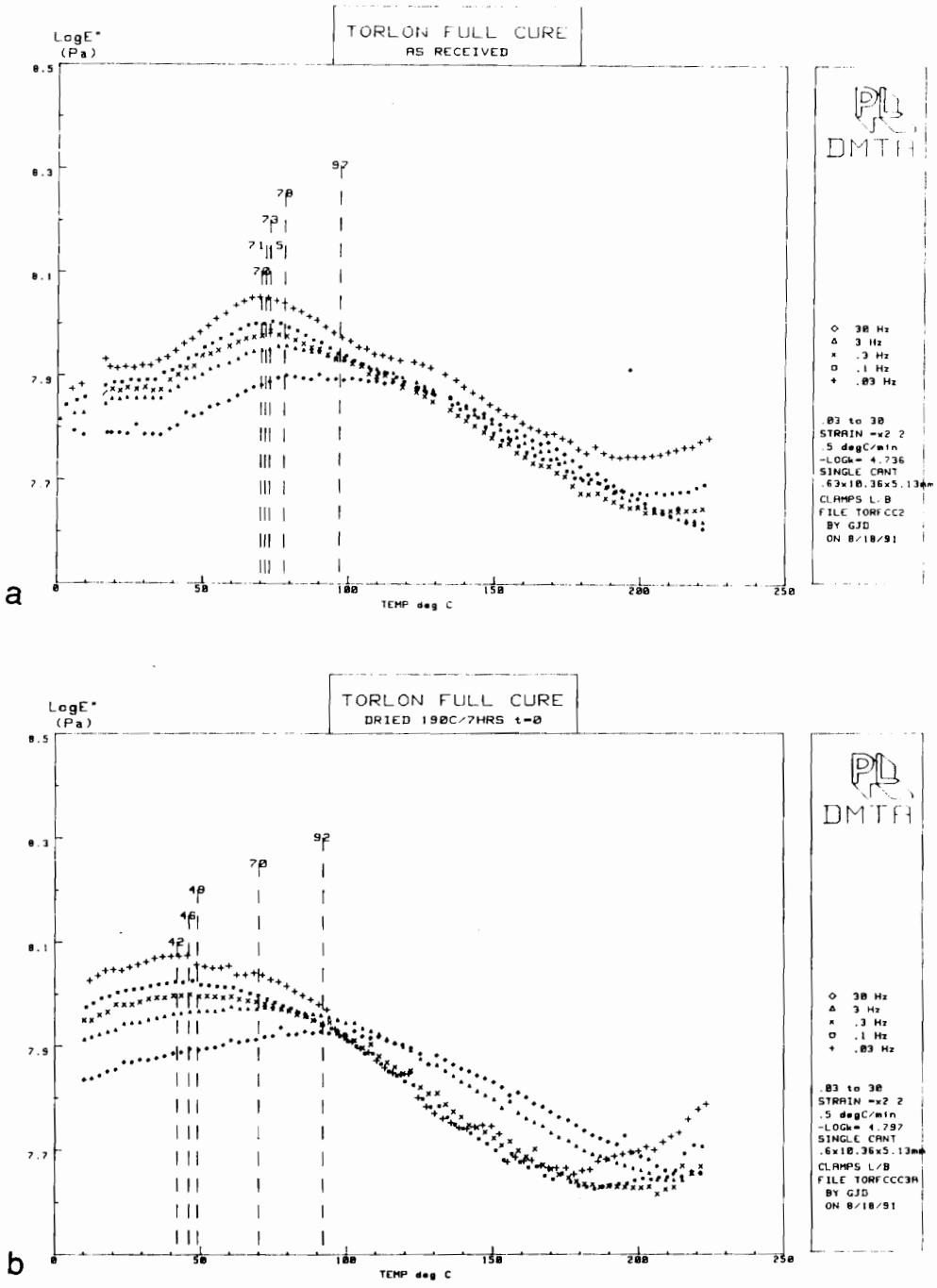

Figure 3.13

a. E" vs. temperature for fully cured as received poly(amide-imide); b. E" vs temperature for the poly(amide-imide) fully cured dried at 190°C and quenched to 20°C and then run immediately.

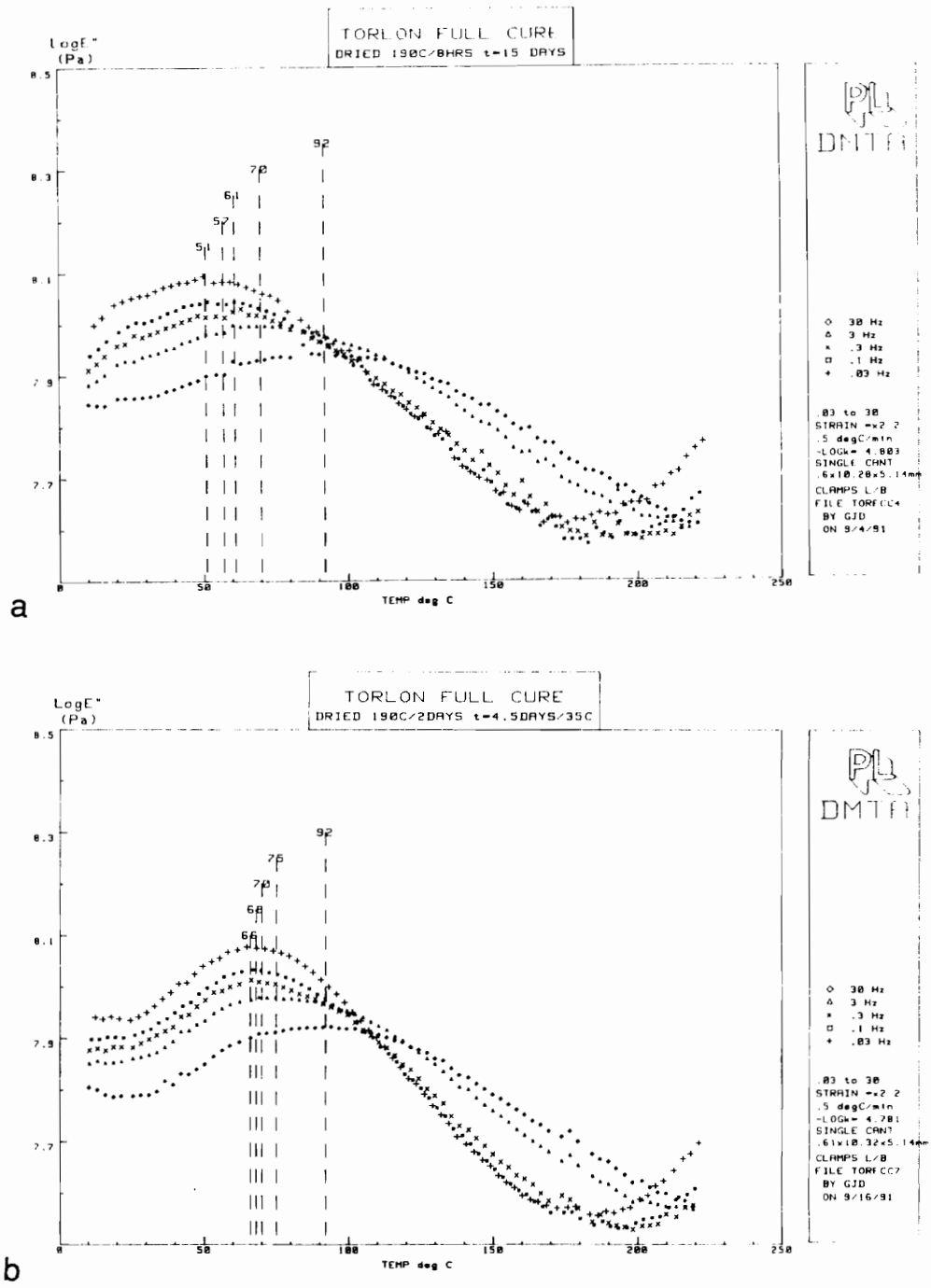

Figure 3.14

a. E" vs. temperature for the poly(amide-imide) aged 15 days at 20°C; b. E" vs. temperature for the poly(amide-imide) aged 4.5 days at 35°C.

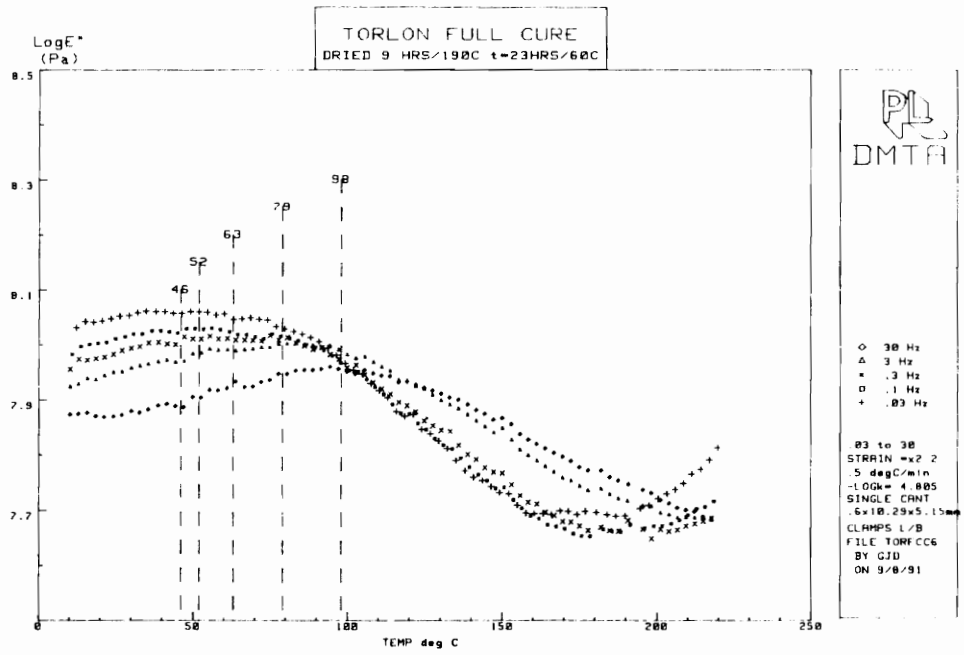

Figure 3.15

A plot of E" vs. temperature for the poly(amide-imide) aged 60°C for 23 hours

Table 3.1

Dynamic Mechanical
Energies of Activation for the β Transition

	ΔG=f(T)	ΔH kJ/M ΔG kJ/M	ΔH kJ/M	ΔS J/M•K
Uncured/As Received		193	187	257
Uncured/Dried		120	114	114
Fully Cured/As Received		316	302	626
Dried 190°C Fully Cured t = 0 20°C		126	117	123
Fully cured Dried t =15 days 20°C		168	163	245
Fully Cured Dried t = 4.5 days 35°C		257	251	490
Fully Cured Dried t = 23 hrs 60°C		129	124	127
		ΔG kJ/M Per mole of hydrogen bonds	ΔH kJ/M	ΔS J/M•K
Water		29	27	25

time of aging below the β transition were all shown to affect the mechanical storage and loss spectra. The extent of cure affected the region of large scale macromolecular motion, or T_g. Also, water content and aging time significantly increased the β transition. An increase in water from dried to saturated with water shifted the β peak up to higher temperatures and increased its height, while also broadening the transition. This shift to higher temperatures could be due to association of the water with the groups that cause the β transition. The possible enthalpic interactions from association with water would require more thermal energy to make the new water β transition structure oscillate, thus shifting the motion to higher temperatures. This however, cannot be concluded by this method. The only conclusive statement that can be made is that there is a correlation between water content and β transition peak height.

The addition of water to the poly(amide-imide) has been shown to occur in two stages, which involve two different structures. At less than 2% weight of water, the water adds in the free volume or interstices as hydrogen bonded molecules. The enthalpies of activation compare favorably with literature values for pure water between 14 to 32 kJ/M of H-bonds [32]. Above 2 to 2.5% by weight water, the water increases the magnitude of the β transition.

The calculations of the activation energies were made by linearizing the log frequency maximum vs. 1/T maximum data. A 30 Hz value for as received poly(amide-imide) could not be determined, so the peak of the 30 Hz value from the companion experiment (of 92°C) was chosen. The 60°C experiment was conducted to determine the upper temperature for physical aging. A 50°C for 24 hours experiment on the companion sample showed intermediate aging, while the 60°C showed less. Therefore, for fully

cured poly(amide-imide), changes in activation energy for the β transition was detected between ~20 to 50°C. This is not to say that changes in activation energy might also occur at longer time scales and lower temperatures.

The thermoreversibility of the β transition was shown by comparing the ΔG^* for the fully cured as received, which had been aged many months (316 kJ/M) to the fully cured sample aged at 35°C for 4.5 days (257 kJ/M). The intermediate aging times produce intermediate values. The ΔH and ΔS values for this series showed that the enthalpic interactions increase with aging and that a more dense structure was developed with aging as indicated by an increase in ΔS^*. Thus, for water content less than 2% by weight, the activation energy for motion of the β transition was governed by the interactions within the poly(amide-imide) and not water-polymer interactions.

The self-consistency of the activation energies can be examined by deriving ΔS from $(\Delta H - \Delta G)/T$ and comparing it to the ΔS calculated by the Kauzmann method. The values obtained in this way comparable if one assumes a 20% slope error. The 20% error was obtained with 95% confidence in slope, calculated by simple regression. Typical errors for ΔS calculated by the Kauzmann method were 50 J/(M•K). This worked well for all calculations except the fully cured as received and the fully cured dried, aged 35°C for 4.5 days. An explanation might be that the β transition was not a single relaxation; this was reasonable given the breadth of the relaxation or that ΔG was temperature dependent for this mechanical motion.

3.7.3 Conclusions

The dynamic mechanical properties of the poly(amide-imide) sheet were governed by cure and were transient with respect to water desorbtion and aging between 20 - 35°C. The DMTA can be used to identify the increase in T_g in the fully cured system compared to the partially cured system. The β transitions in both fully cured and uncured poly(amide-imide)s were sensitive to volatiles content. An increase in water to 4 - 4.5% by weight increases the temperature and broadens the temperature range of the β transition. The E" as a function of time can be used to follow the transient mechanical properties of the poly(amide-imide) film saturated with water for both fully cured and uncured systems. The larger changes in mechanical properties occur with the uncured system instead of the fully cured system. The uncured poly(amide-imide)'s mechanical loss values were reduced by about 0.4 log units. The time scale of the change corresponds well with the time scale for volatiles desorbtion as shown by TG.

Aging a fully cured poly(amide-imide) sample below the β transition at 20 to 35°C increases the activation enthalpy for mechanical motion. The activation energy for the sample aged at 35°C for 4.5 days was 257 kJ/M within 20% experimental error was indistinguishable from the as received value of 316 kJ/M.

3.8 Dielectric Thermal Analysis 0.1 - 100 kHz

3.8.1 Results

In Figures 3.16a and b are ε', ε" vs. temperature from -140 to 230°C for the poly(amide-imide) as received and the poly(amide-imide) dried. The frequencies used were 1 - 100 kHz. The poly(amide-imide) was dried at 190°C for four hours. Three sets of peaks were obtained in the poly(amide-imide) as received as shown in Figure

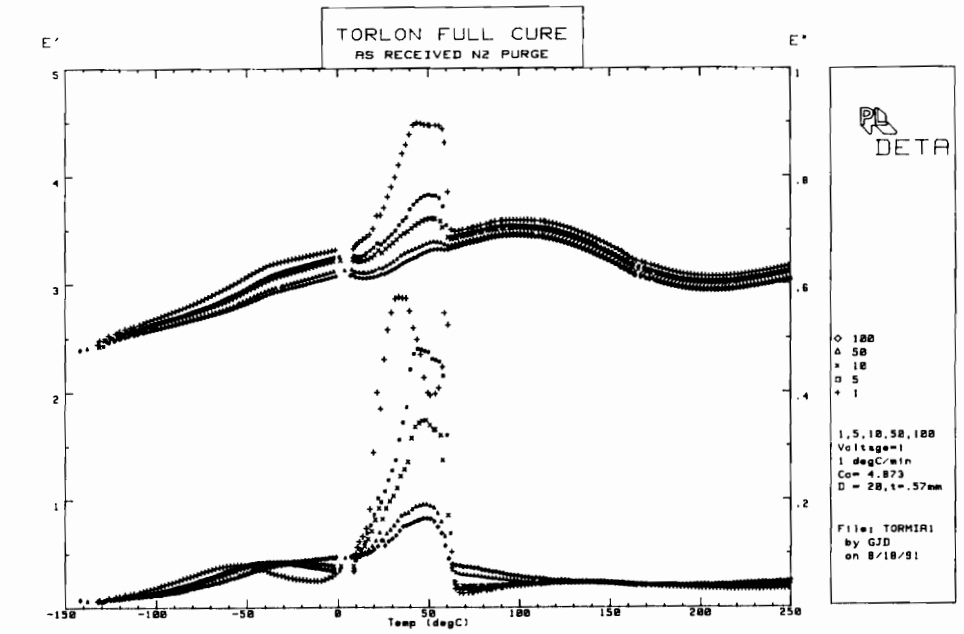

a

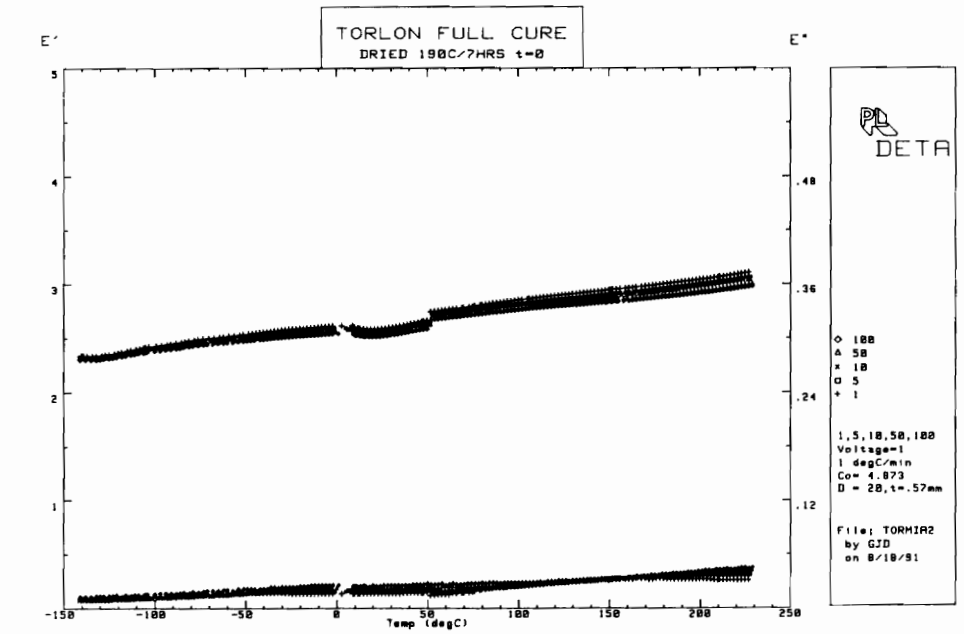

b

Figure 3.16

a. A plot of ε', ε" vs. temperature from -140 to 230°C for fully cured as received poly(amide-imide); b. A plot of ε', ε" vs. temperature for fully cured dried 190°C for 4 hours.

3.16a. They covered the following temperature ranges: from -50 to 0°C, from 0 to 50°C and from 175 to 230°C. Figure 3.16b shows the poly(amide-imide) dried spectra, in which there was only one set of peaks from 175 to 230°C.

The dielectric storage vs. temperature for as received poly(amide-imide) shown in Figure 3.17a increased as a function of temperature until 0°C. From 0 to 50°C, the storage values go through a maximum. The storage continues to increase with temperature until ~100°C. From 100 to 175°C the storage decreases, then increases from 200 to 250°C. The storage values for the dried poly(amide-imide) showed a gradual increase with temperature through the whole temperature range.

3.8.2 Discussion

There were three sets of peaks for the as received poly(amide-imide) shown in Figure 3.16a. The two lower temperature sets were associated with the volatiles, though the loss mechanism of each was different. The low temperature peaks between -50 and 0°C were associated with dipolar losses from hydrogen bonded water. The peaks between 0 and 50°C were primarily associated with conductive losses, probably due to water clusters. This compares favorably to Johnson's differential scanning work shown in Figure 3.1b and dielectric work shown in Figure 3.1a [14]. The conductive losses were determined by a log ε'' vs. log f plot. A linear plot was generated. Its slope, however did not equal -1, (see Equation 2.2). A plot of $\varepsilon''f$ vs. f showed a linear plot with separate conductive and other losses. The conductive losses were determined from the intercept and the other contributions were deduced from the slope of Equation 2.4. The shape of this peak was similar to that predicted for ions in a contained area [43], see insert of Figure 2.3. The conductive losses could be due to water associating or clustering with

the ions in the polymer. The ions were probably left in the polymer from the synthesis of the acid chloride with the aromatic amine. The higher temperature peaks between 175 and 230°C were associated with the β transition. The α transition was above the 300°C temperature limit of the instrument at the frequencies used. Drying the sample both removes the low temperature peaks and leaves the high temperature β transition. This is seen by comparing Figure 3.16a to 3.16b.

Comparing the DMTA in Figure 3.11a and DETA shown in Figure 3.16a for as received poly(amide-imide) shows the difference between the propagation of dielectric and mechanical waves through a material. A comparison between the 0 - 50°C range of each spectra reveals that ionic conductivity is a highly electricaly lossy mechanism, while it is virtually insignificant mechanically. Both of the low temperature peaks between -100 and 0°C for the dielectric and dynamic mechanical experiments seem to both be associated with water and have activation energies of 30 kJ/(M of hydrogen bonds). The high temperature peaks were always apparent whether the sample was dried or not and whether the experiment was electrical or mechanical. This indicates that the β transition was a part of the polymer structure and was a weakly polar transition compared to water.

The dielectric storage values should go through step increases when a new storage mechanism has been activated with increasing temperature. This occurs until ~30°C. The reason for the maximum was not presently understood by this author. However, knowing that the loss mechanism was conductive and not dipolar would lead one to speculate that the ability of ions to store electric energy can be turned off with increasing thermal energy. The decrease in dielectric storage, ε', from 100 to 175°C

was probably due to the desorbtion of water from the polymer as the experiment was proceeding, as this does not occur for the dried sample shown in Figure 3.16b. The temperature range was the correct one for volatile desorbtion as determined by thermogravimetry as shown in Figure 3.5.

The dielectric storage values for the dried sample coincide at the upper and low temperature regions with those of the as received sample. This makes sense at both temperature regions, since, the water will have little effect on the total storage of the sample. In the low temperature region all mechanisms for water storage were turned off and in the upper region, the water has desorbed. The dried samples storage values for the middle temperature region were lower than the as received values. This was in agreement with the notion that water can contribute to dielectric properties at these temperatures.

3.8.3 Conclusions

There were three sets of peaks for the poly(amide-imide) as received in the dielectric spectra. The low temperature peaks from -50 to 0°C were associated with dipolar losses of water. The peaks between 0 and 50°C were primarily associated with conductive losses in the poly(amide-imide). The upper temperature set was due to the motion of the β transition. Also, the spectra for DMTA and DETA were similar, but the exact mechanism of wave propagation was different and does generate significantly different spectra.

The storage values were increased with the addition of water in the temperature range

from -50 to 100°C for frequencies between 1 to 100 kHz. The storage values for the dried sample overlap the storage values of the as received sample at the low and high temperature region. Thus, 2 - 2.5% water can increase the dielectric storage values 10 - 30% depending on the temperature and frequency of the experiment.

3.9 Dielectric Thermal Analysis 2.45 GHz

3.9.1 Results

The ε' and ε" at 2.45 GHz were obtained for the poly(amide-imide) rod as a function of temperature from room temperature to ~285°C. Figures 2.24 a and b are plots of ε' and ε" vs. temperature for the poly(amide-imide) uncured as received and dried and for the poly(amide-imide) fully cured, which had been out in a normal room environment for 20 days. The plot of ε" vs. temperature for the poly(amide-imide) uncured dried sample reveals a slight increase in these values until ~260°C, where the ε" increases more significantly with temperature. The fully cured sample, which had been dried 20 days before shows slightly more ε" than the uncured poly(amide-imide) dried. Its ε" values increase with temperature until it reaches its T_g, and afterward the ε" increases much more rapidly. The uncured as received has significantly higher ε" at all temperatures than the dried one. At T_g the ε" drops dramatically and overlaps the previous two. The ε' as a function of temperature showed a similar ordering with respect to volatile content and a slight increase near T_g.

In Figures 3.17 a and b there is a comparison of weight loss vs. time at 155°C from thermogravimetry and ε" vs. time at 150°C. The ε' and ε" as a function of time were used to examine volatile desorbtion for the uncured system. This is shown in Figures

3.18 a and b at a temperature of 155°C. The ε' and ε" vs. time for the fully cured dried poly(amide-imide) at 260°C are shown in Figures 3.19 a and b. These values do not change over the time scale of the experiment. They were obtained to showed the stability of the signal.

3.9.2 Discussion

The flat signal for the fully cured dried sample shows that the technique works well, since no dielectric events should occur (Figure 3.20a and b). The dielectric values vs. time again showed that changes in ε" or ε' were due to desorbtion of volatiles. The changes in dielectric properties vs. time are similar to the changes in weight loss vs. time as shown in Figure 3.17a and b.

The dielectric values vs. temperature indicated that the water significantly contributes to ε" and ε'. These values came from an average of six points taken one every 10 seconds for one minute. At temperatures above 150°C, the water would desorb and change the dielectric values slightly within the one minute time span. Each of these isothermal readings was taken at least 20 minutes after increasing the heater dial to the next temperature. This was the time needed for both the sand bath and the waveguide to become isothermally stable. The resonant frequency of the waveguide was sensitive to the length of the waveguide. The resonant frequency would change with

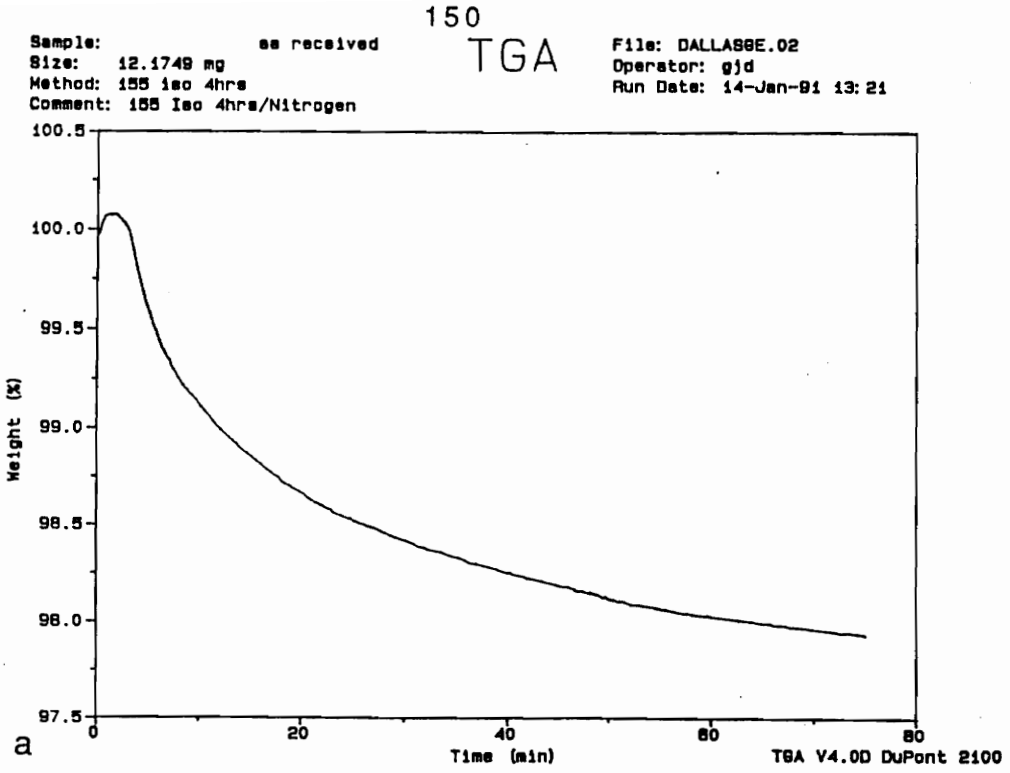

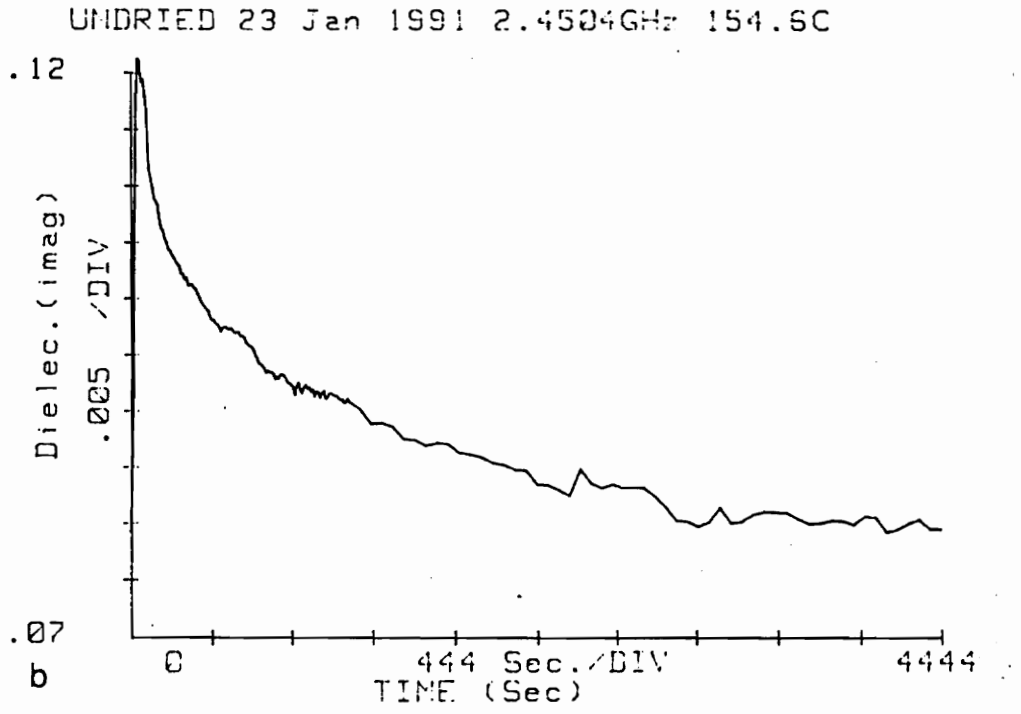

Figure 3.17

a. Illustrates weight loss vs. time at 150°C; b. shows ε" as a function of temperature for the poly(amide-imide) fully cured dried at 155°C

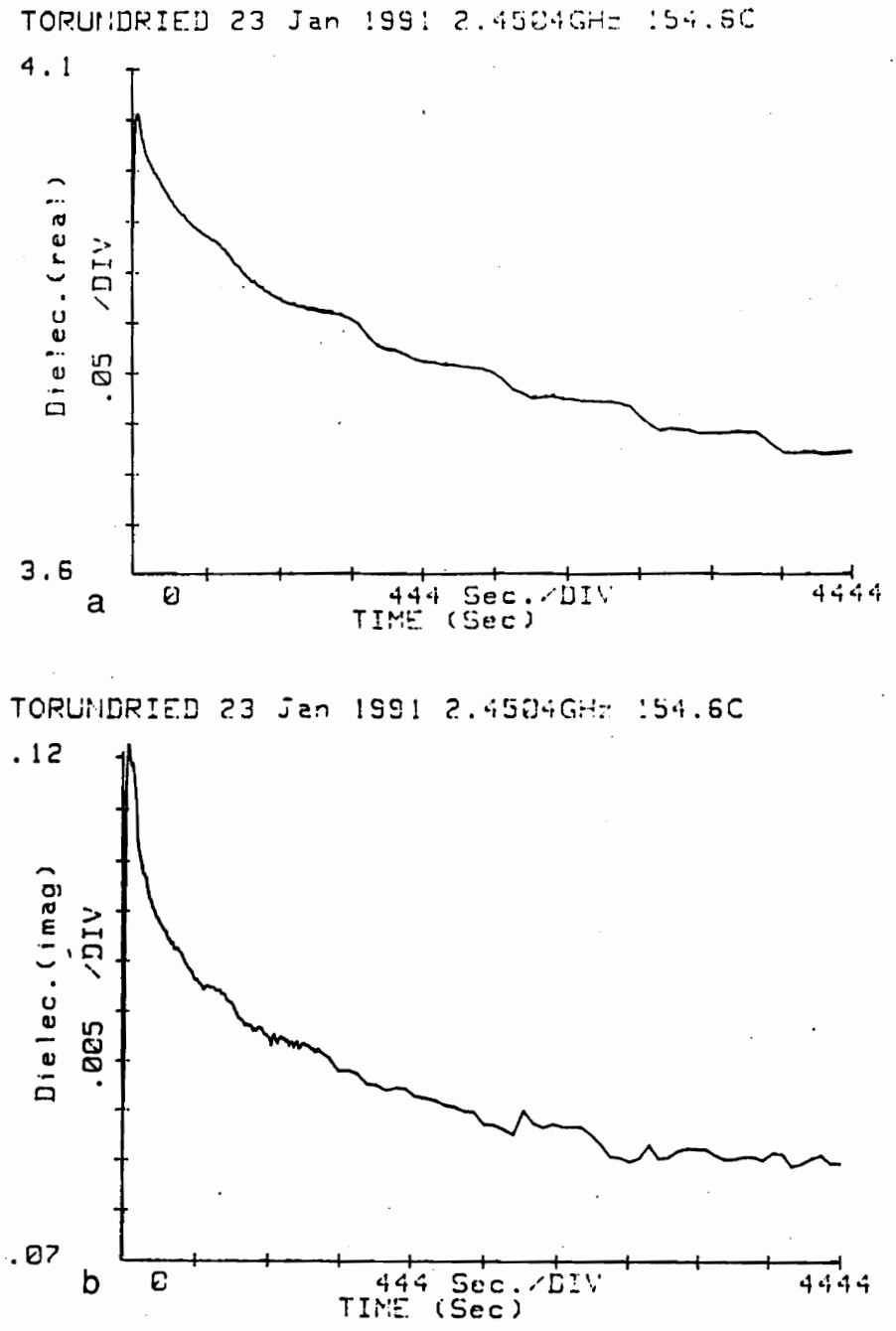

Figure 3.18

Plots of (a) ε' and (b) ε" vs. time at 155°C for the poly(amide-imide) uncured as received.

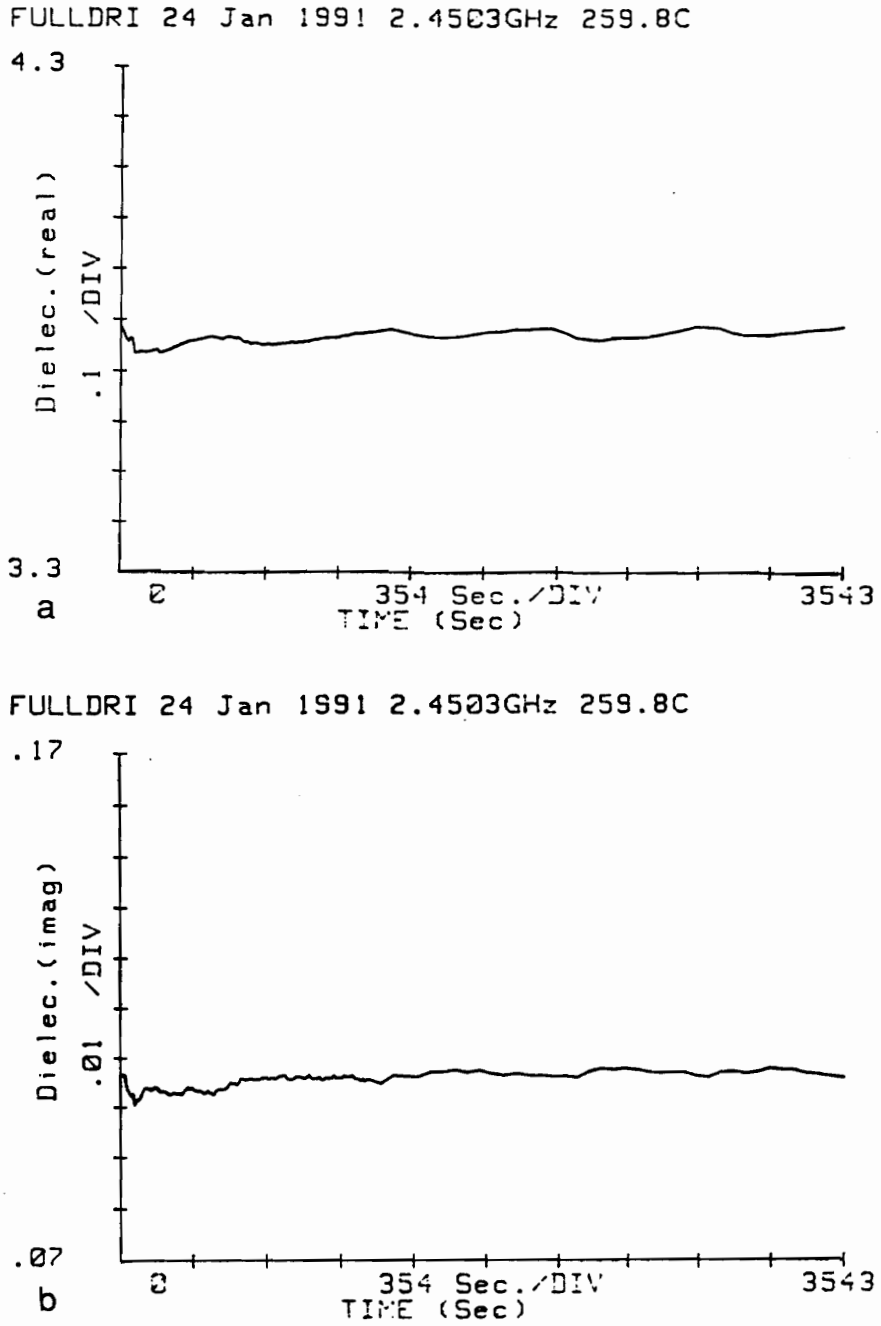

Figure 3.19

Plots of (a) dielectric storage (ε') and (b) dielectric loss (ε") vs. time at 260°C for the poly(amide-imide) fully cured dried.

changing temperature. Thus, isothermal conditions must be met to insure accurate dielectric measurements.

Sample movement within the Teflon® tube caused noise in the dielectric measurements. Shortening the sample so that it just filled the width of the waveguide increased the signal to noise by reducing sample flutter within the Teflon® tube. Temperature instability was not noticed over the time scales utilized so it could not be a cause for noise. Accurately determining temperature above 260°C was difficult; temperatures varied ± 10°C. These temperatures approached the upper limit of the sand bath hot nitrogen heater. Sometimes the temperature probe would touch the Teflon® tube walls, giving a reduced temperature reading. This may be why the increases in ε'' near T_g for cured and uncured samples were similar.

3.9.3 Conclusions

The dielectric properties at 2.45 GHz of the poly(amide-imide) as a function of temperature or time were significantly influenced by the addition of volatiles. Drying the sample reduces the volatiles and the dielectric values. The ε'' and ε' as a function of temperature increased steadily until T_g, where they increased more rapidly as a function of temperature. The ε'' and ε' as a function of time decreased over the same time scale as the weight loss, which was determined by thermogravimetry. The dried samples showed no dielectric changes over the same time scale.

3.10 Thermal and Microwave Processing of the Poly(amide-imide)

3.10.1 Results

The thermal processing of the poly(amide-imide) parts takes a few days to cure completely the parts while maintaining their dimensional stability. Shorter processing times are desired. Microwave processing offers controlled temperature vs. time profiles by properly controlling the power vs. time profiles. Optimizing temperature vs. time cure cycles may reduce processing times. Since the poly(amide-imide) contains residual solvents, their removal was essential to a part's dimensional stability. Thus initial experiments focused on the following:

- Sample preparation
- Heatability of the poly(amide-imide) films and balls
- Controlled temperature vs. time profiles
- Dimensional stability
- Comparison of structures formed after microwave and thermal processing of the poly(amide-imide) balls

Initial curing experiments were done with the as received poly(amide-imide) films and balls; blistering and foaming were observed. These were determined quantitatively by thermomechanical analysis as a function of temperature. An expansion started below the glass transition temperature of 265°C at 235°C for as received uncured and 265°C for uncured dried poly(amide-imide) sheet as shown in Figures 3.8a and b. A drying schedule was used to eliminate the small molecules and therefore the expansion. The poly(amide-imide) was dried at ~190°C under vacuum for 3 hours to remove residual solvents. The content of volatiles was monitored by thermogravimetry. The percent weight loss in the volatiles region decreased from ~3% to < 1% after drying. The blistering and foaming were reduced by this procedure.

Microwave heating was dependent upon the dipole moment, the concentration of dipoles, and their mobility, among other factors explained previously. Microwave heating results from the dipoles dissipating their energy with their local environment when they are forced to oscillate by the applied electric field. The poly(amide-imide) has carbonyl and amide functional groups, which are dipolar and have dielectric loss in the microwave region. The poly(amide-imide) was heated in the cavity at initial heating rates of 200°C/min at 30 W to ~90°C/min at 20 W of input power. The poly(amide-imide) parts were processed by three distinct temperature vs. time profiles. The first one at 30 W until a temperature of 280 - 285°C was reached and held for 900 seconds. The second profile at 20 W until 280 - 285°C was reached and held for 900 seconds. The third was a step method at 20 W until 230 - 235°C was reached and held for 5 minutes then heated to 280 - 285°C was reached for 900 seconds shown in Figure 3.20. A typical power vs. time curve for 20 W is shown in Figure 3.21. This indicated that when the desired temperature was reached, the reflected power was increased to reduce the total electric field strength within the cavity. This power vs. time curve accompanies the 20 W temperature vs. time profile shown in Figure 3.20. These data showed that the poly(amide-imide) can easily be heated in a microwave cavity to a desired temperature.

The three microwave temperature vs. time profiles were compared to the thermal heating of a the poly(amide-imide) ball in a thermal oven at 287°C. A comparison of the thermal and microwave profiles is made in Figure 3.20. The thermal cure was the parabolic one. Initially, the heating rate was similar to the 30 W profile. After ~120 seconds the temperature deviates from that profile and asymptotically approaches the

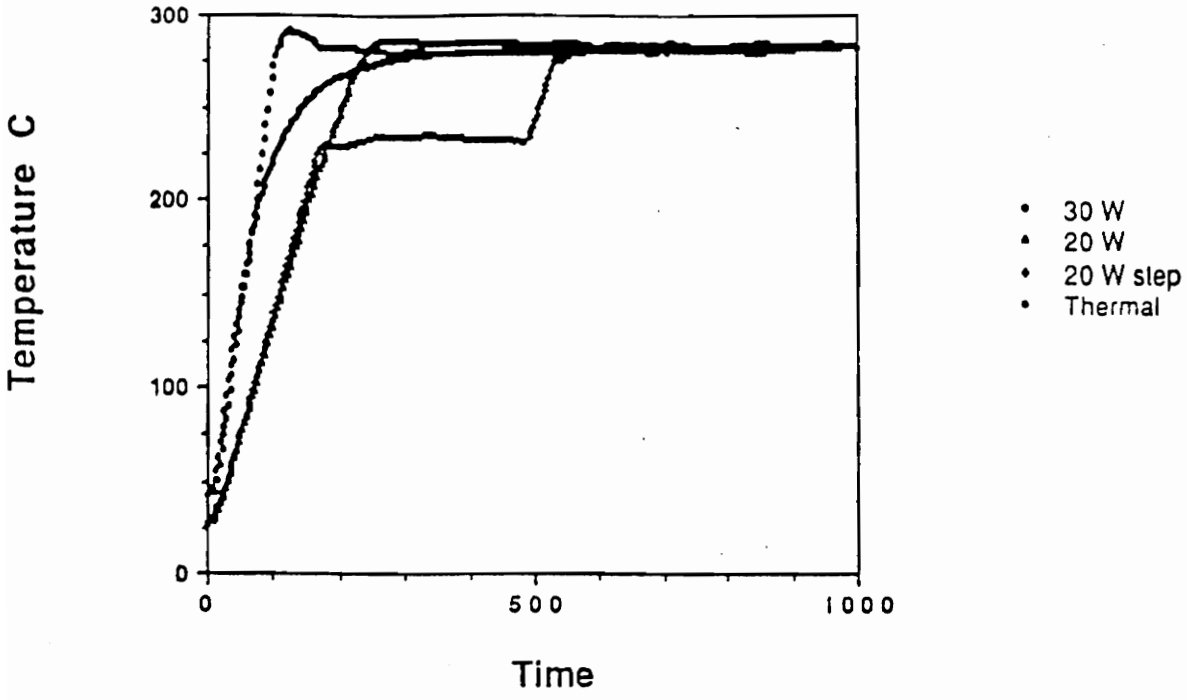

Figure 3.20

Temperature vs. time for microwave and thermally heated poly(amide-imide) balls.

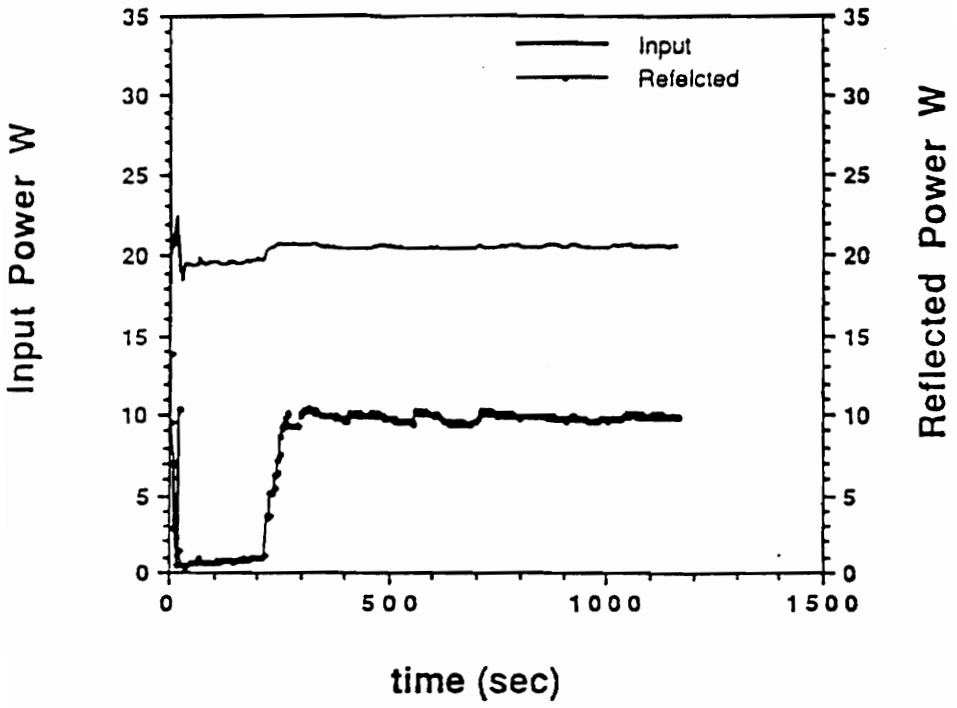

Figure 3.21

Input and reflected power vs. time for 20W temperature vs. time.

Table 3.2
Poly(amide-imide) Ball Dimensions (0.001")

	30 Watts	20 Watts Step
As Received		
Before	0.532"	0.532"
After	0.592"	0.541"/0.52" Seam
Dried		
Before	0.516"	0.536"/0.52" Seam
After	0.534"	0.536"/0.524" Seam

maximum temperature, coming within 5°C after 350 seconds. Thus, microwave processing can be used to control the thermal energy within the sample better than thermal heating.

The effects of drying and temperature vs. time profiles from Figure 3.20 on dimensional stability of 0.5" poly(amide-imide) balls were investigated. Table 3.2 contains the dimensions of the poly(amide-imide) balls in thousandths of an inch. The top row refers to the power used i. e. 30 W and 20 W step conditions. In the first column, the dried and as received conditions are given. The data in each quadrant refers to dimensions "before" and "after" heating. In addition, one "before" and most "after" dimensions are given for either the seam or the other axis. A comparison of Row 1 to Row 2 reveals that the dried balls maintained more dimensional stability than the as received ones. In comparing the 30 W to 20 W step conditions, the lower power and five minute step at 230 - 235°C reduced the distortion caused during processing. Therefore, sample preparation and controlled temperature vs. time profiles were controllable variables that can be used constructively to influence the processing of the poly(amide-imide).

Microwave and thermal processing of uncured poly(amide-imide) balls were both significantly influenced by drying. The dimensional instability was primarily caused by absorbed volatiles. A thermal experiment was devised in order to determine whether the water, which caused the dimensional instability was absorbed or generated during the synthesis. The thermal experiment involved heating the as received and dried poly(amide-imide) balls in an oven set to 288°C. A temperature above T_g was chosen so both sources of waters (generated by synthesis and asorbed volatiles) would cause dimensional instability. The temperature vs. time profile was recorded by a fluoroptic

probe in the center of a poly(amide-imide) ball (Figure 3.3). The balls were kept in the oven so the one poly(amide-imide) ball's central temperature was greater than or equal to 280°C for 900 seconds. Their dimensional changes were measured on two axes. This experiment shows the effect of the total amount of the water adsorbed and that from chemical synthesis on dimensional stability. These dimensional changes will be compared to the dimensional changes that occur when the poly(amide-imide) balls were dried for 12 hrs at 160°C under vacuum. This will show the dimensional instability due to only the water produced during ring closure of the amic acid. The average of ten 0.4" poly(amide-imide) balls shows that the as received poly(amide-imide) ball's dimensions on both axes increased by 0.050", while the dimensional changes of the dried poly(amide-imide) ball's increased by 0.006" along the seam and 0.003" along the non-seam axis. Thus, dimensional instability for uncured poly(amide-imide) balls was caused primarily by adsorbed water. This agrees with the thermomechanical data Figure 3.8a and b.

Thermal and microwave processing techniques were compared on either 0.4" and 0.5" in diameter uncured poly(amide-imide) balls. The SEM's were compared for the dried and as received uncured poly(amide-imide), which had been processed either thermally or in a microwave cavity. These were the same poly(amide-imide) balls that were used to generate the temperature vs. time profile shown in Figure 3.21. The structures obtained after either microwave or thermal processing clearly indicated the influences of each heating type. Thermal processing showed the formation of a skin on the poly(amide-imide) ball, while microwave heating did not show a skin formation. The microwave temperature vs. time profile was obtained by subjecting a 0.5" poly(amide-imide) ball to 30 W in a 7" cylindrical resonant cavity. The temperature increase was

somewhat linear to 285°C where it was held constant. The thermal processing was done with 0.4" poly(amide-imide) balls put in an oven preset to 280°C. The initial temperature increase was similar to the microwave one, but became parabolic with time.

Figures 3.22 a and b are electron micrographs for microwave and thermal as received poly(amide-imide) balls. Figures 3.22 c and d are electron micrographs for microwave and thermal dried uncured poly(amide-imide) balls. In comparing Figures 3.22 a and b it can be observed that the thermally processed poly(amide-imide) balls have a skin with a porous structure on the interior. The skin must have formed first, trapping the volatiles and causing a closed cell structure to occur in the interior of the ball. The microwave edge clearly shows deformation caused by escaping volatiles and a smoother interior. The exterior of each ball cannot be seen. The thermally cured ball was dark green and has a "tortoise shell" appearance, while the microwave ball was smooth and only slightly discolored. The dried poly(amide-imide) balls showed less structure than the as received ones. The thermally cured ball showed no cell structure but the edges were still not smooth. The surface also was irregular with a tortoise shell appearance, though not as pronounced as the undried one. The microwave processed ball was smooth on the interior and exterior. At the center there was a dark green color.

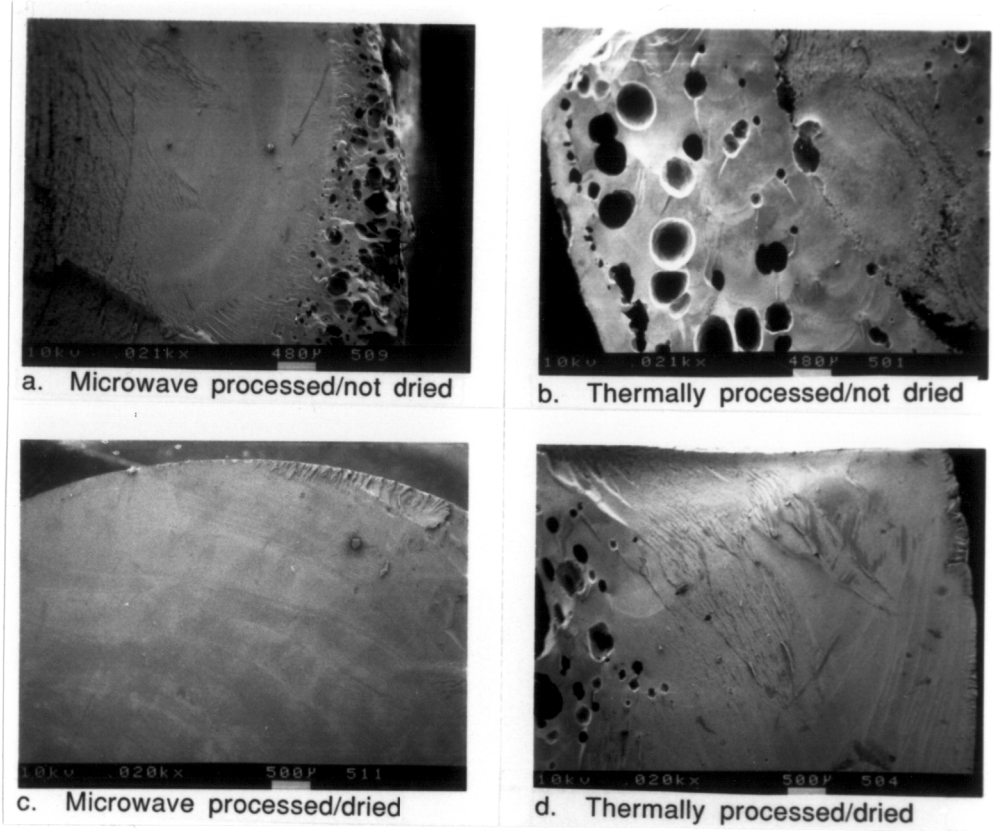

Figure 3.22

Scanning electron micrographs of: a. as received poly(amide-imide) ball microwave processed; b. as received poly(amide-imide) ball thermally processed; c. dried poly(amide-imide) ball processed by microwaves; d. dried poly(amide-imide) ball procesed thermally.

The advancement of cure by microwave radiation was examined for 0.3" poly(amide-imide) rods. The rod was placed in a rectangular waveguide at a maximum in electric field strength Figure 2.8. The temperature was monitored at the interior of the rod by placing a fluoroptic probe in a hole drilled in the center of the rod. The interior temperature was taken to 290°C for three, six, or eight hours. The uncured T_g was 270°C. The three hour cure showed no advancement of cure, while the six and eight hour cures showed advancements in T_g to 275 and 278°C respectively. These T_g values were compared to those T_g values obtained by isothermal curing of poly(amide-imide) fiber at 285°C Figure 3.23.

To examine the effects of water on initial heating rate, a comparison between the heating rates of as received uncured poly(amide-imide) balls and dried uncured poly(amide-imide) balls were made. The high powered heating rates of 0.5" in diameter poly(amide-imide) balls (dried and undried) was obtained in a cylindrical cavity in the TE_{111} mode. The heating rates were shown to be similar at 2°C/sec. The reabsorbed water was 1% by weight.

3.10.2 Discussion

The difference in structure must be caused by the large temperature gradients within the poly(amide-imide) balls. The thermally processed poly(amide-imide) parts were placed in an oven set at 280°C, so the exterior of the ball immediately goes to that temperature, while the interior may take 10 to 15 minutes to reach 270°C.

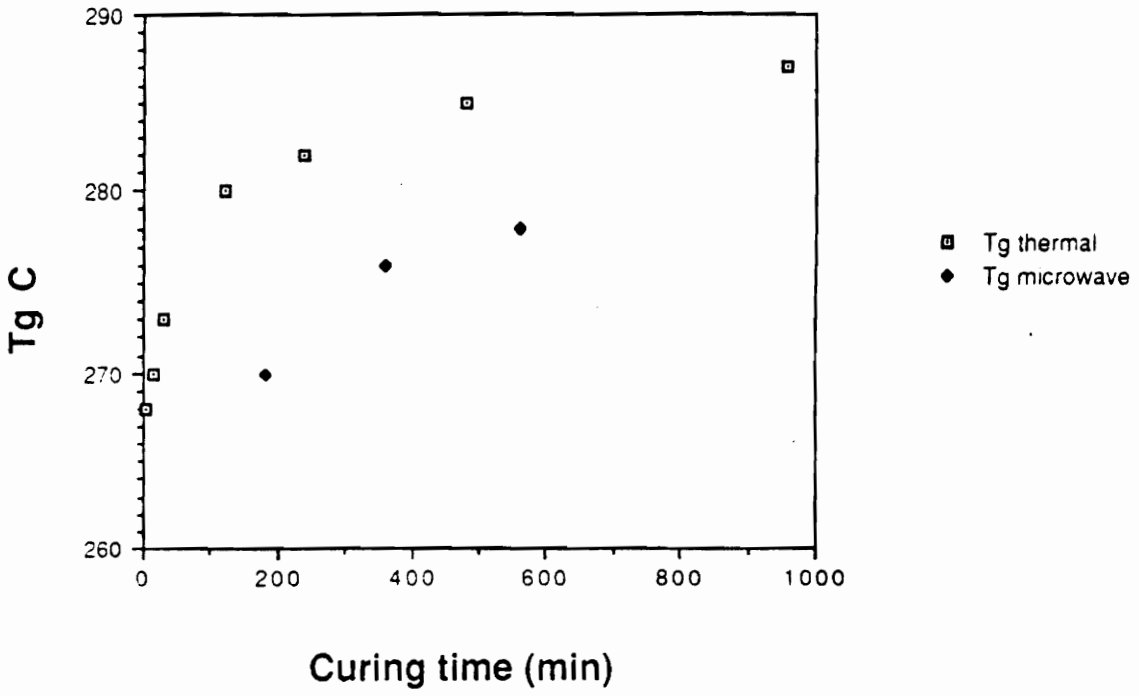

Figure 3.23

T_g vs. time for thermally processed poly(amide-imide) fiber and microwave processed poly(amide-imide) rod.

The interior of the microwave processed ball's was at 285°C within two minutes, while the exterior was in contact with ambient temperature air. Thus, water can escape from the less cured surface and was driven toward the cooler exterior. Therefore, since the relationship between dimensional stability and volatiles was known, an accelerated thermal temperature vs. time profile was attempted on dried poly(amide-imide) balls.

The objective was to look at cure advancement and dimensional stability with dried thermally processed poly(amide-imide) balls. Ten 0.4" poly(amide-imide) balls were dried for 24 hours at 160°C under vacuum. They were given the following temperature vs. time profile of 30 to 225°C at 5°C/min, 225 to 260°C at 1°C/min, and 260 to 275°C at 0.2°C/min, and then hold at 275°C for 1 hour then cool to 30°C at a 1°C /min. The results were the dimensions along the seam and non-seam axes did not change by more than 0.001". The central T_g of the ball was the same as the uncured one of 268°C. Drying the poly(amide-imide) balls at 160°C for 24 hours allows the oven temperature to be brought to cure temperature within a few hours and maintains dimensional stability of the balls. Although the Tg did not advance from this cure cycle.

The microwave curing of poly(amide-imide), which was compared to thermal curing, showed a lower T_g as a function of time. This comparison assumes that the temperature sensors would exhibit the same values. The temperature sensors for the thermogravimetric analyzer have a sigmoidal temperature response and were not linearized. This could possibly show a lower than accurate value, thus causing higher T_g's as a function of time. The fluoroptic probes were linearized and have been compared to NBS thermometers, and were considered reliable to within a few degrees. The heating rate experiments for the poly(amide-imide) balls showed there was no significant

increase in heating rate for as received compared to dried poly(amide-imide) balls. The reabsorbed water must penetrate from the surface inward. It was possible that the surface had a high water concentration but the interior, where the temperature probe was, did not. The reabsorbed water was 1% by weight, which was not significant enough to increase the total ε" and influence the dT/dt of the as received poly(amide-imide) ball.

3.10.3 Conclusions

Microwave energy can be efficiently coupled with the poly(amide-imide) for controlled temperature vs. time profiles. Volatiles greatly contribute to the dimensional instability of the poly(amide-imide). The dimensional instability can be monitored by thermal mechanical analysis. Although, the boiling point of water is 100°C, much higher temperatures (>180°C under vacuum for 3 to 10 hours for parts less than 0.5" thick) were necessary to force the water to desorb from the glassy matrix within a few hours. This was sufficient to remove volatiles and improve dimensional stability. The desorbtion of water can be monitored by thermogravimetry, dielectric, and dynamic mechanical instruments. Proper drying leads to accelerated temperature/time profiles compared to current processing schemes. Dimensional stability also was improved. Thus, removal of volatiles leads to accelerated thermal temperature vs. time profiles and dimensional stability within a few hours. Microwave heating experiments showed that 0.5" balls with less than 1% water uptake by weight had a heating rate similar to dried ones. Microwave processing of the poly(amide-imide) rod at 290°C has been shown to advance T_g by 8°C within eight hours, though preliminary results indicated that it was not as fast as a thermally cured poly(amide-imide) fiber. Microwave processing also

causes a different structure within the poly(amide-imide) balls compared to thermally processed ones. Microwave heating causes the volatiles to escape through the air-surface interphase, while thermal heating produces a skin formation and a cell structure underneath.

3.11 Summary of Chapter 3

The dynamic mechanical and dielectric experiments were used to identify the effects of water and low temperature aging on a poly(amide-imide). Also, the effects of water on the morphology of thermally or microwave processed poly(amide-imide) spheres was examined.

Water has been shown to ingress into the poly(amide-imide) in steps and selectively influence the dynamic mechanical and dielectric properties. The dynamic mechanical properties show a low temperature water peak from -100 to -50°C at less than 2 weight percent . At greater than 2 weight percent water increases the breadth of the β transition. The influence of water on the dielectric spectra shows a water peak between -50 to 0°C and a peak between 0 to 50 °C. This second peak is associated with conductive losses. The fundamental difference between dynamic mechanical and dielectric losses can be seen by comparing the 0 - 50 °C regions of the dynamic mechanical and dielectric spectra. The dielectric loss mechanism is conductive, which is electrical and does not require a significant amount of mechanical motion to generate a mechanical loss peak. Water desorption also caused a decrease of mechanical and dielectric behavior vs. time 150°C.

The activation energy for the β transition, determined by dynamic mechanical thermal analysis was dependent upon the temperature and time of aging. Isothermal aging at 20°C resulted in less change in the activation energy, relative to no aging, than aging at 35°C for 4.5 days. Aging at 60°C resulted in an activation energy similar to that for no aging. Therefore, water and low temperature aging resulted in many features in dielectric and dynamic mechanical spectra as a function of temperature and time.

Water influenced the morphology of thermally and microwave processed poly(amide-imide) spheres. The microwaved spheres had the volatiles migrate to the surface, leaving the interior of the sphere smooth. The thermally processed spheres had the surface of the sphere cure, which trapped the volatiles and caused a closed cell structure.

References

1. Apicella, A. and L. Nicolais, *Effect of Water on the Properties of Epoxy Matrix and Composite,* in *Advances in Polymer Science,* K. Dusek, Editor. 1985, Springer-Verlag: New York. p. 69-76.

2. Starkweather, H.W., *Water in Nylon,* in *Water in Polymers,* S.P. Rowland, Editor. 1980, American Chemical Society: Washington, D. C. p. 433-440.

3. Fuzek, J.F., *Glass Transition Temperature of Wet Fibers,* in *Water in Polymers,* S.P. Rowland, Editor. 1980, American Chemical Society: Washington, D. C. p. 515-530.

4. Moore, R.S. and J.R. Flick, *The Influence of Water Concentration on the Mechanical and Rheo-Optical Properties on Poly(methyl methacrylate),* in *Water in Polymers,* S.P. Rowland, Editor. 1980, American Chemical Society: Washington, D. C. p. 555-570.

5. Bretz, P.E., *et al., Effect of Moisture on Fatigue Crack Propogation in Nylon 66,* in *Water in Polymers,* S. Rowland, Editor. 1980, Washington, D. C. p. 531-554.

6. Ellis, B. and H.U. Rashid, *Water Absorption Isotherms for Cured Bisphenol A Type Epoxy Resins: Effects of Isotherm Temperture and Resin Hardener.* Journal of Applied Polymer Science. 1984. **29**: p. 2021-2038.

7. Moy, P. and F.E. Karasz, *The Interactions of Water with Epoxy Resins,* in *Water in Polymers,* S.P. Rowland, Editor. 1980, American Chemical Society: Washington, D. C. p. 505-514.

8. Apicella, A. and C. Carfagna, *Physical Degradation by Water Clustering in Epoxy Resins.* Journal of Applied Polymer Science. 1983. **28**: p. 2881-2885.

9. Derbyshire, W. and I.D. Duff, *NMR of Agarose Gels.* Discussions of the Faraday Society. 1974. **57**: p. 243-253.

10. Child, T.F., *Pulsed NMR Study of Molecular Motion and Environment of Sorbed Water on Cellulose.* Polymer. 1972. **13**: p. 259-264.

11. Brown, G.L., *Clustering of Water in Polymers,* in *Water in Polymers,* S.P. Rowland, Editor. 1980, American Chemical Society: Washington, D. C. p. 441-450.

12. Froix, M.F. and R. Nelson, *The Interaction of Water with Cellulose from Nuclear Magnetic Resonance Relaxation Times.* Macromolecules. 1975. **8**(6): p. 726-730.

13. Apicella, A., *et al., Thermokinetics and Chemorheology of the Cure Reactions of the Tetraglycidyl Diamino Diphenyl Methane-Diamino Diphenyl Sulfone Epoxy Systems.* Journal of Applied Polymer Sciences. 1984. **29**: p. 2083-2096.

14. Johnson, G.E., *et al., Water Sorption and Its Effect on a Polymer's Dielectric Behavior,* in *Water in Polymers,* S.P. Rowland, Editor. 1980, American Chemical

Society: Washington, D. C. p. 451-468.

15. Dagani, R., *Water Cluster Cradles H30+ Ion In Stable Cagelike Structure,* in *Chemical and Engineering News.* 1991, p. 47-48.

16. Duplessix, R., *et al., Water Absorption in Acid Nafion Membranes,* in *Water in Polymers,* S.R. Rowland, Editor. 1980, American Chemical Society: Washington, D. C. p. 469-486.

17. Rodmacq, B., *et al., Water Absorption in Neutralized Nafion Membranes,* in *Water in Polymers,* S.P. Rowland, Editor. 1980, Stanley P. Rowland: Washington, D. C. p. 487-504.

18. Seferis, J.C., J.D. Keenan, and J.T. Quinlivan, *Effects of Moisture and Stoichiometry on the Dynamic Mechanical Properties of a High-Performance Structural Epoxy.* Journal of Applied Polymer Science, 1979. **24**: p. 2375-2387.

19. Seferis, J.C., *et al., Evaluation of Structural Changes in Epoxy Systems by Moisture Sorption-Desorption and Dynamic Mechanical Studies.* Polymer Composites, 1982. **3**(3): p. 118-124.

20. Wright, W.W., *Characterization of a Bisphenol A Epoxy Resin. A Collaborative Study Carried out by Technical Panel PTP3 of the Technical Cooperation Programme.* British Polymer Journal, 1983. **15**: p. 224-242.

21. Illinger, J.L. and N.S. Schneider, *Water-Epoxy Interactions in Three Epoxy Resins and Their Composites,* in *Water in Polymers,* S.P. Rowland, Editor. 1980, American Chemical Society: Washington, D. C. p. 571-584.

22. Hartmann, B. and G.F. Lee, *Impact Resistance and Secondary Transitions.* Journal of Applied Polymer Science, 1979. **23**: p. 363903650.

23. Boyer, R.F., *Dependence of Mechanical Properties on Molecular Motion in Polymers.* Polymer Engineering and Science, 1968. **8**(3): p. 161-185.

24. Boyer, R. *Introductory Remarks: Symposium on Thermomechanical Analysis.* in *Symposium on Thermomechanical Analysis.* 1974. Mercel Dekker.

25. Boyer, R., *Mechanical Motions in Amorphous and Semi-Crystalline Polymers.* Polymer, 1976. **17**(November): p. 996-1008.

26. McCrum, N.G., B.E. Read, and G. Williams, *Anelastic and Dielectric Effects in Polymers Solids.* 1967, London: John Wiley and Sons.

27. Hunston, D., W. Carter, and J.L. Rushford, *Linear Viscoelastic Properties of Solid Polymers as Modeled by a Simple Epoxy,* in *Developments in Adhesion,* A.J. Kinlock, Editor. 1980, Applied Science: p. 125-174.

28. Hadley, D.W. and I.M. Ward, *Mechanical Properties,* in *Encyclopedia of Polymer Science and Engineering.* 1985, John Wiley and Sons: New York. p. 379-466.

29. Mohajer, Y., G.L. Wilkes, and J.E. McGrath, *Influence of Tacticity and Sorbed Water on the Material Properties of Poly(N,N"-dimethylacrylamide).* Journal of Applied Polymer Science, 1981. **26**: p. 2827-2839.

30. Robeson, L.M., A.G. Farnham, and J.E. McGrath, *Dynamic Mechanical Characteristics of Polysulfone and Other Polyarylethers,* in *Midland Macromolecular Institute Monographs,* D.J. Meier, Editor. 1978, Gordon Breach: p. 405-426.

31. Gillham, J.K., Y. Ozari, and R.H. Chow, *A Water-Sensitive Thermomechanical Transition in a Polyimide.* Journal of Applied Polymer Science, 1979. **23**: p. 1189-1201.

32. Pimentel, G. and A.L. McClellan, *The Hydrogen Bond.* ed. L. Pauling. 1960, San Francisco: W. H. Freeman.

33. von Hippel, A., *The Dielectric Relaxation Spectra of Water, Ice, and Aqueous Solutions, and their Interpretation.* IEEE Transactions on Electrical Insulation, 1988. **23**(5): p. 817-840.

34. Struik, L.C.E., *Physical Aging in Amorphous Polymers and Other Materials.* 1978, Amsterdam: Elsivier.

35. Van Krevelen, D.W., *Properties of Polymers.* 3 rd ed. 1990, Amsterdam: Elsevier.

36. Aklonis, J.J., *Kinetic Treatment of Glass Transition Phenomena and Viscoelastic Properties of Glasses.* Polymer Engineering and Science, 1981. **21**(14): p. 896-902.

37. Lee, H. and F.J.M. Garry, *Glass and B Transitions of Atactic Polystyrenes Monitored by Volume Dilatrometry.* Journal of Macromolecular Science Physics Edition, 1990. **B29(2&3)**: p. 185-202.

38. Moraglio, G. and F. Danusso, *A New Transition in Polystryene.* Polymer, 1963. **4**: p. 445-447.

39. Bianchi, U. and C. Rossi, *A Transition of Atactic Polystyrene in Bulk.* Polymer, 1963. **4**: p. 447-448.

40. Read, B.E. and G.D. Dean, *Time-Dependent Deformation and Craze Initiation in PMMA: Volume Effects.* Polymer, 1984. **25**: p. 1679-1686.

41. Errede, L.A., *et al.,* Journal of Polymer Science: Polymer Chemistry Edition, 1988. **26**: p. 3375.

42. Kauzmann, W., *Dielectric Relaxation as a Chemical Rate Process.* Reviews of Modern Phsyics, 1942. **14**: p. 12-44.

43. von Hippel, A.R., *Dielectrics and Waves.* 1954, New York: John Wiley and Sons.

4. Recommendations

This work clearly establishes Virginia Tech as having a strong fundamental understanding of materials response to electromagnetic radiation in the kHz - GHz frequency region. Attention can be refocused equally to fundamental and applied research. The fundamental research might examine the influence of local environment on dipole moment of a particular molecular structure. Though, this will require many orders of magnitude in frequency (kHz - GHz) to get the $\varepsilon'_{relaxed}$ and $\varepsilon'_{unrelaxed}$ values. This could be complimented by extending the single dipole moment data to dielectric solution properties of stereoregular polymers with the same molecular structure in the backbone. Ceramics could also be included with materials for microwave processing. Fundamental structure-property relationships and concentration behavior could be obtained.

On the fundamental side, an extension of the bisphenol solution data would be to compare the thermal and microwave synthesis of the poly(hydroxether) from bisphenol A and the diglycidylther of bisphenol A. The solution data show that the reactive functional groups are simultaneously the microwave active ones. Any differences in reactivities or activation energies would be more easily interpreted with this selective molecular structure. The photochemical switching of azobenzene could be used as a tool to selectively promote microwave absorption by converting the azobenzene from the cis, which has a dipole moment to the trans form, which does not have a dipole moment. Low power dielectric analysis could be compared to high power heating rates.

Diisobutyldicarbonate could be decomposed both thermally and by a microwave field to examine the influence of electromagnetic radiation on decomposition kinetics. Finally, modified films, with both metal and magnetic filler could be made to compare the absorption characteristics to low power dielectric values.

APPENDIX I

The objective is to determine the derivative of the reflection coefficient (R) as the film thickness (d) goes to zero.

$$\frac{\partial |R|}{\partial d}_{d \to 0} \qquad \text{Eq. A1.1}$$

The definition of the reflection coefficient for a D layer is given by Equation A1.2.

$$\tilde{R} = \frac{(|z/z_o|_r - 1) + i|z/z_o|_i}{(|z/z_o|_r + 1) + i|z/z_o|_i} \qquad \text{Eq. A1.2}$$

Substituting $y = z/z_0$ and knowing that

$$|x + yi| = \sqrt{x^2 + y^2}$$

from the pythagorean theorem, the square of the reflection coffecient becomes Equation A1.3.

$$|R|^2 = \frac{(y_r - 1)^2 + y_i^2}{(y_r + 1)^2 + y_i^2} \qquad \text{Eq. A1.3}$$

Taking the derivative with respect to film thickness (d) results in Equation A1.4.

$$2|R|\frac{\partial R}{\partial d} = 2|R|\frac{\partial (y_r - 1)^2 + y_i^2}{\partial (y_r + 1)^2 + y_i^2} \qquad \text{Eq. A1.4}$$

The derivative was obtained by using the quotient rule, Equation A1.5, which resulted in Equations A1.6 and A1.7.

$$\frac{du/v}{dx} = \frac{\frac{vdu}{dx} - u\frac{dv}{dx}}{v^2} \qquad \text{Eq. A1.5}$$

$$2|R|\frac{\partial R}{\partial d} = \frac{1}{(y_r + 1)^2 + y_i^2}\left[2(y_r - 1)\frac{\partial y_r}{\partial d} + 2y_i\frac{\partial y_i}{\partial d}\right] - \frac{(y_r - 1)^2 + y_i^2}{\left((y_r + 1)^2 + y_i^2\right)^2}\left[2(y_r + 1)\frac{\partial y_r}{\partial d} + 2y_i\frac{\partial y_i}{\partial d}\right]$$

Eq. A1.6

$$2|R|\frac{\partial R}{\partial d} = 2\frac{\partial y_r}{\partial d}\left[\frac{(y_r - 1)}{(y_r + 1)^2 + y_i^2} - \frac{\left[(y_r - 1)^2 + y_i^2\right](y_r + 1)}{(y_r + 1)^2 + y_i^2}\right]$$

$$+ 2y_i\frac{\partial y_i}{\partial d}\left[\frac{1}{(y_r + 1)^2 + y_i^2} - \frac{(y_r - 1)^2 + y_i}{\left[(y_r + 1)^2 + y_i^2\right]^2}\right] \qquad \text{Eq. A1.7}$$

At the limit of the film thickness goes to zero the impedences go to zero.

$y_r, y_i \text{---> } 0$ with $d \text{---> } 0$

and

$|R| \text{---> } 1$ for the D layer This leaves the derivative of reflection coefficient described by Equation A1.8.

$$\frac{\partial|R|}{\partial d} = \frac{2}{2}\frac{\partial y_r}{\partial d}[-1\ -1] = \frac{-4}{2}\frac{\partial y_r}{\partial d} \qquad \text{Eq. A1.8}$$

Substituting the value of the impedence ratio as a function of distance leaves Equation A1.9.

$$\frac{\partial|R|}{\partial d} = -2\frac{w}{c}\mu'' \qquad \text{Eq. A1.9}$$

This shows that the value of the reflection coeffieicnt as the film thickness goes to zero is only a function of one material property (μ'').

APPENDIX 2

The starting Equation is Equation A2.1. The objective is to differentiate ln k with respect to 1/T. Assuming that ΔG is also temperature dependent.

$$\ln k = \frac{-\Delta G}{RT} \qquad \text{Eq. A2.1}$$

The derivative will be taken as a function of dT, yielding Equation A2.2.

$$\frac{d \ln k}{dT} = - \frac{d \Delta G}{dT} \frac{1}{RT} - \Delta G \frac{d1/RT}{dT} \qquad \text{Eq. A2.2}$$

Substituting for - d ΔG / dT results in Equation A2.3.

$$\frac{d \ln k}{dT} = \frac{\Delta S}{RT} + \frac{\Delta G}{RT^2} \qquad \text{Eq. A2.3}$$

Putting over a common denominator and substituting for the numerator yields Equation A2.4

$$\frac{d \ln k}{dT} = \frac{\Delta H}{RT^2} \qquad \text{Eq. A2.4}$$

Knowing $d(1/T)/dT = 1/T^2$, one can substitute for dT, which yields the final results Equation A2.5.

$$\frac{d \ln k}{d\, 1/T} = - \frac{\Delta H}{R} \qquad \text{Eq. A2.5}$$

APPENDIX 3

```
10    DIM POW (3, 3500), powsen (3), DIO% (2), DAT% (4), LT% (3)
20    DIM S$ (4), YT (4), YP (4), SPEC$ (7), PS (4), temp (4)
30    WIDTH 80
40    COLOR 2,0
50    FLAG = SET
60    CLS: LOCATE 9, 25: PRINT "Microwave Data Acquisition"
70    LOCATE 10, 30: PRINT "and Control"
80    LOCATE 17, 20: PRINT "Virginia Polytechnic Institute and State University"
90    LOCATE 19, 20: PRINT "Blacksburg, VA"
100   LOCATE 21, 50: PRINT "VERSION 1.4      1/10/89"
110   LOCATE 24, 30: INPUT "Press RETURN to Continue" ; B$
120   SCREEN 0, 0, 0
130   COLOR 12, 1
140   CLS
150   LOCATE 2, 20: PRINT "Plot Menu"
160   LOCATE 6, 5: INPUT  "INPUT MAXIMUM TIME: ", TIMAX
170   LOCATE 9, 5: INPUT  "INPUT DELAY TIME: ",  DEL
180   LOCATE 12, 10: INPUT "FULLSCALE POWER SETTING ON INPUT POWER
      METER/mW:   ", powsen (0)
190   LOCATE 14, 10: INPUT "FULLSCALE POWER SETTING ON REFLECTED POWER
      METER/mW:   ", powsen (1)
200   LOCATE 16, 10: INPUT "FULLSCALE POWER SETTING ON TRANSMITTED POWER
      METER/mW:   ", powsen (2)
210   LOCATE 18, 10: INPUT "INPUT FILENAME  (8 CHARACTERS MAX): ", F1$
211   'Correction for Fullscale Power Reading
212   FOR I = 0 TO 2
213   IF powsen (I)  =  .3 THEN powsen (I)  =  .316
214   IF powsen (I)  =  3 THEN powsen (I)  =  3.16
215   IF powsen (I)  =  30 THEN powsen (I)  =  31.6
216   IF powsen (I)  =  300 THEN powsen (I)  =  316
217   NEXT I
220   SCREEN 0, 0, 0
230   COLOR 14, 1
240   CLS
250   'LUXTRON PROBE SELECT AND GRAPH LIMITS
260   PRINT "LUXTRON PROBE SELECT AND GRAPH LIMITS"
270   LOCATE 5, 5: PRINT "TEMPERATURE PROBES SELECTED": LOCATE 5, 60 PRINT"
      1     2     3     4"
300   LOCATE 25, 50: COLOR 14, 1: PRINT "Press <esc> to set graph limits";
310   LOCATE 5, 60, 1
320   ROW=5: COL=60
340   A=1: B=1
350   'Waits for input from keyboard
360   KB$=INKEY$
370                 IF LEN (KB$)=2 THEN KB$=MID$ (KB$,2)
380                 IF KB$ = " " THEN KB = ELSE KB = ASC (KB$)
410                 IF KB   = 75  THEN GOSUB 550    'left arrow
420                 IF KB   = 77  THEN GOSUB 580    'right arrow
430                 IF KB   = 13  THEN GOSUB 700   '13=<CR>
440                 IF KB   = 27  THEN GOTO   860   '27=Escape
450   GOTO 340
```

```
550   'Sub to move cusor horizontally
560   B=-1
570                   IF COL<64 THEN RETURN
580                   IF ROW=5 THEN GOTO 600
590                   IF ROW<>20 THEN RETURN
600                   IF B<O THEN GOTO 650
610                   IF ROW<>5 THEN GOTO 630
620                   IF COL>79 THEN RETURN
630                   IF ROW<>20 THEN GOTO 650
640                   IF COL>59 THEN RETURN
650                   COL=COL+(B*5)
660                   LOCATE ROW,COL
670   RETURN
680   COL=60:LOCATE ROW,COL
690   RETURN
700   'Sub for return acknow.
710         IF ROW=5 THEN GOTO 740
730   RETURN
740   V=SCREEN(ROW,COL,1)
750   B=V MOD 16
760   Y=(COL - 60) /5+1
770   IF B<>14 THEN COLOR 14,1:PS(Y)=0:GOTO 790
780   PS(Y)=1:COLOR 9,4
790   LOCATE ROW,COL-1
800   PRINT Y
810   LOCATE ROW,COL-1
820   RETURN
850   '*********************Remote    Configuration*****************
860   'Tell LUXTRON which temperature probes have been selected
870      PS$=""
880      IF PS(1)=1 THEN PS$="1,"
890      IF PS(2)=1 THEN PS$=PS$+"2,"
900      IF PS(3)=1 THEN PS$=PS$+"3,"
1000     IF PS(4)=1 THEN PS$=PS$+"4,"
1005  COLOR 14,1
1010  LOCATE 8,5:PRINT"MAXIMUM TEMPERATURE':LOCATE 8,50:INPUT"",
      TEMPMAX
1020  LOCATE 11,5:PRINT"MAXIMUM POWER":LOCATE 11,50:IMPUT"",PMAX
1040  OPEN"C:\MICRO\"+F1$+".DAT" FOR APPEND AS #3
1060  'Set Up Function Keys
1070     ON KEY(1) GOSUB 2460 ' Pause
1080     ON KEY(2) GOSUB 2420 'Restart
1090     ON KEY(4) GOSUB 1750 ' Acquire Data
1100     ON KEY(5) GOSUB 2570 ' Exit
1120     key(1)  on :key(2)  on: key(3)  on: key(4)  on: key(5)  on
1130  'Set Up Luxtron and Dash8
1140  OPEN"COM1:1200" AS #2
1150  PRINT #2,CHR$(20)     'STANDBY
1160  LINE INPUT#2,EKO$
1161  PRINT #2,CHR$(27);"PS =";PS$;CHR$(13)  'PROBES SELECTED
1162  LINE INPUT #2,EKO$
```

```
1170 PRINT#2,CHR$(27) ; "SF=F"  'SEND FULL LINE FORMAT
1180 LINE INPUT#2, EKO$
1190 PRINT #2,CHR$(27 ; "ST=.1" ; CHR$(13)  '.1 SEC SAMPLE TIME
1200 LINE INPUT#2,EKO$
1210 PRINT #2,CHR$(27) ; "MU=";DEL;CHR$(13)   'MEASUREMENT UPDATE TIME
     (DELAY)
1220 LINE INPUT #2, EKO$
1230 PRINT #2,CHR$ (27) ; "UN=C"; CHR$(13)  'TEMPERATURE IN DEGREES
     CELCIUS
1240 LINE INPUT #2, EKO$
1270 BASADR%=&H300
1280 MD%=0:CALL DASH8 (MD%,BASADR%,FLAG%)  'Initialize
1290 LT%(0)  =  0
1300 LT%(1)  =  3
1310 MD% =1: CALL DASH8 (MD%, LT%(0), FLAG%) 'Set multiplexer high/low
     limits
1320 COM(1) ON:KEY(1) ON:KEY(2) ON:KEY(3) ON:KEY (4) ON:KEY(5)  ON:KEY(6)
     ON
1330 'This routine puts marks onto axes and labels
1340 SCREEN 9, 0, 0, 0: CLS
1350 LOCATE 25, 1
1360 PRINT" F1 PAUSE F2 RESTART      F4 ACQUIRE DATA     F5 EXIT";
1370 LINE   (100,  20)  -  (500,20)
1380 LINE   -  (500,  270)
1390 LINE   -  (100,  270)
1400 LINE   -  (100,  20)
1410         LOCATE 23, 35
1420         PRINT"Time / s"
1430         POWER$="Power / W"
1440         TEMP$="Temperature / C"
1450         LOCATE 4, 5
1460 FOR I=1  TO  15
1470 PRINT  TAB(5): MID$(TEMP$,  I,  1)
1480 NEXT
1490         FOR I = 1  TO 9
1500         LOCATE 7 + I, 75:PRINT MID$ (POWERS, I, 1) :NEXT
1510         FOR I = 0  TO 4
1520         X  =  100  +  I*80
1530         Y  =  20  +  I*50
1540         LINE  (X,  270)  -  (X,  265)
1550         LINE  (100,  Y)  -  (108,  Y)
1560         LINE  (500,  Y)  -  (492,  Y)
1570         NEXT
1580 'Labels for tick marks
1590     T1$=STR$(TEMPMAX)
1600     T2$=STR$(TIMAX)
1610     T3$="0"
1620     T4$=STR$(PMAX)
1630     LOCATE  21, 13:PRINT T3$
1640     LOCATE  21, 60:PRINT T2$
1650     LOCATE  2, 9: PRINT T1$
```

```
1660     LOCATE  20, 11: PRINT T3$
1670     LOCATE  2, 67: PRINT T4$
1680     LOCATE  20, 67: PRINT T3$
1690     XT1 = 100
1700        FOR I = 0 TO 3
1710        YT(I) = 150:YP(I) = 150:NEXT
1720      WHILE  C = 0
1730        C$ = INKEY$
1740        IF LEN(C$) = 2 THEN C$ = MID$(C$, 2)
1745        IF C$ = "" THEN C = 0 ELSE C = ASC(C$)
1746      WEND
1747      C = 0
1748 TIM = 0
1749 FLAG = 0
1750 TIM1 = 0
1751 '**********Timed Data Acquisition with Delay ***************
1760 START ! = TIMER
1770 S = DEL*.99
1780 Q = TIMAX-S
1781     PRINT  #2,CHR$(18)  'TURN ON Luxtron
1782     LINE INPUT  #2,EKO$
1790 WHILE TIM < Q
1800     FINISH! = TIMER
1810     TIM = FINISH! - START!
1825     IF FLAG = SET THEN TIM = TIM + TIM1
1820     CH% = 0
1830     MD% = 2:CALL DASH8  (MD%,CH%,FLAG%)  'Set multiplexer address
1840 'Temperature Acquisition from Luxtron
1850     PRINT  #2,  CHR$(9)
1860     LINE INPUT #2, EKO$
1870     PRINT  #2,  CHR$(17)
1880     LINE INPUT #2, EKO$
1890     LINE INPUT #2, A$
1900     temp (1) = VAL (MID$(A$, 6, 8))
1910     temp (2) = VAL (MID$(A$, 20, 8))
1920     temp (3) = VAL (MID$(A$, 34, 8))
1930     temp (4) = VAL (MID$(A$, 48, 8))
1940 ' Power Acquisition Dash8
1950         WHILE CH% < 2
1960         MD% = 3:CALL DASH8 (MD%, CH%, FLAG%)  'Read multiplexer
1970         MD%= 4:CALL DASH8 (MD%, DIO%, FLAG%)  'Perform A/D conversion
1980         DAT%(DH%) = DIO%
1985         POW(CH%, TIM) = (DAT% (CH%) + 2048) / 4096
1987         WEND
1990 ******This routine plots the acquired data in real time***********
2100 LOCATE 1, 5: PRINT USING " ####.#    ";TIM,TEMP(1), TEMP(2), TEMP(3),
     TEMP(4)
2110     XT  =  100 + (TIM.TIMAX) *400
2120     FOR I=0  TO 4
2140         IF TEMP (I) = 0  THEN GOTO 2180
2150         YT1 = YT(I)
```

```
2160        YT(I) = 270 - TEMP (I)/TEMPMAX*250
2170        LINE  (XT1, YT1) - (XT, YT(I)), I + 2
2180     NEXT I
2190 'This is for plotting the power values
2192 'Correction for Attenuation
2193 POW (O, TIM)  =  POW (O, TIM) *powsen (0) /10
2194 POW (1, TIM)  =  POW (1, TIM) *powsen (1) *10
2195 POW (2, TIM)  =  POW (2, TIM) *powsen (2) *10
2200     FOR I = 0 TO 2
2215     'IF POW (I, TIM)  =  0 THEN GOTO 2250
2220     YP1=YP(I)
2230     YP  (I)  =  270-POW(I,  TIM)  /PMAX*250
2240     LINE (XT1, YP1) - (XT, YP (I)), I + 5
2250     NEXT I
2260 XT1 = XT
2265 'Prints to C drive formatted for Cricket Graph
2270                        PRINT   #3,   USING "####.# ";TIM;
2275                        PRINT   #3,   CHR$(9);
2280                        FOR J = 0 TO 2
2285                        IF POW (J, TIM)  =  0  THEN GOTO 2300
2290                        PRINT   #3, USING "##.## "; POW (J,TIM);
2300                        PRINT   #3, CHR$(9);
2310                        NEXT J
2320                        FOR K = 0 TO 3
2325                          IF TEMP (K)  =  0  THEN GOTO 2360
2330                          PRINT  #3,  USING  "###.##";  TEMP  (K);
2340                          IF K = 3  THEN GOTO 2350
2350                          PRINT #3, CHR$ (9);
2360                        NEXT K
2370                        PRINT #3, TEMP (K)
2400
2410 WEND
2420 'Restart Routine
2421 COM (1) OFF:KEY(1) OFF:KEY(2) OFF KEY(3) OFF KEY(4) OFF:KEY(5)   OFF
2430 PRINT#2,  CHR$(&H14)
2431 LINE INPUT #2, ECO$
2432 PRINT  #2,  CHR$(&H4)
2433 LINE INPUT #2, ECO$
2434 RESET
2436 ERASE POW,POWSEN,DIO%,DAT%,LT%,S$,YT,YP,SPEC$,PS,TEMP
2437 CLOSE
2438 TIMAX = 0 ; TIM = 0:FLAG = 0
2440 RETURN 10
2460 'Pause subroutine
2470 PRINT  #2,  CHR$(&H14)
2471 LINE INPUT #2,ECO$
2472 PRINT  #2,  CHR$(&H4)
2473 LINE INPUT#2,ECO$
2474 FLAG = SET
2475 TIM1  =  TIM
2476 FINISH!  =  0
```

```
2480 LOCATE 20, 30:PRINT "Press enter to continue"
2500 WHILE GB = 0
2510         GB$ = inkeys
2520         IF LEN(GB$0 = 2 THEN GB$ = mid$(GB$,2)
2530         IF GB$ = "" THEN GB = 0 ELSE GB = ASC(GB$)
2540 WEND
2550 GB = 0:START! = TIMER
2560 RETURN 1781
2570 PRINT #2,CHR$(20)  'STANDBY
2580 LINE INPUT #2,EKO$
2590 CLOSE
2600 END
```

Vita

The author, George John Dallas was born on July 9, 1960 in New London Connecticut. He is the son of Mr. and Mrs. George Dallas. He finished high school at East Lyme High in East Lyme Connecticut in June 1978. He then entered Roger Williams College in Bristol Rhode Island. After one semester he transferred to Hartwick College in Oneonta, New York. He completed he Bachelor of Science in Chemistry in May, 1982. He then enrolled in San Jose State University in San Jose California and graduated with a Master of Science in Chemistry under Dr. Joseph Pesek. He then enrolled in Virginia Polytechnic Institute and State University in Blacksburg, Virginia. He commenced towards a Ph. D in the Materials Engineering Science Program at this university under Dr. Thomas C. Ward and completed the degree in the Fall of 1991.